UNIVERSITY OF CALIFORNIA SAN DIEGO

Cardiac function modulates endocardial cell dynamics to shape the cardiac outflow tract

A dissertation submitted in partial satisfaction of the requirements for the degree of Doctor of Philosophy

in

Biology

by

Pragya Sidhwani

Committee in charge:

Professor Deborah Yelon, Chair
Professor Neil Chi
Professor Kimberly Cooper
Professor James Posakony
Professor Xin Sun

2019

The Dissertation of Pragya Sidhwani is approved, and it is acceptable in quality and form for publication on microfilm and electronically:

Chair

University of California San Diego

2019

DEDICATION

I would like to dedicate this dissertation to my parents: to my mother, who sparked in me my passion for science, and to my father, who imbued in me the strength to pursue it.

EPIGRAPH

Outside in

Begin, till sweat erodes your skin,

Work, till it permeates your flesh,

Endure, till it saturates your blood,

Finish, when it forges your heart.

Inside out

Begin, till blood bears its path,

Work, till it perfuses your core,

Endure, till It chisels its realms,

Finish, when it forges your heart.

TABLE OF CONTENTS

LIST OF FIGURES

ACKNOWLEDGEMENTS

I have gotten to know many wonderful people over the last 6 years, many of whom I owe my deepfelt gratitude for supporting me through this journey. First, I would like to thank my advisor Debbie, who has been a mentor to me in every sense of the word. She has taught me not only how to think rigorously and scientifically, but also how to handle situations and people scientifically, with care interspersed with logic. I briefly worked with her on the bench in early 2017 when, unbeknown to her, I was feeling bored with the monotony of my own experiments. By just being her meticulous self, she changed my perspective on science—she made me realize that when you do things systematically, with the love and attention they deserve, they automatically become less mundane and more exciting. I have learnt more from you than you know, Debbie, and I hope that some day, I can impart this wisdom to others in a “signaling cascade” of knowledge.

I would also like to thank Aman, who has been there for me every step of the way. I went from living at home in India to living alone in a new country within a year. This transition would have been harder if it were not for Aman. He fed me good food, listened to my incessant rants about failed experiments, and provided me with unconditional support to be where I am today.

I could not have achieved what I have without constant support from my family, especially my parents, who made me, and made me who I am, my brother Pranav, who I am connected to on a very basal level, my naniji, whose “aashirwaad” got me through tough times, and Akki, who inspired me with her creativity and artistic aplomb.

Finally, I would like to my friends, both in lab and outside. I owe much to my labmates, for their scientific inputs as well as emotional support. I feel especially grateful to have known Andrew, Tami, Elliot, Jessyka, Dena, Hannah, Arjana and Kai. Henry and Kirstin were wonderful undergraduates to work with. My friend and roommate Akshay Rangesh introduced me to great music and anime, while also helping me through some of my toughest times last year. Suneer, Adi, Katharine, Mai, Ami and Anupriya were always there for me. My closest friends Muna, Kashish and Priya reminded me of happier times when I was down.

Chapter 2, in full, is currently being prepared for submission to *eLife* for publication of the material. Sidhwani, Pragya; Boezio Giuilia; Yang, Hongbo; Chi, Neil; Roman, Beth; Stainier, Didier; Yelon, Deborah. “Cardiac function modulates endocardial cell dynamics to shape the cardiac outflow tract” *In preparation.* The dissertation author was the primary investigator and author of this material. Please note that a portion of the material presented in Chapter 1 is adapted from Chapter 2.

Preliminary experiments in Chapter 3 were designed and performed by the dissertation author. Please note that a portion of material presented in Chapter 3 is adapted from Chapter 2.

The appendix, in full, is a reformatted reprint of the following book chapter: Sidhwani, P., Yelon, D., 2019. “Fluid forces shape the embryonic heart: insights from zebrafish”, in *Current Topics in Developmental Biology* 2019; 132: 395-416. The dissertation author was the primary investigator and author of this paper. Please note that portions of the material presented in Chapter 1 and Chapter 3 are adapted from the appendix.

VITA

2011	Bachelor of Science, University of Delhi, India
2013	Master of Science, University of Delhi, India
2019	Doctor of Philosophy, University of California San Diego

PUBLICATIONS

Sidhwani, P., Yelon, D. Fluid forces shape the embryonic heart: insights from zebrafish. *Current Topics in Developmental Biology* 2019; 132: 395-416

Pradhan, A., Zeng, X.X., Sidhwani, P., Marques, S.R., George, V. Targoff, K.L., Chi, N.C., Yelon, D. FGF signaling enforces cardiac chamber identity in the developing ventricle. *Development* 2017; 144: 1328-1338

Khare, G., Reddy, P.V., Sidhwani, P., Tyagi, A.K. KefB inhibits phagosomal acidification but its role is unrelated to *M. tuberculosis* survival in host. *Scientific Reports* 2013; 3: 3527

ABSTRACT OF THE DISSERTATION

Cardiac function modulates endocardial cell dynamics to shape the cardiac outflow tract

by

Pragya Sidhwani

Doctor of Philosophy in Biology

University of California San Diego, 2019

Professor Deborah Yelon, Chair

Physical inputs orchestrate cellular dynamics to sculpt organs of various morphologies. In the embryonic heart, for example, functional cues engendered by blood flow and contractility regulate cell size, shape and number to create the curvatures of the ventricular chamber. However, we have limited understanding of the

many ways by which forces associated with function integrate diverse cellular mechanisms in multiple tissues to build a composed organ. Here, we leverage the junctional location and precise dimensions of the cardiac outflow tract (OFT), a cylindrical carrier of blood between the heart and the vasculature, to address this question. Since the OFT is formed by late-differentiating second heart field cells annexing to the arterial pole of a contractile heart tube, we hypothesize that function could influence the earliest steps of OFT development. Using high-resolution morphometrics in the optically accessible zebrafish embryo, we show that in the context of normal cardiac function, the OFT expands via concerted accumulation of inner endocardial and outer myocardial cells. However, in mutants with disrupted cardiac function, OFT endocardial growth ceases and the arrangement of the overlying myocardial cells is altered. By evaluating patterns of cell behavior in both wild-type and mutant embryos, we identify essential roles for cardiac function in promoting both the proliferation of the OFT endocardium and the addition of endothelial cells to the OFT from the adjacent aortic arches. Intriguingly, loss-of-function of the TGFβ receptor Alk1 leads to reduced addition of endothelial cells to the OFT endocardium without inhibiting OFT endocardial proliferation, suggesting that these two endocardial cell behaviors can be uncoupled through molecular, and possibly physical, mechanisms. Overall, our studies illuminate the cellular basis for essential early phases of OFT morphogenesis, while also pointing toward molecular mechanisms by which cardiac function shapes OFT development.

CHAPTER 1

Functional cues in heart morphogenesis and cardiac outflow tract development

Abstract

"Form ever follows function, and this is the law," as stated by the architect Louis Sullivan, can also be applied to the biological process of morphogenesis. In the embryonic heart for example, both contractility and blood flow have been shown to influence cell shape, size and proliferation to modulate chamber expansion. However, this relationship has not yet been established in the outflow tract (OFT), a cylindrical structure constructed at the arterial pole of the beating heart tube, which acts as a primary portal for blood flow between the heart and the periphery. The OFT is derived from late-differentiating "second heart field" (SHF) progenitors that proliferate, differentiate and accrete onto the early heart tube. Although these processes are concordant with the initiation of cardiac function, which could suggest a role for functional influences on the initial structure of the OFT, the cellular, molecular and physical mechanisms guiding early OFT shape remain generally unknown. In this chapter, we provide a primer on how forces impact multiple aspects of cardiac morphogenesis, followed by an introduction to outflow tract development, morphogenesis and anomalies, all the while highlighting considerable gaps in our knowledge that this dissertation aims to address. In summary, this chapter argues for the importance of uncovering the mechanical mechanisms governing early OFT morphogenesis, especially given that 30% of congenital heart diseases contain OFT abnormalities.

1.1 Physical inputs sculpt the developing heart

Biomechanical forces are important regulators of embryonic morphogenesis. As early as gastrulation, circumferential contractions and flow-frictional mechanisms drive the spreading of the enveloping cell layer over the zebrafish yolk (Behrndt et al., 2012). Compressing and stretching the apical surface of cells induces apoptosis and proliferation, respectively, to shape the overall structure of the Drosophila wing (Diaz de la Loza & Thompson, 2017). The periodic spacing of feather follicles in chick is governed by competing interactions between cellular contractility and substrate stiffness (Shyer et al., 2017). In many contexts, physical cues provoke specific cellular behaviors that ultimately give rise to tissue morphology.

Forces are especially crucial during cardiac development, since blood flow and cardiac contractility produce distinct physical inputs while heart formation is underway (Freund et al., 2012; Haack & Abdelilah-Seyfried, 2016) (Figure 1-1). Contractility, for example, stretches cells in a direction perpendicular to the flow of blood. It is also particularly interesting to consider how flow-induced forces create spatiotemporally heterogeneous patterns that provide regionalized cues within the developing organ. Fluid frictional forces are thought to induce shear stress that deforms cells in the direction of blood flow. Blood pressure, on the other hand, causes cells to stretch circumferentially. Finally, the direction of blood flow can itself administer distinct mechanical cues to cells: reversing or retrograde flows, for instance, are thought to activate specific downstream pathways. Together, these fluid forces sculpt the heart, in a biological manifestation of “form follows function”.

How do fluid forces prompt cardiac cells to enlarge, elongate, divide, converge, and protrude as they create the specific architecture of the embryonic heart? Despite awareness of several mechanosensitive pathways that operate in endothelial cells (Baratchi et al., 2017), we do not yet fully understand the cellular and molecular mechanisms that drive cardiac morphogenesis in response to hemodynamic cues. To gain insights into these mechanisms, we need to be able to integrate *in vivo* assessment of fluid forces, high-resolution analysis of cell behaviors, and precise manipulation of mechanosensitive genes. The zebrafish embryo serves as an ideal model organism in this regard: its optical clarity allows real-time visualization of fluid dynamics as well as live imaging of morphogenesis at cellular resolution, and its genetic tractability permits both classical genetic screens and cutting-edge genome editing (Collins & Stainier, 2016; Li et al., 2016). Importantly, zebrafish offer the unique advantage that they can survive throughout embryogenesis without convective oxygen, allowing the analysis of cardiovascular defects without confounding lethality. Finally, although the zebrafish heart is anatomically simpler than the mammalian heart, the mechanosensory pathways operating during cardiac development appear to be highly conserved (Goddard et al., 2017). Together, these benefits of zebrafish have facilitated a number of investigations into the ways in which function influences form in the developing heart.

1.2 Fluid forces regulate multiple aspects of vessel development

When considering how fluid forces influence cardiac morphology, it is instructive to reflect upon our understanding of the influence of flow on vessel development. The

impact of physical forces on endothelial cells in the vasculature is especially relevant to the potential roles of such forces on the endocardium, the specialized inner layer of endothelium that lines the muscular myocardial layer of the heart. Numerous studies in cultured endothelial cells have shown that endothelial cells rearrange their cytoskeleton and alter their gene-expression patterns in response to flow-induced forces (Helmlinger et al., 1991). Interestingly, endothelial cells respond differently to laminar flow and oscillatory flows (Noris et al., 1995), which has motivated the idea that the direction or pulsatile nature of flow could have a distinct impact on cellular behaviors. In this section, we will provide a few recent perspectives on how processes like lumen growth and vessel remodeling respond to fluid forces in zebrafish.

Blood flow has been shown to regulate vessel diameter through its influence on several types of endothelial cell behaviors. For example, Endoglin, a TGF-β receptor, modulates endothelial cell shape in response to hemodynamic cues, thereby restricting the diameters of the dorsal aorta and posterior cardinal vein (Sugden et al., 2017). In the caudal vein, shear forces lead to an increase in endothelial cell number via mechanosensation by Pkd2/Trpp2, a calcium channel present on endothelial cilia (Goetz et al., 2014). In the cranial vasculature, flow-induced expression of the TGF-β receptor Alk1 regulates the migration of endothelial cells in the direction opposite to blood flow, thereby limiting vessel caliber (Corti et al., 2011; Rochon et al., 2016) (Figure 1-2). Finally, Yap1, a Hippo pathway effector, localizes to the nucleus in a flow-dependent manner in the dorsal longitudinal anastomotic vessel, where it regulates the maintenance of lumen size (Nakajima et al., 2017).

Fluid forces are also critical for the morphogenetic processes that are involved in vessel remodeling. For instance, flow regulates the apical membrane invagination that is required for successful tube formation during vessel fusion (Herwig et al., 2011). Blood flow is also important for the establishment of planar cell polarity in endothelial cells (Kwon et al., 2016), which could influence vessel regression, as has been predicted in mice (Franco et al., 2015). Indeed, vessel regression in the zebrafish eye (Kochhan et al., 2013) and midbrain (Chen et al., 2012) have been shown to occur in response to blood flow, potentially via flow-mediated cell rearrangement and migration.

Together, these studies underscore the importance of fluid forces during multiple aspects of vascular morphogenesis and provide inspiration for the ways in which blood flow could influence cell shape, cell number, migration, and polarity during heart development. In the following sections, we will examine the impact of cardiac function and fluid forces on cell behavior during three essential phases of cardiac morphogenesis: chamber emergence, atrioventricular canal differentiation, and ventricular trabeculation.

1.3 Chamber emergence requires hemodynamic inputs

In the early embryo, the primitive heart is a simple, relatively linear cylinder positioned at the embryonic midline. As development proceeds, the heart tube enlarges and transforms into a morphologically distinct series of cardiac chambers, each expanding into its characteristic curvatures (Collins & Stainier, 2016). Since chamber emergence takes place while the heart is beating and the blood is flowing, biomechanical inputs generated by cardiac function have the potential to influence this

process. Indeed, surgical obstruction of blood flow into the embryonic chick heart results in aberrant chamber morphology (Broekhuizen et al., 1999). Mouse mutants lacking atrial contractility due to a mutation in *atrial myosin light chain 2a* exhibit abnormal ventricular morphogenesis (Huang et al., 2003), further supporting a connection between blood flow and cardiac chamber development. In cultured neonatal rat cardiomyocytes (CMs), mechanical stretch induces expression of proto-oncogenes and many other gene programs, all of which are thought to induce hypertrophic growth (Lindsey et al., 2014; Ruwhof & van der Laarse, 2000; Rysa et al., 2018). Taking advantage of the opportunities for examining chamber emergence in the context of the zebrafish embryo, a number of studies have delved deeper into the cell behaviors that shape the chambers in response to biomechanical cues.

In zebrafish, as the ventricle and atrium emerge from the linear heart tube, distinct convex and concave surfaces form the outer and inner curvatures of each chamber. These tissue shape changes are associated with regional patterns of cell shape change: in the ventricle, for example, outer curvature cardiomocytes enlarge and elongate during chamber emergence, while inner curvature cardiomyocytes remain relatively small and round (Auman et al., 2007). Analysis of cardiomyocyte morphology in mutant embryos has suggested that cell shape change at the ventricular outer curvature depends upon inputs generated by cardiac function. In *weak atrium* (*amhc*) mutants, which lack atrial contractility and therefore have reduced blood flow into the ventricle, outer curvature cardiomyocytes are smaller and rounder than in the wild-type ventricle (Auman et al., 2007); these cells also exhibit diminished myofibril maturation (Lin et al., 2012). In contrast, *half-hearted* (*vmhc*) mutants, which lack ventricular

contractility, display excessively enlarged and elongated cells in the ventricular outer curvature (Auman et al., 2007) (Figure 1-3). These studies suggest that forces produced by both blood flow and contractility modulate cardiomyocyte shape and size and therefore contribute to the regulation of chamber emergence.

In conjunction with the outward expansion of the myocardium, the inner endocardial layer of the heart also grows as the chambers emerge. Cellular proliferation drives this endocardial expansion, while local differences in endocardial cell morphologies correlate with the curved chamber contours (Dietrich et al., 2014). Interestingly, in conditions where fluid forces are reduced, proliferation of the ventricular endocardium is markedly decreased (Dietrich et al., 2014) (Figure 1-4). Endocardial cells also fail to acquire normal morphologies under these circumstances. Together, these results suggest a model in which fluid forces trigger proliferation of endocardial cells, causing an overall enlargement of the endocardium that provokes cell shape changes within the myocardium, thereby facilitating synchronous expansion of both cardiac layers.

Which molecular pathways might drive chamber emergence in response to fluid forces? Exposure of endothelial cells to shear stress *in vitro* induces the expression of *KLF2*, which encodes a mechanoresponsive transcription factor (Dekker et al., 2002), and the expression of the zebrafish homolog *klf2a* also appears to be flow-responsive (Vermot et al., 2009). The *klf2* pathway is thought to contribute to the regulation of chamber emergence, since *klf2a* morphants exhibit aberrant endocardial morphology in the ventricle (Dietrich et al., 2014). Micro-RNAs are also interesting candidates for mechanoresponsive functions, since they can be regulated rapidly in response to flow

(Banjo et al., 2013). Indeed, function-dependent expression of *miR-143* in both the myocardium and the endocardium impacts the process of ventricular emergence (Miyasaka et al., 2011). In the myocardium, *miR-143* targets *adducin3*, which regulates cytoskeletal actin dynamics and can thereby influence cardiomyocyte morphology (Deacon et al., 2010). In the endocardium, *miR-143* limits retinoic acid signaling by directly targeting *raldh2* and *rxrab* (Miyasaka et al., 2011). Intriguingly, *miR-143* morphants exhibit gaps in the ventricular endocardium (Miyasaka et al., 2011), hinting at defects in endocardial cell number. In future studies, it will be valuable to identify not only additional mechanosensitive genes that are relevant to chamber emergence but also additional downstream effectors responsible for executing the patterns of proliferation in the endocardium and cell shape change in the myocardium.

1.4 Retrograde flow drives atrioventricular canal differentiation

As the cardiac chambers emerge, the junction between the atrium and the ventricle constricts to form the atrioventricular canal (AVC). Within this region, distinct differentiation pathways create the endocardial cushions, specialized structures that will subsequently remodel to create the atrioventricular valve. Endocardial cushion formation has been examined with cellular precision in zebrafish, owing to the optical accessibility of the embryo. At early stages, endocardial cells accumulate both through proliferation and via convergence to the AVC region (Boselli et al., 2017; Steed et al., 2016b), while also acquiring distinctive cuboidal morphologies (Beis et al., 2005; Steed et al., 2016b). Following this, the endocardial cells invaginate as a sheet into the extracellular matrix, ultimately forming valve leaflets (Pestel et al., 2016).

Early work in chick had shown that impediment of mechanical forces in the heart, via surgical alteration, can result in abnormal morphology of the atrioventricular valve (Sedmera et al., 1999). Following this, several studies in zebrafish have indicated that cardiac function provides essential cues for endocardial cushion formation. Endocardial cushions fail to form in *silent heart* mutants and *cardiofunk* mutants, both of which have defects in cardiac contractility (Bartman et al., 2004; Beis et al., 2005). Similarly, physical occlusion of blood flow into the zebrafish heart impairs atrioventricular valve development (Hove et al., 2003).

The oscillatory component of wall shear stress, or retrograde flow, is known to be particularly elevated within the AVC (Heckel et al., 2015), suggesting that the magnitude and the direction of fluid forces could influence AVC differentiation. To examine the effects of these types of mechanical inputs, the phenotypes generated by knocking down *gata1* and *gata2*, genes involved in hematopoiesis, were examined (Vermot et al., 2009) (Figure 1-5). Since both genes contribute to erythrocyte development, knockdown of either should reduce shear forces in the heart. In addition, *gata2* morphants display a reduction in retrograde flow fraction (RFF) in the AVC, whereas *gata1* morphants display an increased RFF. Furthermore, *gata2* morphants fail to develop valve leaflets, whereas *gata1* morphants appear strikingly normal. Likewise, valve formation fails in *weak atrium* mutants, which also exhibit a reduced RFF in the AVC (Kalogirou et al., 2014). Notably, the valve defects in *gata2* morphants are preceded by a failure to accumulate endocardial cells at the AVC, as well as irregular cellular morphologies (Vermot et al., 2009). The former is consistent with the observation that endocardial convergence at the AVC fails in *silent heart* mutants (Boselli et al., 2017). Together,

these findings imply that retrograde flow, and not shear, is the driving force for atrioventricular valve formation, potentially through its influence on cellular rearrangement during AVC differentiation.

Investigation of the molecular pathways triggered by retrograde flow in the AVC has primarily centered on *klf2a*. Expression of *klf2a* in the AVC endocardium is reduced in *gata2* morphants (Heckel et al., 2015; Vermot et al., 2009), and *klf2a* morphants resemble *gata2* morphants in that their AVC endocardial cells are reduced in number as well as abnormally elongated and flat (Vermot et al., 2009). Moreover, the calcium channels Trpp2 and Trpv4 appear to regulate *klf2a* expression in response to oscillatory flow patterns within the AVC endocardium (Heckel et al., 2015). Downstream effectors of Klf2 in the AVC endocardium include the extracellular matrix component Fibronectin: *fibronectin1b* morphants have defective cell clustering at the AVC, similar to *klf2a* morphants and *gata2* morphants (Steed et al., 2016b). In addition, *wnt9b* acts a paracrine factor downstream of *klf2a* during AVC differentiation (Goddard et al., 2017).

Given the importance of *klf2a* to mechanosensation at the AVC, it is reasonable to imagine that the levels of *klf2a* expression must be carefully controlled. In accordance with this, the cerebral cavernous malformation (CCM) proteins Ccm1 and Ccm2 have been shown to restrict *klf2a* expression, with Ccm2 acting in a manner independent of cardiac function (Renz et al., 2015). Interestingly, the expression of Heg1, which acts to stabilize Ccm1, appears to be dependent on both cardiac function and *klf2a*, suggesting that *klf2a* acts in a negative feedback loop to influence its own expression (Donat et al., 2018). Altogether, studies of the factors upstream and downstream of *klf2a* place it as a key node in a retrograde flow-regulated pathway that drives AVC differentiation.

When considering additional factors that may act in or parallel to the *klf2a* pathway in this context, it is again interesting to examine the possible roles of micro-RNAs. For example, *miR-21* is expressed in the AVC in a function-dependent manner, and *miR-21* morphants fail to exhibit normal atrioventricular valve formation (Banjo et al., 2013). *miR-21* is thought to activate the MAP kinase cascade by targeting *sprouty2*, suggesting a possible mechanism for its influence on endocardial cell behavior during AVC differentiation. Further work will be necessary to evaluate whether these and/or other players interface with the *klf2a* pathway in executing the biomechanical regulation of AVC differentiation by retrograde flow.

1.5 Functional regulation of ventricular trabeculation

Following cardiac chamber emergence, the architecture of the ventricle becomes more elaborate through the formation of trabeculae – myocardial ridges that extend into the ventricular lumen. Analyses in zebrafish have shown that trabeculation is driven by the directional migration of cells that delaminate from the compact layer of the myocardium (Liu et al., 2010; Staudt et al., 2014). This delamination process involves constriction of the abluminal cardiomyocyte surface and is dependent upon the proper apicobasal polarization of the myocardial tissue (Jimenez-Amilburu et al., 2016; Staudt et al., 2014). In a noncontractile zebrafish heart, trabeculation fails: in *silent heart* morphants, for example, cardiomyocytes still extend protrusions into the ventricular lumen, but these protrusions frequently retract and stable trabeculae do not form (Staudt et al., 2014). These findings indicate that cardiac function is important for regulating trabeculation, consistent with prior observations in chick, where ventricular

afterload has been implicated in regulating the thickening of the compact and trabecular layers (Sedmera et al., 1999).

Do fluid forces play a key role in controlling the cell behaviors that underlie trabeculation? Indeed, reduction of blood flow in both *weak atrium* mutants and *gata1* morphants inhibits trabeculation (Lee et al., 2016; Peshkovsky et al., 2011; Staudt et al., 2014; Vedula et al., 2017). Furthermore, studies in *weak atrium* mutants and morphants suggest that both the initial formation of luminal protrusions and their progression into stable trabeculae could be sensitive to the patterns of blood flow through the ventricle (Peshkovsky et al., 2011; Staudt et al., 2014). Flow parameters at the onset of ventricular trabeculation have not yet been carefully examined; however, the oscillatory shear index has been shown to be higher in trabecular grooves and lower in trabecular ridges at 4 days post-fertilization, after mature trabeculae are in place, and this distinct pattern is perturbed when trabeculation is inhibited (Vedula et al., 2017). In future studies, it will be valuable to investigate flow patterns in the ventricle at earlier stages in order to discern whether parameters like the oscillatory shear index can predict where trabecular protrusions will form.

Several signaling pathways that are known to be important regulators of trabeculation are also responsive to biomechanical cues. For example, the Neuregulin signaling pathway, operating through the Erbb2 receptor tyrosine kinase, is required for trabeculation (Liu et al., 2010), and expression of both *erbb2* (Lee et al., 2016) and its ligand *nrg2a* (Rasouli & Stainier, 2017) have been shown to be dependent on cardiac function. Function-mediated Notch signaling activity in the endocardium has also been implicated in trabeculation, potentially via its role in regulating expression of the Erbb2

ligand *nrg1* (Samsa et al., 2015), as has been suggested in mice (Grego-Bessa et al., 2007). Wwtr1, a Hippo pathway effector that localizes to the nucleus in response to function, is an essential regulator of the compact wall architecture supporting trabeculation, where it can also influence myocardial Notch signaling (Lai et al., 2018). Furthermore, Erbb2 signaling can direct Wwtr1 localization (Lai et al., 2018) and Notch signaling in the myocardium (Jimenez-Amilburu et al., 2016). Finally, cardiac function, Erbb2, Wwtr1, and Notch have all independently been shown to be important for the relocalization of N-cadherin in delaminating cardiomyocytes (Cherian et al., 2016; Han et al., 2016; Lai et al., 2018). Collectively, these data signify complex spatiotemporal interactions between cardiac function and the Erbb2, Notch, and Hippo signaling pathways during the modulation of trabeculation. Ongoing studies will continue to illuminate the precise nature of these interactions, while also deciphering how these pathways instruct cell behaviors as trabeculae form.

1.6 The cardiac outflow tract: a valuable model to study functional influences on cardiovascular morphogenesis

In previous sections, we emphasized the many ways in which cardiac function influences morphogenesis in the heart. Given that several of these processes are spatiotemporally correlated, these findings provoke an intriguing model where cardiac function synchronizes development of many tissue types, including the endocardium, the endothelium and the myocardium, to construct a continuous cardiovascular system. However, we have little insight into how multiple functional influences trigger diverse cellular behaviors to build a composite organ. The cardiac outflow tract (OFT), a tubular

portal that lies at the junction of the heart and the vessels, is an interesting model for investigation of this topic. Importantly, the OFT is built in the context of active blood flow and contractility, suggesting a potential involvement of function in guiding the earliest phases of its morphogenesis. In the following sections, we present our current understanding of OFT development, highlight critical gaps in our knowledge, and demonstrate the significance of illuminating the mechanical regulation of OFT construction.

1.7 Outflow tract development: an overview

Vertebrate heart development takes place in two phases: in the first phase, “first heart field” (FHF) progenitors in the anterior lateral plate mesoderm (ALPM) differentiate and fuse to form the early heart tube. Following this, “second heart field” (SHF) progenitors differentiate and accrete onto both poles of linear heart tube, giving rise to much of the atrium, the right ventricle and the OFT (Kelly, 2012). The OFT is a particularly important SHF-derived structure: misregulation of its development is known to occur in 30% of the cases of congenital heart diseases, highlighting the importance of understanding this process in cellular and molecular detail (Neeb et al., 2013). Moreover, since the OFT acts as a pivotal conduit for blood flow between the heart and the periphery, its appropriate dimensions are critical for its function. Despite its importance, however, the cellular underpinnings of OFT shape remain largely mysterious.

To begin understanding the cellular mechanisms that construct the OFT, we must first revisit the cellular origins of the OFT. Much is known about the location of

OFT myocardial precursors at various stages of development (Fig. 1-6). Fate-mapping studies in zebrafish suggest that in the early blastula, OFT progenitors are located dorsal to ventricular progenitors, which are clustered close to the embryonic margin (Hami et al., 2011). Subsequently, cardiac progenitors exist in bilateral populations in the ALPM. At this time, OFT progenitors are located medial to ventricular and atrial progenitors (Hami et al., 2011), where they express the SHF-progenitor marker *mef2cb* (Lazic & Scott, 2011) and the cardiac progenitor marker *nkx2.5* (Guner-Ataman et al., 2013). Live imaging in zebrafish has shown that cardiac progenitors within the ALPM continuously differentiate within an epithelial sheath that converges at the embryonic midline (Felker et al., 2018) (Figure 1-7): in this way, the medio-lateral placement of OFT, ventricular and atrial cells in the ALPM appears to translate into antero-posterior positions within the heart tube. Moreover, studies in chick and mice suggest that, prior to appending to the heart, SHF progenitors are found in the dorsal pericardial wall (DPW), from where they are deployed to the arterial pole of the heart tube (Ramsbottom et al., 2014; van den Berg et al., 2009).

In mice, SHF cells in the DPW are further subdivided into an anterior population, which gives rise to the OFT, and a posterior population that is thought to contribute to the venous pole (Kelly, 2012; Vincent & Buckingham, 2010). While such a distinction has not been classified in zebrafish, SHF progenitors generating the outflow tract and inflow tract regions can be distinguished based on the timing of differentiation and requirement of Fgf signaling and Isl1, respectively (de Pater et al., 2009). At the arterial pole, SHF progenitors are identifiable with markers like *ltbp3* and *mef2cb* (Lazic & Scott, 2011; Zhou et al., 2011). Additionally, a transgenic reporter driven by the *cis*-regulatory

elements of the *draculin* gene was recently found to specifically mark FHF-derived cells, and hence can be used to distinguish between FHF- and SHF- derived cells in zebrafish (Mosimann et al., 2015). It is important to note, however, that since the SHF also appends to the distal portion of the ventricle, none of these markers are specific to the OFT myocardium.

While we have many clues to the location of OFT myocardial precursors, less attention has been paid to the origins of the OFT endocardium. Studies in zebrafish have suggested that endocardial progenitors lie in the lateral marginal zone of the blastula, in the same region as, and intermingled with, myocardial progenitors (Keegan et al., 2004). In the ALPM, endocardial progenitors are thought to lie rostral to myocardial progenitors (Schoenebeck et al., 2007). The migration of endocardial cells towards the midline is spatiotemporally coordinated with that of the myocardium, such that within the heart tube, myocardial cells are encasing endocardial cells. Interestingly, endocardial cells are thought to be developmentally related to both the myocardial lineage as well as the endothelial lineage. Several studies in zebrafish and chick suggest a common precursor for the myocardium and endocardium: markers like Mesp1 and Flk1 are expressed in both myocardial and endocardial cells (Devine et al., 2014; Misfeldt et al., 2009). Furthermore, in the ALPM of zebrafish *cloche* mutants, which lack an endocardium, the expression of the myocardial progenitor marker *hand2* is expanded rostrally (Schoenebeck et al., 2007). The endocardium is also thought to be a subset of the endothelium: known endothelial markers, including *flk1* and *etv2*, are expressed in the endocardium as well (Bussmann et al., 2007; Schoenebeck et al., 2007); moreover, although no markers specific to non-endocardial endothelium have

been discovered, an endocardium-only maker, NFATc1, does exist (de la Pompa et al., 1998). Interestingly, genes like *tie2* in mice and *cloche* in zebrafish are absolutely essential for endocardial development but appear to be dispensable for vascular development (Puri et al., 1999; Stainier et al., 1995), which reaffirms the idea that the endocardium is a specialized endothelium.

With respect to the OFT endocardium in particular, however, not much is understood. After heartbeat initiates, the endocardium expresses genes like *klf2a*, *notch1b* and *wnt9b*, all of which progressively concentrate in the OFT and atrioventricular canal endocardium (Goddard et al., 2017; Vermot et al., 2009). Eventually, endocardial cells in these two regions develop valves, which are flaps that prevent backflow of blood. Therefore, although the OFT endocardium eventually exhibits specialized characteristics, we do not know if and how the early OFT endocardium is molecularly different from the ventricular endocardium and the vascular endothelium. Notably, SHF-derived cells and neural crest cells are known to contribute to the OFT endocardium at later stages (Cavanaugh et al., 2015; Lazic & Scott, 2011; Zhou et al., 2011); however, in zebrafish, this does not happen during the initial stages of OFT formation.

What is known about the signaling pathways guiding OFT development? Canonical Wnt signaling has been shown to act upstream of other signaling pathways like Fgf to positively regulate SHF proliferation in mice (Li et al., 2007; Cohen et al., 2007). Recently, studies in our lab compared microarray profiles of zebrafish embryos treated with the Fgf inhibitor SU5402 to untreated embryos, and discovered that the cell adhesion molecule *cadm4* acts downstream of Fgf signaling to restrict SHF proliferation

as well as the timing of their differentiation to the arterial pole; consequently, *cadm4* morphants exhibit a highly elongated OFT (Zeng & Yelon, 2014). Bmp signaling is also thought to promote differentiation of SHF cells in mice via multiple targets including *Tbx3*, *Tbx20* and *Isl1* (Yang et al., 2006). Further, the non-canonical Wnt pathway is thought to be involved in SHF accretion by regulating the formation of a cohesive epithelial sheet of SHF progenitors prior to their deployment to the arterial pole (Sinha et al., 2015). Finally, the AP-1 transcription factor Fosl2 has been implicated in regulating the timing of SHF differentiation (Jahangiri et al., 2016).

As SHF cells deploy to the arterial pole, they must organize into a cylindrical structure of appropriate dimensions. While not much is known about this particular phase of OFT morphogenesis, recent live imaging analysis in zebrafish has emphasized the emerging endocardium as a platform for myocardial assembly (Felker et al., 2018). In this dissertation, we will progressively unravel the cellular and molecular mechanisms governing early endocardial morphogenesis in the OFT, with the hope of elucidating the cellular, molecular and mechanical underpinnings of OFT shape.

1.8 Cardiac outflow tract morphogenesis and anomalies

While not much is understood about early OFT morphogenesis, we have some insights into the cellular characteristics of SHF progenitors prior to their accretion to the arterial pole of the heart, and extensive knowledge of later morphogenetic events like OFT valve development and remodeling. Reviewing this information is crucial for refining our perception of early OFT development.

Epithelial characteristics of SHF progenitors

Recent studies in mice suggest that SHF cells are organized into an apico-basally polarized epithelium in the dorsal pericardial wall (DPW), where the apical side faces the pericardium (Cortes et al., 2018). The epithelial properties of the anterior DPW, which contains OFT progenitors, depend upon Tbx1 function: in the absence of *tbx1*, aDPW cells are rounder, have expanded apical domains, lack basal filopodial extensions, and consequently fail to form a proper OFT (Francou et al., 2014). Further, multiple mutants in which planar cell polarity is disrupted specifically in the SHF, including conditional mutants for *vangl2* and *wnt11*, exhibit a shortened OFT (Ramsbottom et al., 2014; Zhou et al., 2011). Live imaging analysis using a *tbx1*:*eGFP* transgene in zebrafish further shows that the SHF-containing epithelial sheath is continuous with the differentiated ventricular myocardium (Felker et al., 2018) (Figure 1- 7). Work in mice has in fact suggested that this physical interface with differentiating SHF cells exerts epithelial tension on SHF progenitors, which is thought to induce proliferation of SHF progenitors in a YAP/TAZ-dependent fashion (Francou et al., 2017). Finally, cell-cell adhesion also appears to be regulated during SHF development: while expression of the adhesion molecule N-cadherin within the DPW gradually intensifies towards the venous pole, E-cadherin localizes primarily in the anterior DPW, and is maintained in the differentiated OFT myocardium (Francou et al., 2014). Therefore, regulation of multiple cellular characteristics within the SHF, including cell shape, planar cell polarity and adhesion are integral to forming the mature OFT.

OFT remodeling and valve morphogenesis

Later steps in OFT morphogenesis, after the initial formation of the OFT structure, include valve formation, and, in higher vertebrates, OFT remodeling and septation. In four-chambered hearts, aortic and pulmonic valves, jointly called semilunar valves, form at the OFT region (Combs & Yutzey, 2009). Since the zebrafish heart contains a single atrium and ventricle, only a single OFT with one semilunar valve exists.

Semilunar valve development initiates with endocardial cushion formation, which is characterized by endocardial thickening within the OFT. The OFT cushions are derived from both SHF endocardial progenitors and neural crest cells (Wu et al., 2017). Since the cellular and molecular mechanisms underlying OFT and AVC valve development are assumed to be similar, the majority of the studies in multiple model organisms, and especially those in zebrafish, have focused on AVC valve development. In higher vertebrates, endocardial cushion formation begins with the deposition of extracellular matrix between the endocardium and the myocardium. Following this, mesenchymal cells derived from the endocardium proliferate and populate the ECM-rich regions in an epithelial-to-mesenchymal transition (EMT). During zebrafish AVC valve formation, invagination of endocardial cells, and not EMT, appears to drive valve formation, as visualized using high-speed microscopy (Scherz et al., 2008); although we imagine this to be the case for OFT valves in zebrafish, this is yet to be confirmed. Despite these differences, the underlying molecular mechanisms for valve formation appear to be conserved in zebrafish and higher vertebrates (Bakkers, 2011): many signaling pathways, including Bmp, canonical Wnt and Notch

pathways, which have been implicated in regulating EMT and mesenchymal proliferation in higher vertebrates, are also involved in valve development in zebrafish.

Cardiac function is an especially important regulator of valve development. Work in chick has employed a technique called OFT banding, where a suture is tightened around the OFT to constrict its lumen, to reveal multiple influences of hemodynamic stimuli on ECM deposition prior to valve formation (Rennie et al., 2017). This was also recently confirmed in chick OFT explants, where, in addition to defects in ECM components, disturbed flows correlated with disrupted levels of RhoA signaling, TGFβ signaling, and Klf2, and OFT explant morphology also appeared abnormal (Fig. 1-8) (Biechler et al., 2014). As discussed in previous sections, numerous studies in the zebrafish AVC have suggested a pathway where the mechanosensitive channels Trpp2 and Trpv4 regulate *klf*2a expression, which can further mediate *wnt9b* expression for valve formation (Goddard et al., 2017; Heckel et al., 2015). Klf2 is further thought to regulate both cell number, cell shape and fibronectin deposition at the AVC (Steed et al., 2016a; Vermot et al., 2009). Importantly, *klf2a* is also expressed in the OFT endocardium and may play a similar role there (Vermot et al., 2009). Recent work in zebrafish has also implied a function-mediated mechanism involving *notch1b* for OFT valve formation (Hsu et al., 2019). Together, these studies show that function regulates many aspects of valve formation in the OFT and the AVC.

Finally, in higher vertebrates, the left ventricle must acquire an independent OFT, such that the pulmonary outlet is separate from the systemic outlet for blood. To accomplish this, the single OFT undergoes septation and remodeling, where the OFT myocardial wall is thought to rotate in a counter-clockwise direction, in a process that

culminates with the formation of semilunar valves in two distinct outlets. Both cardiac neural crest and SHF cells are thought to contribute to the OFT septum. Notably, the non-canonical Wnt ligand Wnt5a, as well as TGFβ signaling have been implicated in septal morphogenesis as well (Neeb et al., 2013).

Outflow tract anomalies

Congenital heart defects affect approximately 1% of the live births in the United States, 30% of the cases of which include OFT defects. OFT anomalies present as four major defects, many of which occur together (Fig. 1-9) (Neeb et al., 2013). If septation and OFT remodeling proceed normally, separate aortic and pulmonary outlets exit from the right and left ventricles, respectively. In Persistent Truncus Arteriosus (PTA), however, a single OFT exits the right ventricle of the heart. In mouse models where the neural crest population was ablated, the embryos presented with PTA. Multiple mouse mutants confirm the necessity of neural crest cells for proper OFT development: targeted deletions of *acvrl1*, *cdh1* and *ctnnb1* in NC cells that affect migration, differentiation and proliferation, respectively, resulted in PTA (Kaartinen et al., 2004; Kioussi et al., 2002). Global deletion of *tbx1* also results in PTA, suggesting an additional necessity of SHF cells in this process (Merscher et al., 2001).

Another type of OFT abnormality is Double Outlet Right Ventricle (DORV). As the name suggests, DORV is characterized by both of the divided outlets arising from the right ventricle. Wnt1-Cre targeted deletion of *hand2* and *msx1*/*2*, which causes failure of neural crest migration and proliferation, respectively, results in DORV (Holler et al., 2010; Ishii et al., 2005). Endocardial cushion formation and myocardial function

also appear to be important for the etiology of DORV (Azhar et al., 2010; Katz et al., 2003).

A third type of OFT anomaly is Transposition of Great Arteries (TGA), where the positioning of the pulmonary and systemic outlets is reversed, such that the pulmonary outlet arises from the left ventricle and the systemic from the right. Majority of TGA cases are associated with defects in left-right patterning; for example, mouse mutants for *acvr2b* and *gdf1* exhibit characteristics of TGA (Oh & Li, 1997; Rankin et al., 2000). Finally, the fourth kind of OFT abnormality is termed Overriding Aorta (OA), where the aortic outlet is mispositioned over the interventricular septal defect instead of the left ventricle. In most mouse models, OA accompanies PTA and DORV as a consequence of defects in the neural crest population (Neeb et al., 2013).

1.9 Shaping the initial OFT: the missing link

Our review of OFT morphogenesis at various phases during its development highlights a significant gap in our understanding: once SHF progenitors differentiate, how do they organize into a cylindrical structure that is later capable of undergoing valve development and remodeling? In this regard, it is important to note that many studies have in fact suggested that problems with initial OFT dimensions could translate into OFT alignment defects at later stages. For example, *raldh2* mutant mice present with a shorter and wider OFT prior to developing PTA (El Robrini et al., 2016). Similarly, in chick, shortening of the OFT following neural crest ablation leads to PTA and other OFT misalignments (Yelbuz et al., 2002). Therefore, while it is evident that the OFT must attain its proper morphology for its physiological function, the cellular and

molecular mechanisms underlying the stereotypical initial dimensions of the OFT remain unclear. In the following chapter, we begin to address this gap by characterizing the cellular behaviors governing OFT shape in zebrafish.

Since the OFT is formed in the context of active blood flow and contractility, biomechanical forces associated with function could be influencing the earliest steps of OFT development, in addition to their described roles in later steps of cushion formation and valve development. Interestingly, flow-responsive genes like *klf2a* and *notch1b* are expressed in the OFT endocardium at relatively early stages (Vermot et al., 2009) (Figure 1-10). Recent studies in mice have in fact indicated that SHF deployment exerts epithelial tension, which promotes SHF proliferation in a YAP/TAZ-dependent fashion (Francou et al., 2017). In zebrafish too, SHF progenitors are connected to beating cardiomyocytes in a continuous epithelium (Felker et al., 2018); this physical interface with contractile cells likely tugs on SHF progenitors as they differentiate. Together, these data imply that the early OFT could be exposed to, as well as sensitive to, multiple functional influences; however, a role for cardiac function in the initial phases of OFT construction has not been evaluated. In the next chapter, we employ genetic manipulations, high-resolution morphometrics and *in vivo* assays of cell behavior to specifically address this open question.

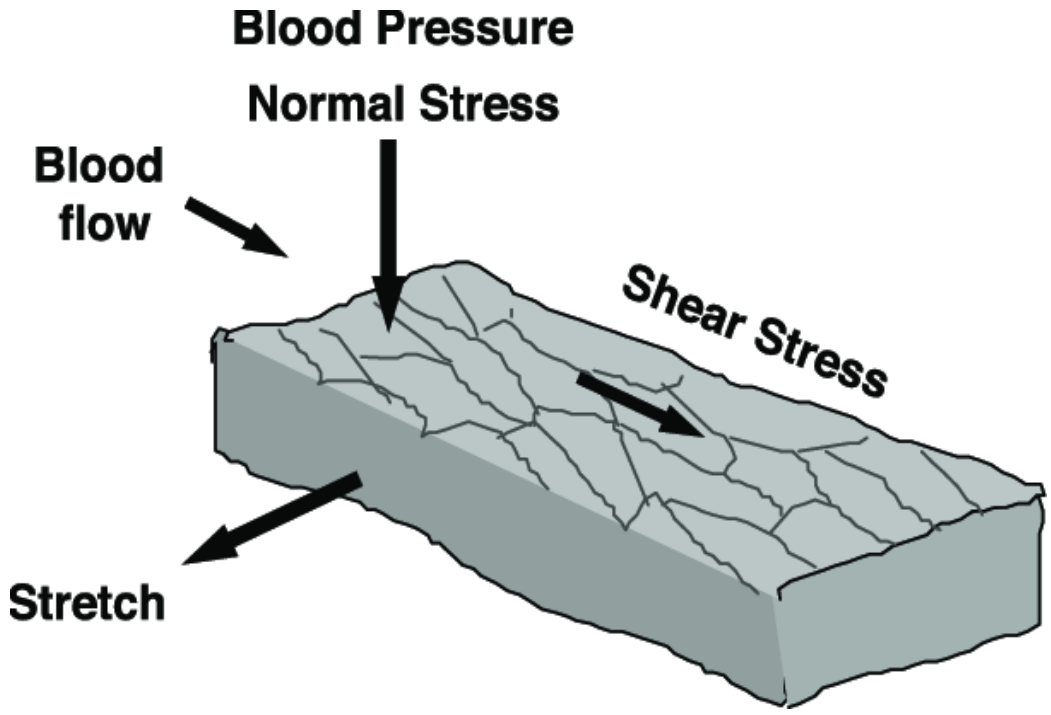

Figure 1-1: Endocardial cells are exposed to multiple distinct forces. Diagram illustrating the many types of forces exerted on the inner, endocardial layer of the heart. While contractility and blood pressure stretch cells in a direction perpendicular to flow, the viscous nature of blood stimulates shearing of cells in a direction parallel to the flow of blood. Figure adapted form Chien, 2007.

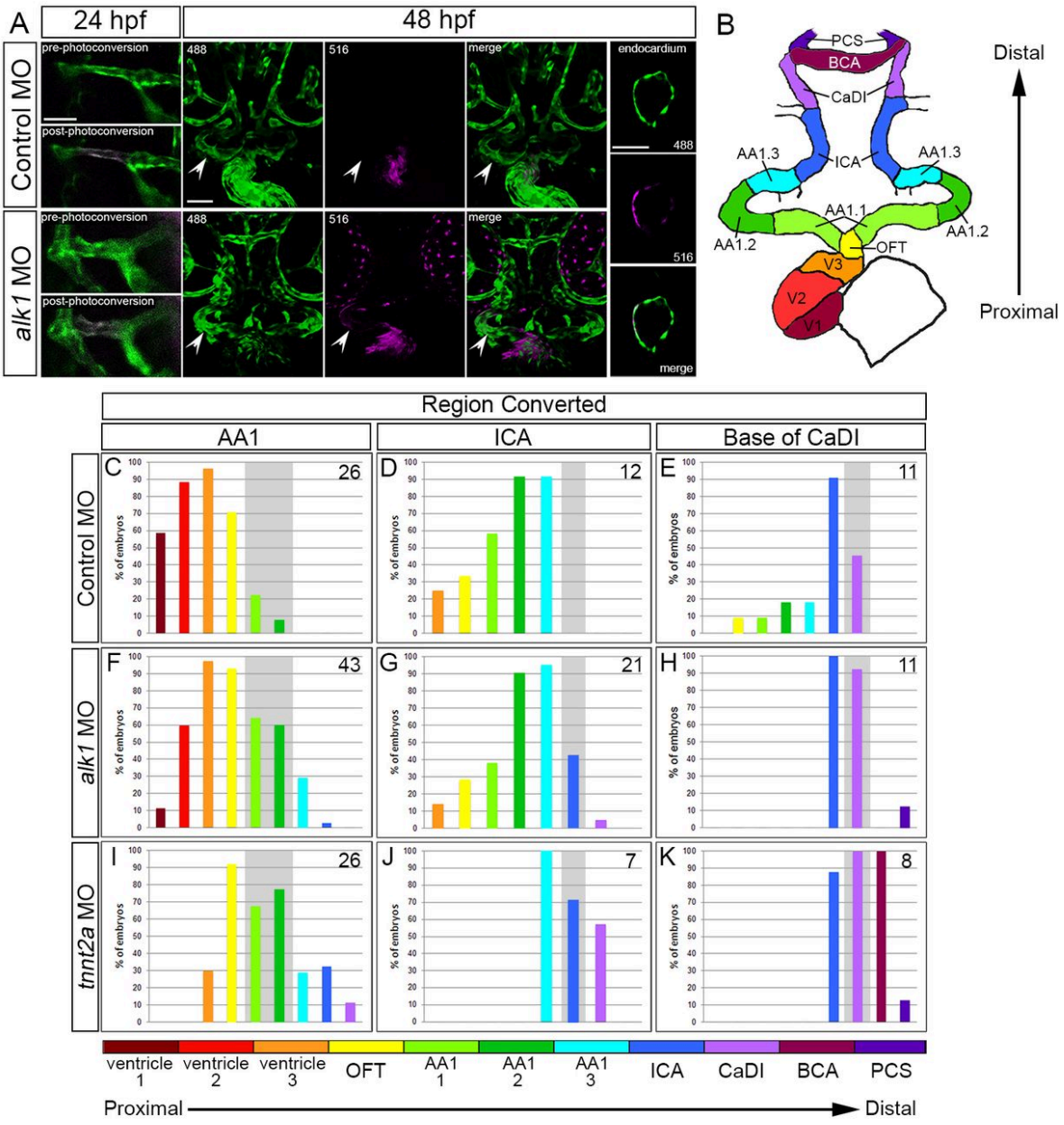

Figure 1-2: Alk1 and cardiac function promote endothelial cell migration against blood flow into the heart. (A-B) At 24 hours-post-fertilization (hpf), various segments of the arterial vasculature, including the aortic arch 1 (AA1), internal carotid artery (ICA) and the caudal division of the internal carotid artery (CaDI) were labeled by photoconversion in control morphants, *alk1* morphants or *tnnt2a* morphants, which lack cardiac function. (C-K) While photoconverted cells were frequently found in the heart by 48 hpf in control morphants (C-E), displacement towards the heart was reduced in both *alk1* morphants (F-H) and *tnnt2a* morphants (I-K). Figure adapted from Rochon et al., 2016.

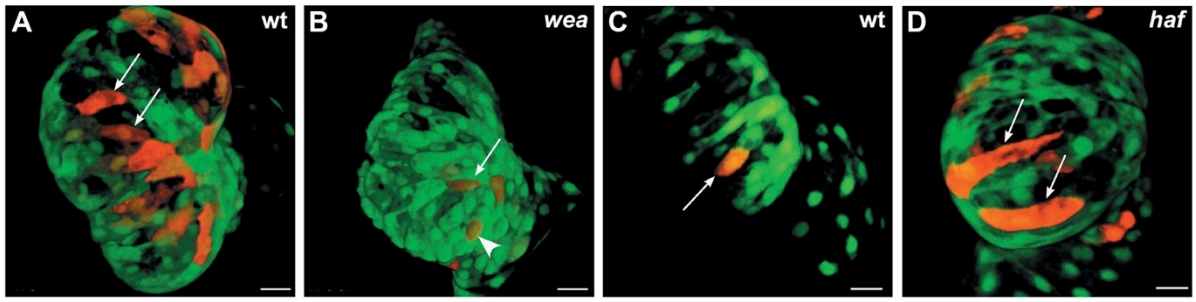

Figure 1-3: Cardiac function modulates cardiomyocyte dimensions in the ventricle. Confocal projections show the ventricle in embryos carrying the transgene *Tg*(*myl7:egfp*), with mosaic expression of *Tg*(*myl7*:*dsRedt4*). (A,C) At 52 hours post-fertilization (hpf), cardiomyocytes in the outer curvature of the ventricle (arrows) have acquired a characteristic size and an elongated morphology. (B) In *weak atrium* (*wea*) mutants, blood flow into the ventricle is reduced, and the cardiomyocytes in the outer curvature are abnormally small (arrow) and circular (arrowhead). (D) In *half-hearted* (*haf*) mutants, the ventricle is non-contractile, and the outer curvature cardiomyocytes are abnormally large and distended (arrows). Images adapted from Auman et al., 2007.

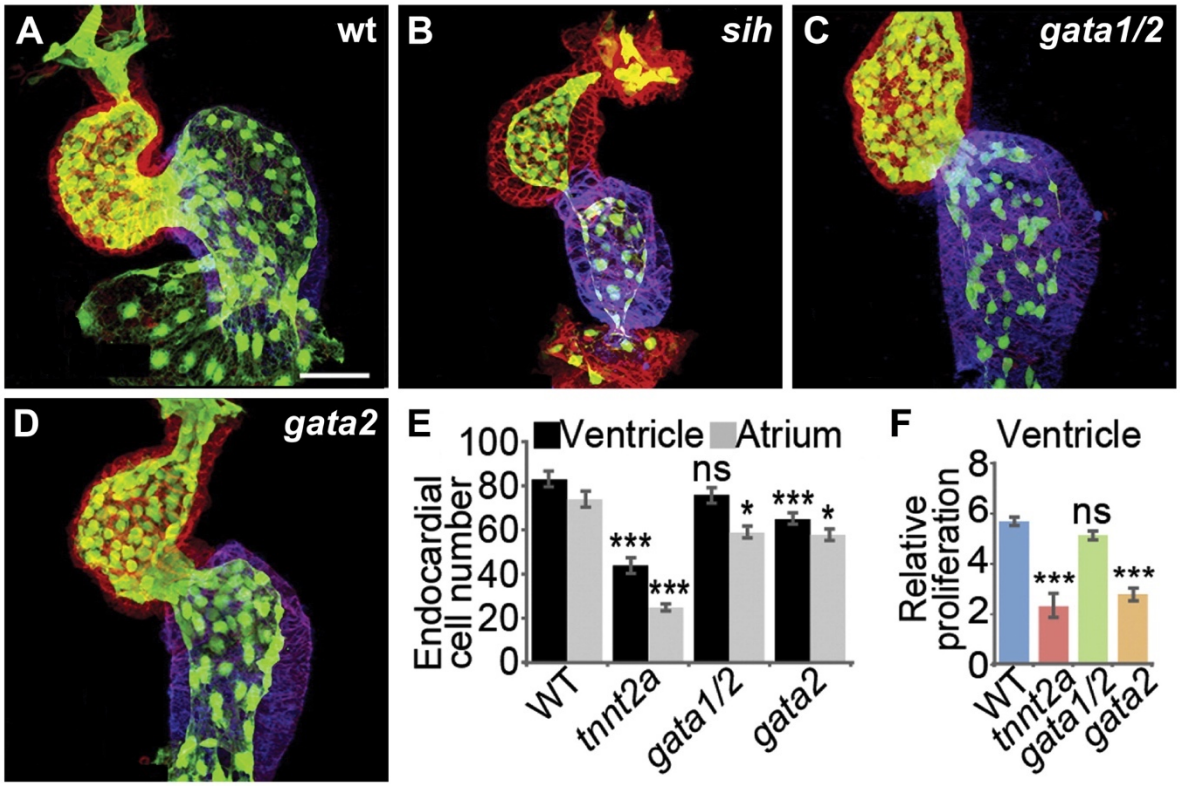

Figure 1-4: Fluid forces influence endocardial cell number during chamber emergence. (A-D) Endocardial cells (green) are indicated by expression of the transgene *Tg*(*kdrl:GFP*); localization of Amhc (blue) and actin (red) are also shown. Whereas wild-type embryos have ~80 and ~70 endocardial cells in the ventricle and the atrium, respectively (A,E), the number of endocardial cells in both chambers is significantly reduced in *silent heart* (*sih; tnnt2a*) mutants (B,E), in which the heart is noncontractile. *gata1/2* morphants, which have diminished shear forces due to their reduced hematocrit, display fewer endocardial cells in the atrium (C,E). In contrast, *gata2* morphants, which have been shown to have reduced retrograde flow in addition to diminished shear forces, display fewer endocardial cells in both chambers (D,E), similar to *sih* mutants. (F) Consistent with this, endocardial proliferation in the ventricle is significantly reduced in *sih* mutants and *gata2* morphants, but not in *gata1*/*2* morphants. Images adapted from Dietrich et al., 2014.

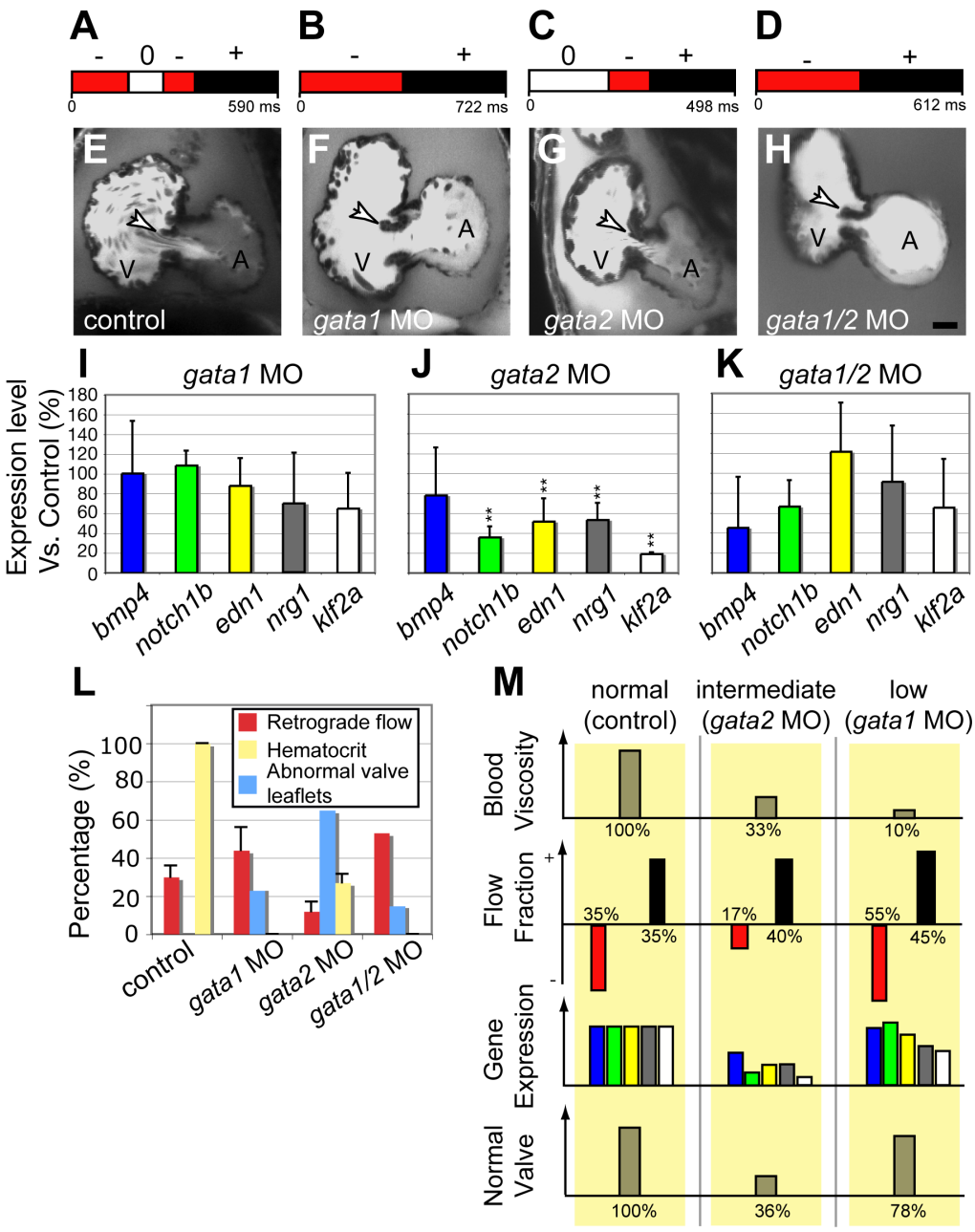

Figure 1-5: Reversing flows drive distinct expression profiles for valve development in the atrioventricular canal. (A-H) Flow patterns of control (A), *gata1* morphants (B), *gata2* morphants (C) and *gata1/2* morphants (D) show that reversing flows (red) are reduced in *gata2* morphants and increased in *gata1* and *gata1/2* morphants. (I-K) These patterns of retrograde flows correspond with expression of mechanotransducive genes like *klf2a* and *notch1b*, which are reduced in gata2 morphants but not affected significantly in *gata1* or *gata1/2* morphants. (L-M) Despite reduced hematocrit levels in *gata1* morphants, they develop normal valves. However, *gata2* morphants fail to develop valves, suggesting that valve development is associated with reversing flows and not shear forces from blood. Figure adapted from Vermot et al., 2009.

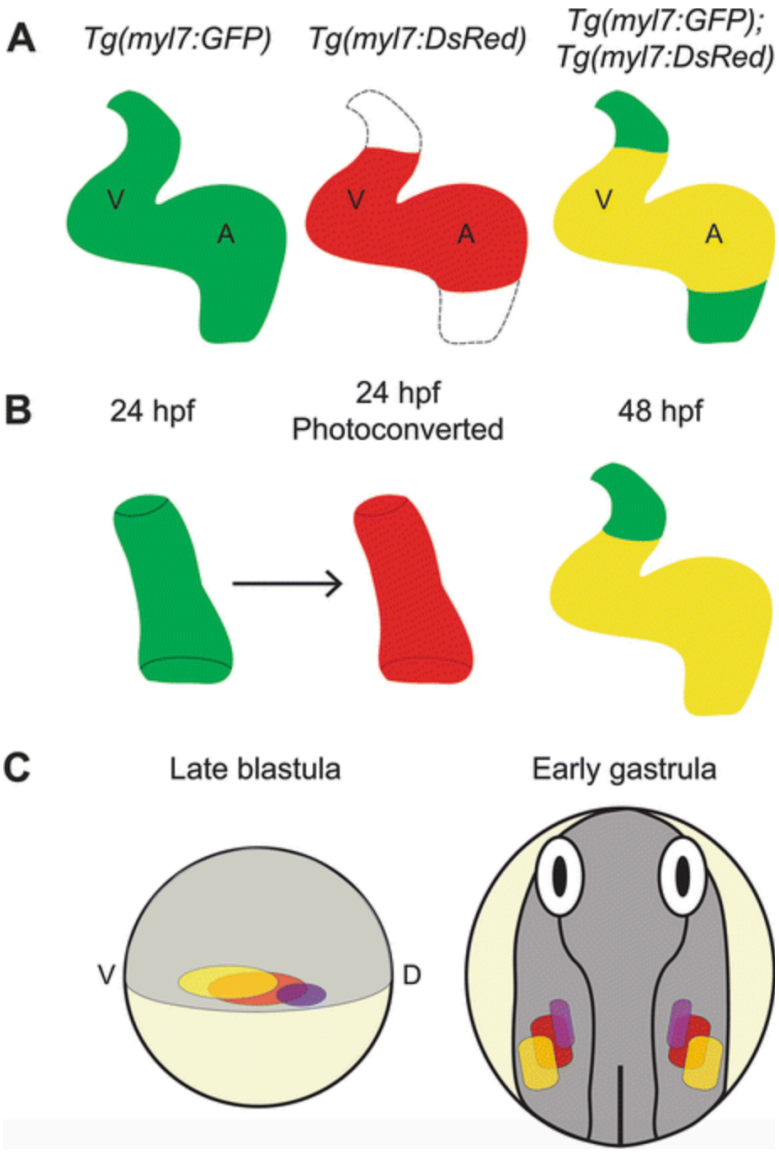

Figure 1-6: Outflow tract myocardial cells are derived from late-differentiating second heart field progenitors. (A-B) In zebrafish, multiple assays confirm that the OFT is derived from late-differentiating cells. Leveraging the slower maturation dynamics of RFP compared to GFP, late-differentiating myocardial cells can be distinguished as "green-only" cells in *Tg(myl7:GFP); Tg(myl7:dsRed)* embryos at 48 hpf. An alternative assay to visualize late-differentiating cells exploits photoconversion labeling techniques, where the entire heart is photoconverted from green to red fluorescence at 24 hpf, and unphotoconverted "green-only" cells are found in the OFT by 48 hpf. (C) OFT progenitors, marked in purple, are found dorsal to ventricular (red) and atrial (yellow) progenitors in the late blastula embryo. At early gastrula stages, when cardiac progenitors are within bilateral fields in the anterior lateral plate mesoderm, OFT progenitors are medial to ventricular progenitors. Reproduced from Knight and Yelon, 2016.

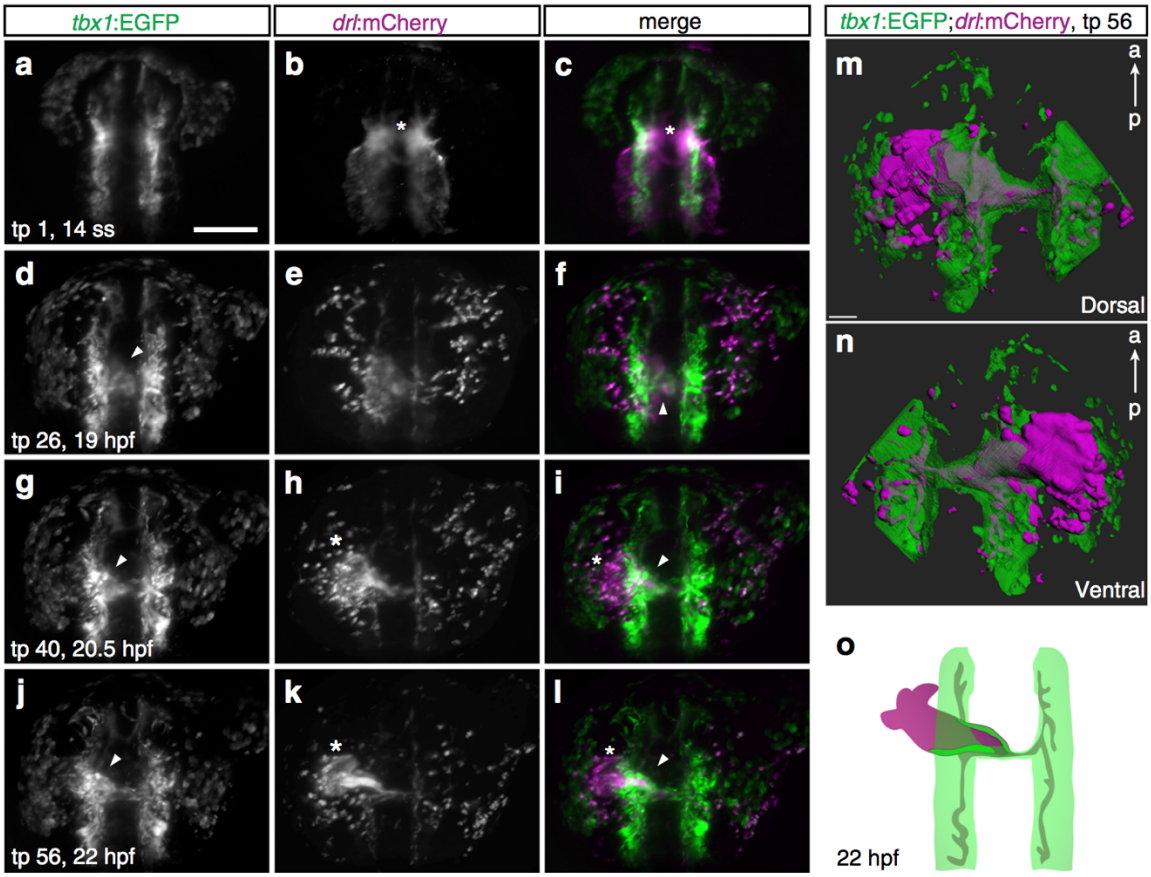

Figure 1-7: Second heart field cells constitute a continuously differentiating epithelial sheath. Stills from live movies collected from 14 somites to 22 hpf using high-speed SPIM imaging of embryos marked with *Tg*(*tbx1*:*EGFP*), which labels cardiac precursors, and *Tg*(*drl*:*mCherry*), which marks first heart field-derived cells. At 14 somites, Tbx1+ cells are present as bilateral populations in the anterior lateral plate mesoderm. By 22 hpf, these cells are differentiating in a continuous epithelium emanating from the bilateral populations towards the linear heart tube, as can be seen from surface representations in M-O. Images adapted from Felker et al., 2019.

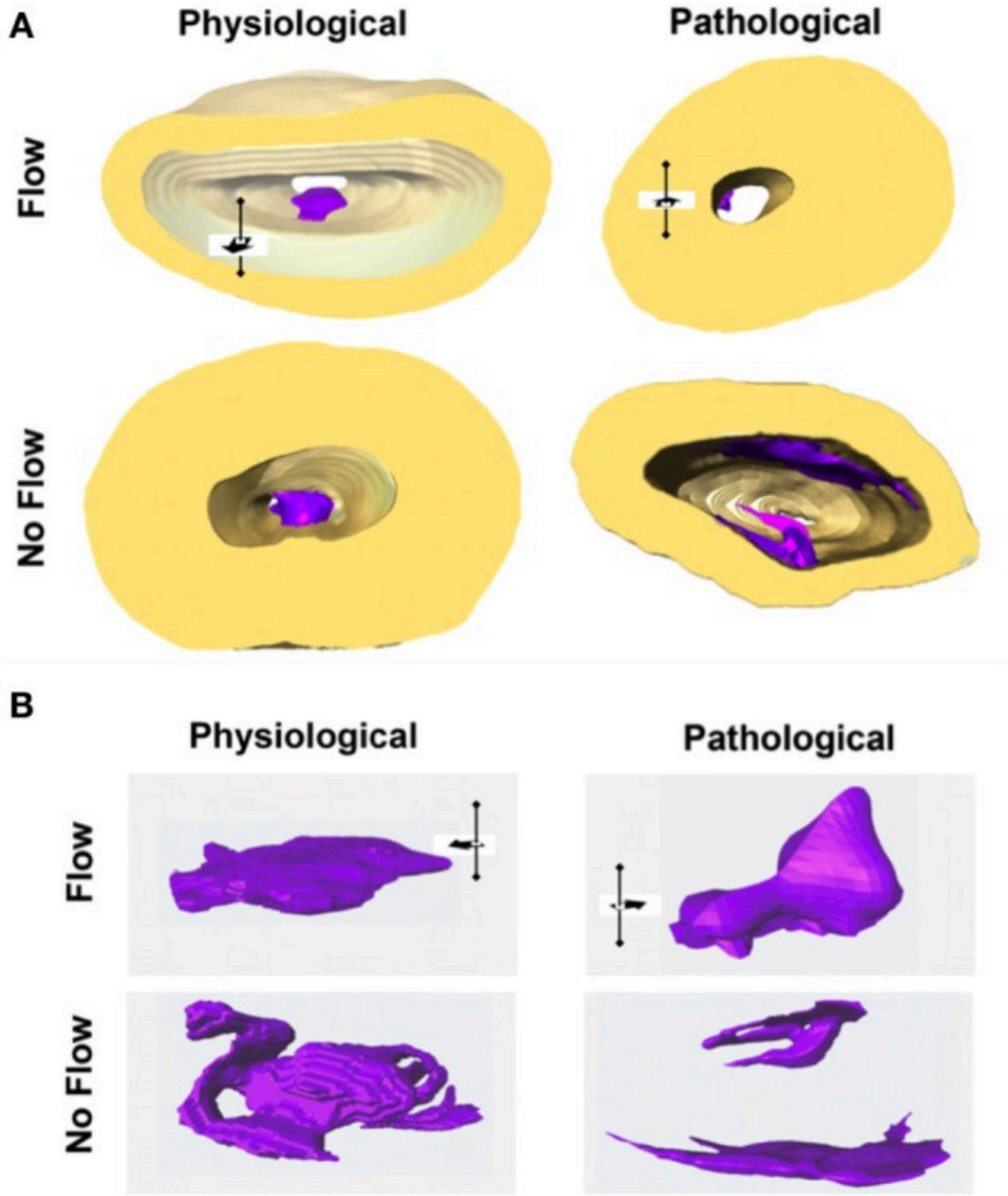

Figure 1-8: Flow regulates outflow tract explant morphology. Chick OFT explants with explant tissue marked in purple and scaffold marked in gold shows that in physiological flow conditions, explants form a mound-like morphology. However, in pathological flow conditions, they retain a leaflet morphology. Finally, in low flow conditions, the explants appear as a loose network that protrudes into the lumen. Reproduced from Biechler et al., 2014.

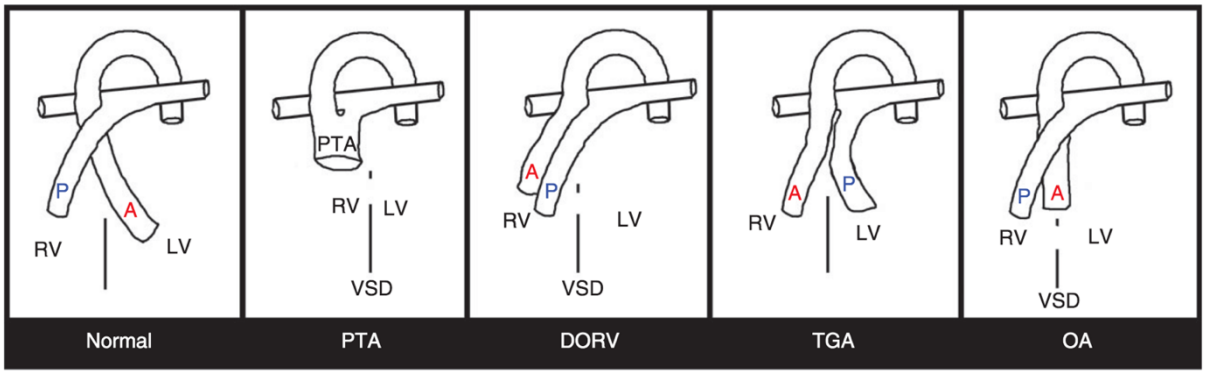

Figure 1-9: Anomalies of the cardiac outflow tract. In normal conditions, the pulmonary outlet arises from the right ventricle, while the systemic or aortic outlet emerges from the left ventricle. In Persistent Truncus Arteriosus (PTA), a single outlet arises from the right ventricle. In contrast, in Double Outlet Right Ventricle (DORV), both outlets are attached to the right ventricle. Patients with Transposition of Great Arteries (TGA) have the wrong connections, whereas in those with Overriding Aorta (OA), the aortic outlet is mispositioned over the Ventricular Septal Defect (VSD), marked with dotted lines. Reproduced from Neeb et al., 2013.

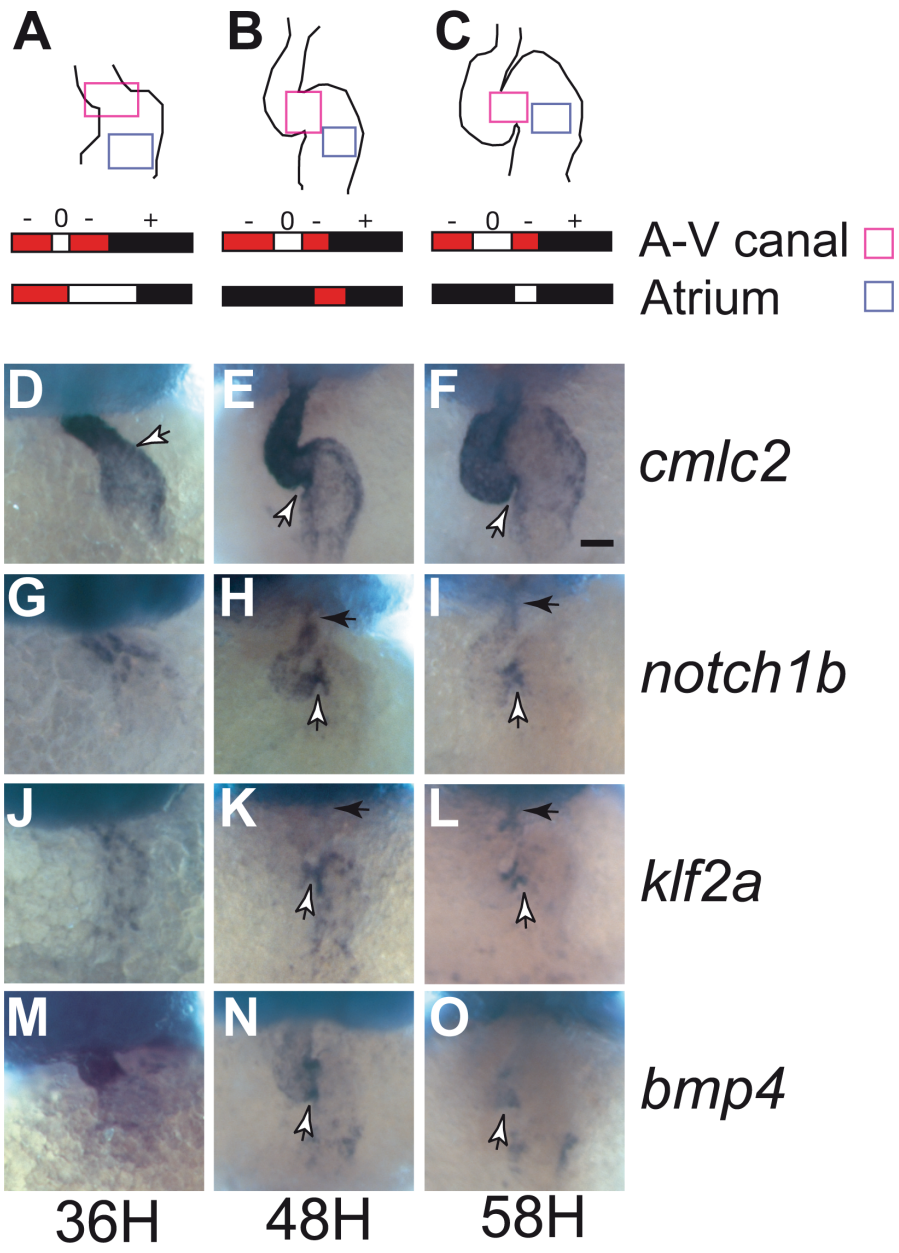

Figure 1-10: Multiple mechanoresponsive genes are expressed in the outflow tract as early as 36 hpf. (A-C) Diagrams showing retrograde flow patterns in the atrioventricular canal (AVC) and atrium over development. As retrograde flows in the AVC increase, mechanoresponsive genes such as *notch1b* and *klf2a* progressively concentrate in the AVC endocardium (white arrow) and outflow tract endocardium (black arrow). Figure adapted from Vermot et al., 2009.

References

Auman, H.J., Coleman, H., Riley, H.E., Olale, F., Tsai, H.J., Yelon, D. (2007). Functional Modulation of Cardiac Form through Regionally Confined Cell Shape Changes. *PLoS Biol*, *5*, e53.

Azhar, M., Wang, P.Y., Frugier, T., Koishi, K., Deng, C., Noakes, P.G., McLennan, I.S. (2010). Myocardial Deletion of Smad4 Using a Novel Alpha Skeletal Muscle Actin Cre Recombinase Transgenic Mouse Causes Misalignment of the Cardiac Outflow Tract. *Int J Biol Sci*, *6*, 546-555.

Bakkers, J. (2011). Zebrafish as a Model to Study Cardiac Development and Human Cardiac Disease. *Cardiovasc Res*, *91*, 279-288.

Banjo, T., Grajcarek, J., Yoshino, D., Osada, H., Miyasaka, K.Y., Kida, Y.S., Ueki, Y., Nagayama, K., Kawakami, K., Matsumoto, T., Sato, M., Ogura, T. (2013).

Haemodynamically Dependent Valvulogenesis of Zebrafish Heart Is Mediated by Flow-Dependent Expression of Mir-21. *Nat Commun*, *4*, 1978.

Baratchi, S., Khoshmanesh, K., Woodman, O.L., Potocnik, S., Peter, K., McIntyre, P. (2017). Molecular Sensors of Blood Flow in Endothelial Cells. *Trends Mol Med*, *23*, 850-868.

Bartman, T., Walsh, E.C., Wen, K.K., McKane, M., Ren, J., Alexander, J., Rubenstein, P.A., Stainier, D.Y. (2004). Early Myocardial Function Affects Endocardial Cushion Development in Zebrafish. *PLoS Biol*, *2*, E129.

Behrndt, M., Salbreux, G., Campinho, P., Hauschild, R., Oswald, F., Roensch, J., Grill, S.W., Heisenberg, C.P. (2012). Forces Driving Epithelial Spreading in Zebrafish Gastrulation. *Science*, *338*, 257-260.

Beis, D., Bartman, T., Jin, S.W., Scott, I.C., D'Amico, L.A., Ober, E.A., Verkade, H., Frantsve, J., Field, H.A., Wehman, A., Baier, H., Tallafuss, A., Bally-Cuif, L., Chen, J.N., Stainier, D.Y., Jungblut, B. (2005). Genetic and Cellular Analyses of Zebrafish Atrioventricular Cushion and Valve Development. *Development*, *132*, 4193-4204.

Biechler, S.V., Junor, L., Evans, A.N., Eberth, J.F., Price, R.L., Potts, J.D., Yost, M.J., Goodwin, R.L. (2014). The Impact of Flow-Induced Forces on the Morphogenesis of the Outflow Tract. *Front Physiol*, *5*, 225.

Boselli, F., Steed, E., Freund, J.B., Vermot, J. (2017). Anisotropic Shear Stress Patterns Predict the Orientation of Convergent Tissue Movements in the Embryonic Heart. *Development*, *144*, 4322-4327.

Broekhuizen, M.L., Hogers, B., DeRuiter, M.C., Poelmann, R.E., Gittenberger-de Groot, A.C., Wladimiroff, J.W. (1999). Altered Hemodynamics in Chick Embryos after Extraembryonic Venous Obstruction. *Ultrasound Obstet Gynecol*, *13*, 437-445.

Bussmann, J., Bakkers, J., Schulte-Merker, S. (2007). Early Endocardial Morphogenesis Requires Scl/Tal1. *PLoS Genet*, *3*, e140.

Cavanaugh, A.M., Huang, J., Chen, J.N. (2015). Two Developmentally Distinct Populations of Neural Crest Cells Contribute to the Zebrafish Heart. *Dev Biol*, *404*, 103-112.

Chen, Q., Jiang, L., Li, C., Hu, D., Bu, J.W., Cai, D., Du, J.L. (2012). Haemodynamics-Driven Developmental Pruning of Brain Vasculature in Zebrafish. *PLoS Biol*, *10*, e1001374.

Cherian, A.V., Fukuda, R., Augustine, S.M., Maischein, H.M., Stainier, D.Y. (2016). N-Cadherin Relocalization During Cardiac Trabeculation. *Proc Natl Acad Sci U S A*, *113*, 7569-7574.

Cohen, E.D., Wang, Z., Lepore, J.J., Lu, M.M., Taketo, M.M., Epstein, D.J., Morrisey, E.E. (2007). Wnt/Beta-Catenin Signaling Promotes Expansion of Isl-1-Positive Cardiac Progenitor Cells through Regulation of Fgf Signaling. *J Clin Invest*, *117*, 1794-1804.

Collins, M.M., Stainier, D.Y. (2016). Organ Function as a Modulator of Organ Formation: Lessons from Zebrafish. *Curr Top Dev Biol*, *117*, 417-433.

Combs, M.D., Yutzey, K.E. (2009). Heart Valve Development: Regulatory Networks in Development and Disease. *Circ Res*, *105*, 408-421.

Cortes, C., Francou, A., De Bono, C., Kelly, R.G. (2018). Epithelial Properties of the Second Heart Field. *Circ Res*, *122*, 142-154.

Corti, P., Young, S., Chen, C.Y., Patrick, M.J., Rochon, E.R., Pekkan, K., Roman, B.L. (2011). Interaction between Alk1 and Blood Flow in the Development of Arteriovenous Malformations. *Development*, *138*, 1573-1582.

de la Pompa, J.L., Timmerman, L.A., Takimoto, H., Yoshida, H., Elia, A.J., Samper, E., Potter, J., Wakeham, A., Marengere, L., Langille, B.L., Crabtree, G.R., Mak, T.W. (1998). Role of the Nf-Atc Transcription Factor in Morphogenesis of Cardiac Valves and Septum. *Nature*, *392*, 182-186.

de Pater, E., Clijsters, L., Marques, S.R., Lin, Y.F., Garavito-Aguilar, Z.V., Yelon, D., Bakkers, J. (2009). Distinct Phases of Cardiomyocyte Differentiation Regulate Growth of the Zebrafish Heart. *Development*, *136*, 1633-1641.

Deacon, D.C., Nevis, K.R., Cashman, T.J., Zhou, Y., Zhao, L., Washko, D., Guner-Ataman, B., Burns, C.G., Burns, C.E. (2010). The Mir-143-Adducin3 Pathway Is Essential for Cardiac Chamber Morphogenesis. *Development*, *137*, 1887-1896.

Dekker, R.J., van Soest, S., Fontijn, R.D., Salamanca, S., de Groot, P.G., VanBavel, E., Pannekoek, H., Horrevoets, A.J. (2002). Prolonged Fluid Shear Stress Induces a Distinct Set of Endothelial Cell Genes, Most Specifically Lung Kruppel-Like Factor (Klf2). *Blood*, *100*, 1689-1698.

Devine, W.P., Wythe, J.D., George, M., Koshiba-Takeuchi, K., Bruneau, B.G. (2014). Early Patterning and Specification of Cardiac Progenitors in Gastrulating Mesoderm. *Elife*, *3*.

Diaz de la Loza, M.C., Thompson, B.J. (2017). Forces Shaping the Drosophila Wing. *Mech Dev*, *144*, 23-32.

Dietrich, A.C., Lombardo, V.A., Veerkamp, J., Priller, F., Abdelilah-Seyfried, S. (2014). Blood Flow and Bmp Signaling Control Endocardial Chamber Morphogenesis. *Dev Cell*, *30*, 367-377.

Donat, S., Lourenco, M., Paolini, A., Otten, C., Renz, M., Abdelilah-Seyfried, S. (2018). Heg1 and Ccm1/2 Proteins Control Endocardial Mechanosensitivity During Zebrafish Valvulogenesis. *Elife*, *7*.

El Robrini, N., Etchevers, H.C., Ryckebusch, L., Faure, E., Eudes, N., Niederreither, K., Zaffran, S., Bertrand, N. (2016). Cardiac Outflow Morphogenesis Depends on Effects of Retinoic Acid Signaling on Multiple Cell Lineages. *Dev Dyn*, *245*, 388-401.

Felker, A., Prummel, K.D., Merks, A.M., Mickoleit, M., Brombacher, E.C., Huisken, J., Panakova, D., Mosimann, C. (2018). Continuous Addition of Progenitors Forms the Cardiac Ventricle in Zebrafish. *Nat Commun*, *9*, 2001.

Franco, C.A., Jones, M.L., Bernabeu, M.O., Geudens, I., Mathivet, T., Rosa, A., Lopes, F.M., Lima, A.P., Ragab, A., Collins, R.T., Phng, L.K., Coveney, P.V., Gerhardt, H. (2015). Correction: Dynamic Endothelial Cell Rearrangements Drive Developmental Vessel Regression. *PLoS Biol*, *13*, e1002163.

Francou, A., De Bono, C., Kelly, R.G. (2017). Epithelial Tension in the Second Heart Field Promotes Mouse Heart Tube Elongation. *Nat Commun*, *8*, 14770.

Francou, A., Saint-Michel, E., Mesbah, K., Kelly, R.G. (2014). Tbx1 Regulates Epithelial Polarity and Dynamic Basal Filopodia in the Second Heart Field. *Development*, *141*, 4320-4331.

Freund, J.B., Goetz, J.G., Hill, K.L., Vermot, J. (2012). Fluid Flows and Forces in Development: Functions, Features and Biophysical Principles. *Development*, *139*, 1229-1245.

Goddard, L.M., Duchemin, A.L., Ramalingan, H., Wu, B., Chen, M., Bamezai, S., Yang, J., Li, L., Morley, M.P., Wang, T., Scherrer-Crosbie, M., Frank, D.B., Engleka, K.A., Jameson, S.C., Morrisey, E.E., Carroll, T.J., Zhou, B., Vermot, J., Kahn, M.L. (2017). Hemodynamic Forces Sculpt Developing Heart Valves through a Klf2-Wnt9b Paracrine Signaling Axis. *Dev Cell*, *43*, 274-289 e275.

Goetz, J.G., Steed, E., Ferreira, R.R., Roth, S., Ramspacher, C., Boselli, F., Charvin, G., Liebling, M., Wyart, C., Schwab, Y., Vermot, J. (2014). Endothelial Cilia Mediate Low Flow Sensing During Zebrafish Vascular Development. *Cell Rep*, *6*, 799-808.

Grego-Bessa, J., Luna-Zurita, L., del Monte, G., Bolos, V., Melgar, P., Arandilla, A., Garratt, A.N., Zang, H., Mukouyama, Y.S., Chen, H., Shou, W., Ballestar, E., Esteller, M., Rojas, A., Perez-Pomares, J.M., de la Pompa, J.L. (2007). Notch Signaling Is Essential for Ventricular Chamber Development. *Dev Cell*, *12*, 415-429.

Guner-Ataman, B., Paffett-Lugassy, N., Adams, M.S., Nevis, K.R., Jahangiri, L., Obregon, P., Kikuchi, K., Poss, K.D., Burns, C.E., Burns, C.G. (2013). Zebrafish Second Heart Field Development Relies on Progenitor Specification in Anterior Lateral Plate Mesoderm and Nkx2.5 Function. *Development*, *140*, 1353-1363.

Haack, T., Abdelilah-Seyfried, S. (2016). The Force Within: Endocardial Development, Mechanotransduction and Signalling During Cardiac Morphogenesis. *Development*, *143*, 373-386.

Hami, D., Grimes, A.C., Tsai, H.J., Kirby, M.L. (2011). Zebrafish Cardiac Development Requires a Conserved Secondary Heart Field. *Development*, *138*, 2389-2398.

Han, P., Bloomekatz, J., Ren, J., Zhang, R., Grinstein, J.D., Zhao, L., Burns, C.G., Burns, C.E., Anderson, R.M., Chi, N.C. (2016). Coordinating Cardiomyocyte Interactions to Direct Ventricular Chamber Morphogenesis. *Nature*, *534*, 700-704.

Heckel, E., Boselli, F., Roth, S., Krudewig, A., Belting, H.G., Charvin, G., Vermot, J. (2015). Oscillatory Flow Modulates Mechanosensitive Klf2a Expression through Trpv4 and Trpp2 During Heart Valve Development. *Curr Biol*, *25*, 1354-1361.

Helmlinger, G., Geiger, R.V., Schreck, S., Nerem, R.M. (1991). Effects of Pulsatile Flow on Cultured Vascular Endothelial Cell Morphology. *J Biomech Eng*, *113*, 123-131.

Herwig, L., Blum, Y., Krudewig, A., Ellertsdottir, E., Lenard, A., Belting, H.G., Affolter, M. (2011). Distinct Cellular Mechanisms of Blood Vessel Fusion in the Zebrafish Embryo. *Curr Biol*, *21*, 1942-1948.

Holler, K.L., Hendershot, T.J., Troy, S.E., Vincentz, J.W., Firulli, A.B., Howard, M.J. (2010). Targeted Deletion of Hand2 in Cardiac Neural Crest-Derived Cells Influences Cardiac Gene Expression and Outflow Tract Development. *Dev Biol*, *341*, 291-304.

Hove, J.R., Koster, R.W., Forouhar, A.S., Acevedo-Bolton, G., Fraser, S.E., Gharib, M. (2003). Intracardiac Fluid Forces Are an Essential Epigenetic Factor for Embryonic Cardiogenesis. *Nature*, *421*, 172-177.

Hsu, J.J., Vedula, V., Baek, K.I., Chen, C., Chen, J., Chou, M.I., Lam, J., Subhedar, S., Wang, J., Ding, Y., Chang, C.C., Lee, J., Demer, L.L., Tintut, Y., Marsden, A.L., Hsiai, T.K. (2019). Contractile and Hemodynamic Forces Coordinate Notch1b-Mediated Outflow Tract Valve Formation. *JCI Insight*, *5*.

Huang, C., Sheikh, F., Hollander, M., Cai, C., Becker, D., Chu, P.H., Evans, S., Chen, J. (2003). Embryonic Atrial Function Is Essential for Mouse Embryogenesis, Cardiac Morphogenesis and Angiogenesis. *Development*, *130*, 6111-6119.

Ishii, M., Han, J., Yen, H.Y., Sucov, H.M., Chai, Y., Maxson, R.E., Jr. (2005). Combined Deficiencies of Msx1 and Msx2 Cause Impaired Patterning and Survival of the Cranial Neural Crest. *Development*, *132*, 4937-4950.

Jahangiri, L., Sharpe, M., Novikov, N., Gonzalez-Rosa, J.M., Borikova, A., Nevis, K., Paffett-Lugassy, N., Zhao, L., Adams, M., Guner-Ataman, B., Burns, C.E., Burns, C.G. (2016). The Ap-1 Transcription Factor Component Fosl2 Potentiates the Rate of Myocardial Differentiation from the Zebrafish Second Heart Field. *Development*, *143*, 113-122.

Jimenez-Amilburu, V., Rasouli, S.J., Staudt, D.W., Nakajima, H., Chiba, A., Mochizuki, N., Stainier, D.Y.R. (2016). In Vivo Visualization of Cardiomyocyte Apicobasal Polarity Reveals Epithelial to Mesenchymal-Like Transition During Cardiac Trabeculation. *Cell Rep*, *17*, 2687-2699.

Kaartinen, V., Dudas, M., Nagy, A., Sridurongrit, S., Lu, M.M., Epstein, J.A. (2004). Cardiac Outflow Tract Defects in Mice Lacking Alk2 in Neural Crest Cells. *Development*, *131*, 3481-3490.

Kalogirou, S., Malissovas, N., Moro, E., Argenton, F., Stainier, D.Y., Beis, D. (2014). Intracardiac Flow Dynamics Regulate Atrioventricular Valve Morphogenesis. *Cardiovasc Res*, *104*, 49-60.

Katz, S.G., Williams, A., Yang, J., Fujiwara, Y., Tsang, A.P., Epstein, J.A., Orkin, S.H. (2003). Endothelial Lineage-Mediated Loss of the Gata Cofactor Friend of Gata 1 Impairs Cardiac Development. *Proc Natl Acad Sci U S A*, *100*, 14030-14035.

Keegan, B.R., Meyer, D., Yelon, D. (2004). Organization of Cardiac Chamber Progenitors in the Zebrafish Blastula. *Development*, *131*, 3081-3091.

Kelly, R.G. (2012). The Second Heart Field. *Curr Top Dev Biol*, *100*, 33-65.

Kioussi, C., Briata, P., Baek, S.H., Rose, D.W., Hamblet, N.S., Herman, T., Ohgi, K.A., Lin, C., Gleiberman, A., Wang, J., Brault, V., Ruiz-Lozano, P., Nguyen, H.D., Kemler, R., Glass, C.K., Wynshaw-Boris, A., Rosenfeld, M.G. (2002). Identification of a Wnt/Dvl/Beta-Catenin --> Pitx2 Pathway Mediating Cell-Type-Specific Proliferation During Development. *Cell*, *111*, 673-685.

Kochhan, E., Lenard, A., Ellertsdottir, E., Herwig, L., Affolter, M., Belting, H.G., Siekmann, A.F. (2013). Blood Flow Changes Coincide with Cellular Rearrangements During Blood Vessel Pruning in Zebrafish Embryos. *PLoS One*, *8*, e75060.

Kwon, H.B., Wang, S., Helker, C.S., Rasouli, S.J., Maischein, H.M., Offermanns, S., Herzog, W., Stainier, D.Y. (2016). In Vivo Modulation of Endothelial Polarization by Apelin Receptor Signalling. *Nat Commun*, *7*, 11805.

Lai, J.K.H., Collins, M.M., Uribe, V., Jimenez-Amilburu, V., Gunther, S., Maischein, H.M., Stainier, D.Y.R. (2018). The Hippo Pathway Effector Wwtr1 Regulates Cardiac Wall Maturation in Zebrafish. *Development*, *145*.

Lazic, S., Scott, I.C. (2011). Mef2cb Regulates Late Myocardial Cell Addition from a Second Heart Field-Like Population of Progenitors in Zebrafish. *Dev Biol*, *354*, 123-133.

Lee, J., Fei, P., Sevag Packard, R.R., Kang, H., Xu, H., Baek, K.I., Jen, N., Chen, J., Yen, H., Kuo, C.C., Chi, N.C., Ho, C.M., Li, R., Hsiai, T.K. (2016). 4-Dimensional Light-Sheet Microscopy to Elucidate Shear Stress Modulation of Cardiac Trabeculation. *J Clin Invest*, *126*, 3158.

Li, M., Zhao, L., Page-McCaw, P.S., Chen, W. (2016). Zebrafish Genome Engineering Using the Crispr-Cas9 System. *Trends Genet*, *32*, 815-827.

Lin, Y.F., Swinburne, I., Yelon, D. (2012). Multiple Influences of Blood Flow on Cardiomyocyte Hypertrophy in the Embryonic Zebrafish Heart. *Dev Biol*, *362*, 242-253.

Lindsey, S.E., Butcher, J.T., Yalcin, H.C. (2014). Mechanical Regulation of Cardiac Development. *Front Physiol*, *5*, 318.

Liu, J., Bressan, M., Hassel, D., Huisken, J., Staudt, D., Kikuchi, K., Poss, K.D., Mikawa, T., Stainier, D.Y. (2010). A Dual Role for Erbb2 Signaling in Cardiac Trabeculation. *Development*, *137*, 3867-3875.

Merscher, S., Funke, B., Epstein, J.A., Heyer, J., Puech, A., Lu, M.M., Xavier, R.J., Demay, M.B., Russell, R.G., Factor, S., Tokooya, K., Jore, B.S., Lopez, M., Pandita, R.K., Lia, M., Carrion, D., Xu, H., Schorle, H., Kobler, J.B., Scambler, P., Wynshaw-Boris, A., Skoultchi, A.I., Morrow, B.E., Kucherlapati, R. (2001). Tbx1 Is Responsible for Cardiovascular Defects in Velo-Cardio-Facial/Digeorge Syndrome. *Cell*, *104*, 619-629.

Misfeldt, A.M., Boyle, S.C., Tompkins, K.L., Bautch, V.L., Labosky, P.A., Baldwin, H.S. (2009). Endocardial Cells Are a Distinct Endothelial Lineage Derived from Flk1+ Multipotent Cardiovascular Progenitors. *Dev Biol*, *333*, 78-89.

Miyasaka, K.Y., Kida, Y.S., Banjo, T., Ueki, Y., Nagayama, K., Matsumoto, T., Sato, M., Ogura, T. (2011). Heartbeat Regulates Cardiogenesis by Suppressing Retinoic Acid Signaling Via Expression of Mir-143. *Mech Dev*, *128*, 18-28.

Mosimann, C., Panakova, D., Werdich, A.A., Musso, G., Burger, A., Lawson, K.L., Carr, L.A., Nevis, K.R., Sabeh, M.K., Zhou, Y., Davidson, A.J., DiBiase, A., Burns, C.E., Burns, C.G., MacRae, C.A., Zon, L.I. (2015). Chamber Identity Programs Drive Early Functional Partitioning of the Heart. *Nat Commun*, *6*, 8146.

Nakajima, H., Yamamoto, K., Agarwala, S., Terai, K., Fukui, H., Fukuhara, S., Ando, K., Miyazaki, T., Yokota, Y., Schmelzer, E., Belting, H.G., Affolter, M., Lecaudey, V., Mochizuki, N. (2017). Flow-Dependent Endothelial Yap Regulation Contributes to Vessel Maintenance. *Dev Cell*, *40*, 523-536 e526.

Neeb, Z., Lajiness, J.D., Bolanis, E., Conway, S.J. (2013). Cardiac Outflow Tract Anomalies. *Wiley Interdiscip Rev Dev Biol*, *2*, 499-530.

Noris, M., Morigi, M., Donadelli, R., Aiello, S., Foppolo, M., Todeschini, M., Orisio, S., Remuzzi, G., Remuzzi, A. (1995). Nitric Oxide Synthesis by Cultured Endothelial Cells Is Modulated by Flow Conditions. *Circ Res*, *76*, 536-543.

Oh, S.P., Li, E. (1997). The Signaling Pathway Mediated by the Type Iib Activin Receptor Controls Axial Patterning and Lateral Asymmetry in the Mouse. *Genes Dev*, *11*, 1812-1826.

Peshkovsky, C., Totong, R., Yelon, D. (2011). Dependence of Cardiac Trabeculation on Neuregulin Signaling and Blood Flow in Zebrafish. *Dev Dyn*, *240*, 446-456.

Pestel, J., Ramadass, R., Gauvrit, S., Helker, C., Herzog, W., Stainier, D.Y. (2016). Real-Time 3d Visualization of Cellular Rearrangements During Cardiac Valve Formation. *Development*, *143*, 2217-2227.

Puri, M.C., Partanen, J., Rossant, J., Bernstein, A. (1999). Interaction of the Tek and Tie Receptor Tyrosine Kinases During Cardiovascular Development. *Development*, *126*, 4569-4580.

Ramsbottom, S.A., Sharma, V., Rhee, H.J., Eley, L., Phillips, H.M., Rigby, H.F., Dean, C., Chaudhry, B., Henderson, D.J. (2014). Vangl2-Regulated Polarisation of Second Heart Field-Derived Cells Is Required for Outflow Tract Lengthening During Cardiac Development. *PLoS Genet*, *10*, e1004871.

Rankin, C.T., Bunton, T., Lawler, A.M., Lee, S.J. (2000). Regulation of Left-Right Patterning in Mice by Growth/Differentiation Factor-1. *Nat Genet*, *24*, 262-265.

Rasouli, S.J., Stainier, D.Y.R. (2017). Regulation of Cardiomyocyte Behavior in Zebrafish Trabeculation by Neuregulin 2a Signaling. *Nat Commun*, *8*, 15281.

Rennie, M.Y., Stovall, S., Carson, J.P., Danilchik, M., Thornburg, K.L., Rugonyi, S. (2017). Hemodynamics Modify Collagen Deposition in the Early Embryonic Chicken Heart Outflow Tract. *J Cardiovasc Dev Dis*, *4*.

Renz, M., Otten, C., Faurobert, E., Rudolph, F., Zhu, Y., Boulday, G., Duchene, J., Mickoleit, M., Dietrich, A.C., Ramspacher, C., Steed, E., Manet-Dupe, S., Benz, A., Hassel, D., Vermot, J., Huisken, J., Tournier-Lasserve, E., Felbor, U., Sure, U., Albiges-Rizo, C., Abdelilah-Seyfried, S. (2015). Regulation of Beta1 Integrin-Klf2-Mediated Angiogenesis by Ccm Proteins. *Dev Cell*, *32*, 181-190.

Rochon, E.R., Menon, P.G., Roman, B.L. (2016). Alk1 Controls Arterial Endothelial Cell Migration in Lumenized Vessels. *Development*, *143*, 2593-2602.

Ruwhof, C., van der Laarse, A. (2000). Mechanical Stress-Induced Cardiac Hypertrophy: Mechanisms and Signal Transduction Pathways. *Cardiovasc Res*, *47*, 23-37.

Rysa, J., Tokola, H., Ruskoaho, H. (2018). Mechanical Stretch Induced Transcriptomic Profiles in Cardiac Myocytes. *Sci Rep*, *8*, 4733.

Samsa, L.A., Givens, C., Tzima, E., Stainier, D.Y., Qian, L., Liu, J. (2015). Cardiac Contraction Activates Endocardial Notch Signaling to Modulate Chamber Maturation in Zebrafish. *Development*, *142*, 4080-4091.

Scherz, P.J., Huisken, J., Sahai-Hernandez, P., Stainier, D.Y. (2008). High-Speed Imaging of Developing Heart Valves Reveals Interplay of Morphogenesis and Function. *Development*, *135*, 1179-1187.

Schoenebeck, J.J., Keegan, B.R., Yelon, D. (2007). Vessel and Blood Specification Override Cardiac Potential in Anterior Mesoderm. *Dev Cell*, *13*, 254-267.

Sedmera, D., Pexieder, T., Rychterova, V., Hu, N., Clark, E.B. (1999). Remodeling of Chick Embryonic Ventricular Myoarchitecture under Experimentally Changed Loading Conditions. *Anat Rec*, *254*, 238-252.

Shyer, A.E., Rodrigues, A.R., Schroeder, G.G., Kassianidou, E., Kumar, S., Harland, R.M. (2017). Emergent Cellular Self-Organization and Mechanosensation Initiate Follicle Pattern in the Avian Skin. *Science*, *357*, 811-815.

Sinha, T., Li, D., Theveniau-Ruissy, M., Hutson, M.R., Kelly, R.G., Wang, J. (2015). Loss of Wnt5a Disrupts Second Heart Field Cell Deployment and May Contribute to Oft Malformations in Digeorge Syndrome. *Hum Mol Genet*, *24*, 1704-1716.

Stainier, D.Y., Weinstein, B.M., Detrich, H.W., 3rd, Zon, L.I., Fishman, M.C. (1995). Cloche, an Early Acting Zebrafish Gene, Is Required by Both the Endothelial and Hematopoietic Lineages. *Development*, *121*, 3141-3150.

Staudt, D.W., Liu, J., Thorn, K.S., Stuurman, N., Liebling, M., Stainier, D.Y. (2014). High-Resolution Imaging of Cardiomyocyte Behavior Reveals Two Distinct Steps in Ventricular Trabeculation. *Development*, *141*, 585-593.

Steed, E., Boselli, F., Vermot, J. (2016a). Hemodynamics Driven Cardiac Valve Morphogenesis. *Biochim Biophys Acta*, *1863*, 1760-1766.

Steed, E., Faggianelli, N., Roth, S., Ramspacher, C., Concordet, J.P., Vermot, J. (2016b). Klf2a Couples Mechanotransduction and Zebrafish Valve Morphogenesis through Fibronectin Synthesis. *Nat Commun*, *7*, 11646.

Sugden, W.W., Meissner, R., Aegerter-Wilmsen, T., Tsaryk, R., Leonard, E.V., Bussmann, J., Hamm, M.J., Herzog, W., Jin, Y., Jakobsson, L., Denz, C., Siekmann, A.F. (2017). Endoglin Controls Blood Vessel Diameter through Endothelial Cell Shape Changes in Response to Haemodynamic Cues. *Nat Cell Biol*, *19*, 653-665.

van den Berg, G., Abu-Issa, R., de Boer, B.A., Hutson, M.R., de Boer, P.A., Soufan, A.T., Ruijter, J.M., Kirby, M.L., van den Hoff, M.J., Moorman, A.F. (2009). A Caudal Proliferating Growth Center Contributes to Both Poles of the Forming Heart Tube. *Circ Res*, *104*, 179-188.

Vedula, V., Lee, J., Xu, H., Kuo, C.J., Hsiai, T.K., Marsden, A.L. (2017). A Method to Quantify Mechanobiologic Forces During Zebrafish Cardiac Development Using 4-D Light Sheet Imaging and Computational Modeling. *PLoS Comput Biol*, *13*, e1005828.

Vermot, J., Forouhar, A.S., Liebling, M., Wu, D., Plummer, D., Gharib, M., Fraser, S.E. (2009). Reversing Blood Flows Act through Klf2a to Ensure Normal Valvulogenesis in the Developing Heart. *PLoS Biol*, *7*, e1000246.

Vincent, S.D., Buckingham, M.E. (2010). How to Make a Heart: The Origin and Regulation of Cardiac Progenitor Cells. *Curr Top Dev Biol*, *90*, 1-41.

Wu, B., Wang, Y., Xiao, F., Butcher, J.T., Yutzey, K.E., Zhou, B. (2017). Developmental Mechanisms of Aortic Valve Malformation and Disease. *Annu Rev Physiol*, *79*, 21-41.

Yang, L., Cai, C.L., Lin, L., Qyang, Y., Chung, C., Monteiro, R.M., Mummery, C.L., Fishman, G.I., Cogen, A., Evans, S. (2006). Isl1cre Reveals a Common Bmp Pathway in Heart and Limb Development. *Development*, *133*, 1575-1585.

Yelbuz, T.M., Waldo, K.L., Kumiski, D.H., Stadt, H.A., Wolfe, R.R., Leatherbury, L., Kirby, M.L. (2002). Shortened Outflow Tract Leads to Altered Cardiac Looping after Neural Crest Ablation. *Circulation*, *106*, 504-510.

Zeng, X.X., Yelon, D. (2014). Cadm4 Restricts the Production of Cardiac Outflow Tract Progenitor Cells. *Cell Rep*, *7*, 951-960.

Zhou, Y., Cashman, T.J., Nevis, K.R., Obregon, P., Carney, S.A., Liu, Y., Gu, A., Mosimann, C., Sondalle, S., Peterson, R.E., Heideman, W., Burns, C.E., Burns, C.G. (2011). Latent Tgf-Beta Binding Protein 3 Identifies a Second Heart Field in Zebrafish. *Nature*, *474*, 645-648.

CHAPTER 2

Cardiac function modulates endocardial cell dynamics to shape the cardiac outflow tract

Pragya Sidhwani[1], Giulia Boezio[2], Hongbo Yang[3,4],

Neil C. Chi[3], Beth L. Roman[5], Didier Y.R. Stainier[2], and Deborah Yelon[1]*

[1] Division of Biological Sciences, University of California, San Diego, La Jolla, CA, 92093, USA

[2] Max Planck Institute for Heart and Lung Research, Department of Developmental Genetics, 61231 Bad Nauheim, Germany

[3] Division of Cardiovascular Medicine, Department of Medicine, University of California, San Diego, La Jolla, CA, 92093, USA

[4] Department of Biochemistry and Molecular Biology, College of Medicine, The Pennsylvania State University, Hershey, Pennsylvania 17033, USA

[5] Human Genetics, Graduate School of Public Health, University of Pittsburgh, Pittsburgh, PA, 15261, USA

*Corresponding author: email: dyelon@ucsd.edu; phone: (858) 534-1822

ABSTRACT

Mechanical inputs orchestrate cellular dynamics in order to precisely shape developing organs. For example, blood flow and contractility generate biomechanical cues that influence cardiovascular morphogenesis, although the relevant cellular and molecular mechanisms remain relatively mysterious. Here, we address the impact of cardiac function on organ dimensions in the context of the cardiac outflow tract (OFT), a crucial portal between the heart and vasculature. In zebrafish, the OFT expands via accumulation of inner endocardial and overlying myocardial cells. However, when cardiac function is disrupted, OFT endocardial growth ceases, accompanied by reduced proliferation and reduced addition of endocardial cells from adjacent vessels. Loss-of-function of the TGFβ receptor Alk1 inhibits addition of endocardial cells without blocking their proliferation, suggesting distinct regulation of these two cell behaviors. Thus, our results indicate that cardiac function leads to endocardial accumulation by triggering both proliferation and cell addition, thereby inducing OFT lumen expansion and shaping OFT dimensions.

INTRODUCTION

Organs are sculpted in a dynamic physical environment, where they are pulled, squeezed and twisted in a spatiotemporally heterogeneous manner. Such anisotropic mechanical influences are indispensable for proper development: they activate specific signaling cascades to drive essential cellular decisions on growth and rearrangement (Eder et al., 2017; Heisenberg & Bellaiche, 2013). In this way, physical influences forge an organ's characteristic contours and proportions, which ultimately facilitates function. Despite their importance, however, the molecular and cellular mechanisms that tune organ shape in response to forces remain elusive in multiple contexts.

The embryonic heart serves as an important system to study how biomechanical cues enforce organ form (Collins & Stainier, 2016; Sidhwani & Yelon, 2019). As blood flows through the sequentially contracting chambers, it sloshes along the grooves and gorges created by the inner endocardial layer of the heart. The resulting perturbations in fluid parameters, as well as contractility intrinsic to the outer myocardial layer, can jointly modulate cellular behaviors to create a heart of the appropriate dimensions. In the zebrafish heart, for example, hemodynamic influences promote regionalized cellular expansion and myofibril maturation, while contractility restricts myocardial cell size, as the characteristic curvatures of the ventricular chamber emerge (Auman et al., 2007; Lin et al., 2012). This myocardial growth is spatiotemporally coordinated with that of the underlying ventricular endocardium, where blood flow instigates proliferation and cellular hypertrophy (Dietrich et al., 2014). In a similar timeframe, function-induced expression of the TGFβ type I receptor Alk1 in arterial vessels facilitates endothelial

migration into the heart, resulting in the restriction of the lumenal diameter of the distal cranial vessels (Corti et al., 2011; Rochon et al., 2016). Flow-related parameters also activate the calcium channels Trpp2 and Trpv4 to upregulate expression of the transcription factor *klf2a* which remodels the endocardial cells lining the atrioventricular canal in a *wnt9b*-dependent manner (Galvez-Santisteban et al., 2019; Goddard et al., 2017; Heckel et al., 2015). Thus, cardiac function impacts multiple tissues – myocardium, endocardium, and endothelium – during the synchronous development of the continuous cardiovascular system.

The cardiac outflow tract (OFT), a tubular portal at the junction where the heart meets the vessels, could provide meaningful insight into the collaboration between cardiac and vascular morphogenesis. Despite the importance of the OFT, the cellular mechanisms that precisely calibrate its dimensions remain largely mysterious. The OFT myocardium is derived from late-differentiating second heart field (SHF) progenitor cells that append to the arterial pole of the contracting primitive heart tube, which itself is formed by early-differentiating first heart field cells (Cortes et al., 2018; Felker et al., 2018; Francou & Kelly, 2016; Knight & Yelon, 2016). Pathways regulating SHF proliferation, epithelialization and differentiation ensure an adequate supply of myocardial cells for construction of the initial OFT. Fgf and canonical Wnt pathways, for example, regulate proliferation of SHF progenitors (Cohen et al., 2007; de Pater et al., 2009; Lin et al., 2007; Zeng & Yelon, 2014). Tbx1-dependent epithelial characteristics and protrusive activity of SHF progenitors are also important for their proper proliferation and differentiation (Francou et al., 2014). Recent live imaging analysis in zebrafish suggests that SHF-derived cells constitute an epithelial sheath that wraps around an

emerging endocardium (Felker et al., 2018). Subsequently, the AP-1 transcription factor Fosl2 is thought to control the timing of SHF differentiation (Jahangiri et al., 2016). Beyond our understanding of SHF progenitor dynamics, however, not much is known about how SHF-derived cells organize into an appropriately shaped OFT.

Since the OFT is formed in the context of active blood flow and contractility, biomechanical forces associated with function could be influencing the initial steps of establishing OFT morphology. Indeed, later phases in OFT morphogenesis, specifically endocardial cushion remodeling and valve formation within the mature OFT, have been shown to depend on cardiac function. For example, flow stimulates the deposition of fibrous extracellular matrix proteins during valve formation in chick OFT explants (Biechler et al., 2014). Function-mediated *notch1b* expression also regulates OFT valve formation in zebrafish (Hsu et al., 2019), consistent with earlier work in chick in which surgical obstruction of blood flow led to OFT valve anomalies (Hogers et al., 1999). Moreover, recent studies in mice indicate that SHF deployment exerts epithelial tension, which promotes SHF proliferation in a YAP/TAZ-dependent fashion (Francou et al., 2017). Together, these data imply that the early OFT could be exposed to, as well as sensitive to, multiple functional influences; however, a role for cardiac function during the initial phases of OFT construction has not been evaluated.

Here, we exploit the utility of zebrafish genetics and high-resolution morphometrics to unravel function-induced mechanisms governing the cellular underpinnings of OFT shape. We find that the expansion of the OFT endocardium and myocardium are accompanied by endocardial cell accumulation from two sources: endocardial proliferation and addition of endothelial cells from the neighboring aortic

arches. Disruption of cardiac function leads to a collapse of the OFT endocardium and inhibits endocardial cell accumulation by interfering with both proliferation and addition of cells. Importantly, we find that loss of Alk1 function interferes with endothelial cell addition without mitigating proliferation, in a manner that is similar to mutants in which atrial function is disrupted, presumably altering the patterns of blood flow into the ventricle and OFT. Together, our studies propose a model where contractility and blood flow concertedly trigger endocardial proliferation and Alk1-dependent endothelial addition in order to construct an endocardial scaffold that myocardial cells encase to mold a bilayered OFT. Our work has broad implications for understanding the potential causes of congenital heart defects, 30% of which include OFT malformations (Neeb et al., 2013), as well as for comprehension of the mechanisms underlying hereditary hemorrhagic telangiectasia type 2, which is caused by mutations in Alk1(Letteboer et al., 2006; Roman & Hinck, 2017) .

RESULTS

Cellular accumulation accompanies outflow tract growth

The cardiac outflow tract (OFT) is morphologically distinct from the ventricle: whereas the ventricle has a bean-shaped appearance following chamber emergence (Auman et al., 2007), the OFT is a tubular structure separated from the expanded ventricle by a defined constriction (Fig. 2-1A,B). Although the OFT can be qualitatively distinguished from the ventricle, we do not understand the cellular mechanisms that build this discrete structure.

OFT morphology could be a cumulative outcome of changes in cell number, cell size and cell shape. To evaluate if cellular accumulation accompanies OFT morphogenesis, we examined the number of OFT cells at two stages: 36 hours post fertilization (hpf), when differentiation of SHF cells is underway, and 51 hpf, when the mature OFT has been formed (Guner-Ataman et al., 2013; Lazic & Scott, 2011; Zhou et al., 2011). Since we do not have a molecular marker that specifically delineates the OFT at these stages, we used reproducible morphological landmarks to demarcate its boundaries: proximally to distally (with respect to the arterial end of the ventricle), the OFT begins at the myocardial constriction between the ventricle and the OFT, and ends at the bifurcation of the aortic arches (Fig. 2-1A,B; see Materials and Methods for more detail). Quantification of endocardial cell number at 36 hpf and 51 hpf revealed that endocardial cells accrue as the OFT develops (Fig. 2-1C, G, S). Myocardial cell number in the OFT also increases during this time (Fig. 2-1K, O, W), concordant with previous studies demonstrating that SHF-derived myocardial cells append to the arterial pole

between 24 hpf and 48 hpf (de Pater et al., 2009; Lazic & Scott, 2011). Corresponding with the observed increases in the total number of cells, the number of endocardial and myocardial cells in a medial cross-section of the OFT also increases during this time interval (Fig. 2-1D, H, L, P, T, X).

To determine if changes in cell morphology also contribute to OFT expansion, we analyzed endocardial and myocardial cell shape and size at 36 hpf and 51 hpf. We focused our analysis on the lateral walls of the OFT, termed outer curvature (OC) and inner curvature (IC) for their differential convex and concave curvatures (see Materials and Methods for more detail). Our results demonstrate that OFT endocardial cells become smaller and rounder during OFT expansion, in both the OC and IC (Fig. 2-1E-F, I-J, U-V). Simultaneously, and in contrast to endocardial cells, OFT myocardial cells become marginally larger, particularly in the OC, while also becoming more circular (Fig. 2-1M-N, Q-R, Y-Z).

Together, our studies indicate that OFT development is accompanied by distinct cellular behaviors in both layers: in the endocardium, cells accrue over time and get rounder and smaller, while in the myocardium, cells also accumulate and get rounder, but instead undergo regionalized expansion. Notably, these trends in endocardial and myocardial cell morphologies are similar to those observed in the ventricle during chamber formation (Auman et al., 2007; Dietrich et al., 2014). How might these cellular processes underlie OFT expansion? Given that endocardial cells are getting smaller and myocardial cells are expanding only within certain areas of the OFT, our data suggest cellular increment as the primary mechanism for OFT growth between 36 hpf and 51 hpf.

Proliferation and addition contribute to OFT endocardial expansion

Reasoning that the endocardium could act as a platform for myocardial assembly, we focused our investigation on potential sources of the additional endocardial cells that accumulate in the OFT. Prior studies in zebrafish have found that ventricular endocardial cells proliferate between 24 hpf and 48 hpf (Dietrich et al., 2014). Recent work has also determined that cells from the arterial vasculature migrate into the heart, in a direction opposing blood flow, during a similar timeframe (Rochon et al., 2016). To begin addressing whether either of these mechanisms contribute to OFT expansion between 36 hpf and 51 hpf, we evaluated whether OFT endocardial cells proliferate during this period. At 36 hpf, we injected embryos with the thymidine analog EdU, which is incorporated into mitotic cells during S phase. At 51 hpf, we consistently observed ~5 EdU+ endocardial cells in the OFT, corresponding to an OFT endocardial proliferation index (PI) of 25.8 ± 1.2 % (Fig. 2-2A-D). To complement this analysis, we incubated embryos with the thymidine analog BrdU between 36 and 51 hpf; BrdU incorporation provided evidence for a similar rate of OFT endocardial proliferation (PI = 28.9 ± 4.2 %; Fig. 2-2E-H). Altogether, our data suggest that proliferation is one mechanism by which endocardial cells accrue over time in the OFT.

Since previous studies indicate that endothelial cells from the arterial vasculature append to the heart (Rochon et al., 2016), we next investigated whether endothelial cells from external sources supply endocardial cells to the OFT between 36 hpf and 51 hpf. To begin evaluating this, we specifically labeled OFT endocardial cells at 36 hpf using photoconversion in *Tg*(*kdrl*:*dendra*) embryos, in which the green-to-red photoconvertible protein Dendra is expressed in the endothelium (Fig. 2-3A). By 51 hpf,

the OFT contained two populations of cells: those expressing only the native form of Dendra, which fluoresces green, and those containing the photoconverted “red” version of Dendra in addition to the newly synthesized “green” form. These data suggest that endocardial addition indeed supplements OFT growth (Fig. 2-3C-H). Interestingly, the “green-only” cells were present around the distal edge of the OFT at 51 hpf, while the proximal edge of the OFT appeared intact, suggesting that cells from the adjacent aortic arches may be contributing to OFT expansion. To test whether cells from the aortic arches come to occupy the OFT, we targeted one of the bilateral first aortic arches (AA1) by photoconversion in *Tg*(*kdrl*:*dendra*) embryos at 36 hpf (Fig. 2-3B). Indeed, we found photoconverted cells in the OFT by 51 hpf, most frequently in the distal parts of the OFT (Fig. 2-3O), suggesting that cells from the AA1 do relocate to the OFT endocardium (Fig. 2-3I-N). Overall, these experiments show that both cellular proliferation and endothelial addition contribute to OFT endocardial growth.

During chamber emergence, myocardial cells in the outer curvature of the ventricle expand, whereas those in the inner curvature retain smaller morphologies (Auman et al., 2007). Such localized cellular growth is thought to engender differential curvatures in the heart, thereby contributing to its functional capacity. We wondered if cellular features of the OFT could similarly provoke changes in its overall structure. To begin addressing this, we analyzed OFT dimensions by creating surfaces representative of the endocardial wall (see Materials and Methods). At 36 hpf, the OFT, as we define it, is a linear structure that appears uniformly wide along the proximal-distal axis (Fig. 2-4A-E). Interestingly, by 51 hpf, the OFT has adopted a funnel-like morphology, such that its opening into the aortic arches is larger than its connection to

the ventricle (Fig. 2-4K-O. Fig. 2-5). This shape could facilitate efficient efflux of blood while restricting reversing flows, a task that is later accomplished by OFT valves (Hinton & Yutzey, 2011). Importantly, this aspect of OFT shape strongly correlates with our observations that cells from the AA1 add primarily to the distal OFT. In addition to the increase in distal sectional area, the enclosed volume of the OFT endocardium also expands between 36 hpf and 51 hpf (Fig. 2-4U). Differences in endocardial volume in fixed samples were confirmed using complementary analysis in live embryos, where, similar to fixed embryos, OFT expansion by 51 hpf is clearly visible (Fig. 2-6). Thus, endocardial cellular accumulation coincides with endocardial growth, which presumably facilitates lumen expansion for unimpeded flow of blood.

Given that the number of myocardial cells also increases during this time, we hypothesized that OFT myocardial volume would also enlarge. Indeed, our results show that the enclosed volume of the myocardium increases markedly during this time (Fig. 2-4V). We also observed an intriguing coupling of endocardial and myocardial volumes at 36 and 51 hpf (Fig. 2-4W), suggesting that the two layers develop in a coordinated manner. Together, these data indicate that the OFT attains a stereotypical morphology by 51 hpf, in a process that is regulated on a cellular level.

Cardiac function promotes OFT endocardial enlargement

Since the OFT is assembled atop a beating heart, we speculated that functional cues are necessary for OFT morphogenesis. To begin investigating this, we analyzed OFT endocardial volume and proximal-distal sectional areas in *silent heart* (*sih*) mutants, which lack contractility, and consequently blood flow, due to a mutation in

troponin T type 2a (*tnnt2a*), a cardiac specific troponin T (Sehnert et al., 2002). At 36 hpf, we found that OFT endocardial volume and sectional areas are indistinguishable between wild type and *sih* (Fig. 2-4A-J, U, X-Y); however, by 51 hpf, whereas the wild-type OFT endocardium has grown in volume and medio-distal sectional area, the *sih* OFT failed to expand (Fig. 2-4K-T, U, X-Y). The OFT myocardial volume is similar in wild-type and *sih* embryos at 51 hpf, suggesting that cardiac function primarily regulates endocardial growth (Fig. 2-4V). Similarly, in live images of *sih* at 51 hpf, the OFT endocardium also appears as a thin row of cells with a significantly different volume than the wild-type endocardium (Fig. 2-6). Strikingly, in *sih*, while the endocardial volume is similar between 36 hpf and 51 hpf, the sectional area is significantly reduced by 51 hpf. In this regard, it is informative to reflect upon recent studies in mice, which suggest that SHF deployment confers epithelial tension on the dorsal pericardial wall (DPW) (Francou et al., 2017). Since the endocardium and myocardium are closely apposed during OFT morphogenesis, epithelial tension between the DPW and the developing myocardium could be influencing OFT proportions. Consequently, in the absence of endocardial growth, the OFT endocardium could appear stretched in the proximal-distal direction, as observed in *sih* at 51 hpf.

Cardiac function promotes OFT endocardial accumulation

We next investigated the cellular mechanisms through which cardiac function promotes OFT endocardial enlargement. Since OFT growth in wild-type is accompanied by cellular accumulation, we first quantified OFT cell number at 36 hpf and 51 hpf in *sih*. At 36 hpf, the number of OFT endocardial cells in wild-type and *sih* is comparable,

consistent with the similarity in OFT endocardial volume at this stage (Fig. 2-7A, C, K). By 51 hpf, however, this number is significantly smaller in *sih* than in wild-type (Fig. 2-7B, D, K); consequently, *sih* mutants have fewer endocardial cells per medial section as well (Fig. 2-7A'-D', L). To confirm that this phenotype is dependent on cardiac function and not on cardiac troponin T specifically, we next evaluated OFT endocardial cell number in *half-hearted* (*haf*) mutants, which lack Ventricular Myosin Heavy Chain, and thus have non-contractile ventricles (Auman et al., 2007). Excitingly, *haf* mutants also exhibit a similar trend in OFT endocardial cell number (Fig. 2-7E-F, K), suggesting that function promotes endocardial accumulation in the OFT. On performing cellular morphometric analysis, we also determined that OFT endocardial cells in *sih* are larger and elongated in comparison to wild-type at 51 hpf (Fig. 2-9). Therefore, in the absence of cardiac function, multiple aspects of the OFT endocardium fail to develop normally. Additionally, although *sih* mutants have a normal number of OFT myocardial cells at 51 hpf, the number of cardiomyocytes in a medial section is strikingly reduced (Fig 2-8). Putting together these observations, we propose that cardiac function promotes OFT endocardial accumulation, which influences cellular arrangement in the overlying myocardium to facilitate overall OFT growth.

Atrial function is required for cellular accumulation in the OFT endocardium

To begin isolating the effects of contractility and blood flow in OFT expansion, we assessed the *weak atrium* (*wea*) mutant, which has a mutation in *atrial myosin heavy chain* (*amhc/myh6)*, an atrial specific myosin isoform (Berdougo et al., 2003). *wea* mutants have non-contractile atria, due to which blood flow into the ventricle and OFT is

thought to be reduced. As in *sih* and *haf*, OFT endocardial cell number is normal in *wea* at 36 hpf (Fig. 2-7G, G', K). However, at 51 hpf, the *wea* OFT has significantly fewer endocardial cells in comparison to wild-type, both in the OFT overall as well as in a medial section (Fig. 2-7H, H', L). To begin dissecting the nature of the fluid force(s) that could be influencing endocardial accumulation, we assayed the number of endocardial cells at 36 hpf and 51 hpf in *gata1* morphants, which have fewer erythrocytes, and hence reduced shear forces (Vermot et al., 2009). At 51 hpf, the number of OFT endocardial cells in *gata1* morphants is comparable to wild-type (Fig. 2-7I-J, K-L), which suggests that shear forces do not influence OFT cell number. Nevertheless, we cannot exclude the possibility that shear forces from blood plasma are sufficient for OFT endocardial accumulation. Overall, our data show that cardiac function and atrial function are both necessary for OFT endocardial growth.

Blood flow drives endothelial displacement but not proliferation in the OFT

What are the cellular mechanisms by which functional cues promote OFT endocardial growth? To answer this, we first inspected OFT endocardial proliferation in *sih* mutants using both EdU and BrdU assays. Interestingly, whereas endocardial cells in the wild-type OFT incorporate EdU between 36 hpf and 51 hpf with a PI of 29.6 ± 3.6 %, the PI in *sih* OFT endocardium is significantly reduced to 10.2 ± 4.3 % (Fig. 2-10A-F, Fig. 2-11C-D). This reduction is recapitulated in the *haf* OFT as well, where the endocardial cells were found to divide with a PI of 15.6 ± 4.8 % (Fig. 2-10G-I, M, Fig. 2-11E-F). Thus, cardiac function bolsters OFT endocardial proliferation, as has been previously suggested for the ventricular endocardium (Dietrich et al., 2014). Next, we

evaluated if cardiac function also induces endothelial addition to the OFT from AA1 between 36 hpf and 51 hpf. For this purpose, we photoconverted AA1 cells in *sih*; *Tg*(*kdrl*:*dendra*) embryos at ~36 hpf, and probed for red cells in the OFT at ~51 hpf. In contrast to wild-type embryos, where 5/5 embryos displayed red cells in the OFT, in *sih*, only 1/6 embryos had red cells in the OFT by 51 hpf (Fig. 2-12A-L, S-T). These observations were also confirmed in *sih* morphants (Fig.2-13). Then, to determine if either or both of these cellular processes depend on blood flow, we inspected proliferation and addition in *wea* mutants. Surprisingly, OFT endocardial cells in *wea* mutants proliferate normally, with a PI of 27.8 ± 6.3 % (Fig. 2-10J-M, Fig. 2-11G-H). In contrast, endothelial addition to the OFT is reduced in *wea* when compared to wild-type (Fig. 2-12M-R, U). Taken together, our experiments suggest that endothelial addition, but not OFT endocardial proliferation, is dependent on blood flow. It is important to note, however, that PI measurements depend on the total number of cells, which itself is impacted by cellular addition; therefore, we cannot preclude a subtle reduction of OFT endocardial proliferation in *wea*.

Klf2a and Klf2b are not essential for endocardial accumulation in the OFT

Functional cues must be interpreted by mechanotransducers in endothelial cells to instigate tissue-wide changes in the OFT. The mechanotransducive transcription factor *klf2a* is highly expressed in the endocardium at 36 hpf, and progressively concentrates at the atrioventricular canal and OFT endocardium by 48 hpf (Vermot et al., 2009). Although Klf2 is known to be an essential mediator of atrioventricular canal development (Goddard et al., 2017; Heckel et al., 2015; Steed et al., 2016; Vermot et

al., 2009), less is known about whether *klf2a* and its paralog *klf2b* play a role in OFT development. To begin testing a role for Klf2 factors in endocardial accumulation in the OFT, we quantified OFT endocardial cell number in wild-type siblings and *klf2a*;*klf2b* double mutants (henceforth called *klf2* mutants) at 51 hpf. Ten out of eleven *klf2* mutants appeared remarkably normal, suggesting that Klf2 factors do not govern OFT endocardial accumulation. We did, however, observe a significant reduction in OFT endocardial cell number in one embryo, suggesting the possibility of a poorly penetrant phenotype, as has been observed for other cardiac phenotypes in *klf2* mutants (Fig. 2-15) (Rasouli et al., 2018). Interestingly, in experiments where *klf2* mutants were selected for analysis prior to fixation based on subtle morphological anomalies, such as distension of the OFT and atrioventricular canal, we observed low OFT endocardial cell number in a higher proportion of mutant embryos (3/7 embryos; data not shown). This phenotype, which is obvious under a stereoscope by 74 hpf (data not shown), is strikingly reminiscent of *sih* and *haf*. Therefore, although it appears that Klf factors could be playing a role in OFT endocardial accumulation, our data suggest that they are not absolutely essential.

The mechanotransducive TGFβ receptor Alk1 is required for OFT growth

Another interesting candidate for a mechanotransducer mediating OFT endocardial development is the TGFβ receptor Alk1, whose expression as well as activity in the arterial endothelium depends on cardiac function (Corti et al., 2011; Laux et al., 2013). Importantly, Alk1 mediates endothelial migration towards the heart between 24 hpf and 48 hpf (Rochon et al., 2016). Although these migrating endothelial

cells culminate in the heart, a role for Alk1 in endocardial morphogenesis has not yet been investigated.

To begin evaluating if Alk1 promotes OFT growth between 36 hpf and 51 hpf, we quantified OFT endocardial cell number in *alk1* morphants. Previous studies have established that *alk1* morphants phenocopy *alk1* mutants; both the mutant and MO-injected embryos exhibit characteristics of hereditary hemorrhagic telangiectasia type 2 (HHT2), where the cranial vessels are visibly dilated by 36 hpf (Corti et al., 2011; Laux et al., 2013; Rochon et al., 2016). At 36 hpf, the number of endocardial cells in the OFT was comparable between uninjected controls and *alk1* morphants, as is the case for functional mutants. Strikingly, by 51 hpf, the OFT endocardial cell number is significantly reduced in *alk1* morphants compared wild-type (Fig. 2-14A-E). We confirmed this phenotype in *alk1* mutants as well (Fig. 2-16). The reduction in cell number manifests as a shortened OFT in most cases (Fig. 2-14) but can sometimes lead to a narrower OFT (data not shown). Notably, *alk1* morphants have normal heart rates at 36 hpf, but exhibit a slight yet significant reduction in heart rate by 51 hpf (Fig. 2-17). Although the declining heart rate could be influencing the severity of the OFT phenotype, given the considerable reduction in OFT endocardial cell number, we do not anticipate that it affects endocardial accumulation substantially.

Alk1 promotes endothelial addition independent of proliferation

To further elucidate the cellular mechanisms that underlie the reduction in endocardial cell number, we assayed OFT endocardial proliferation in *alk1* morphants. Due to the similarity in OFT endocardial cell number in *alk1* morphants and *wea*

mutants, we hypothesized that *alk1* morphants will have normal proliferation and reduced addition from the aortic arches, as is the case in *wea*. Indeed, *alk1* morphants proliferate with a PI of 29.1 ± 2.7 %, in comparison to 21.5 ± 1.9 % in uninjected controls (Fig. 2-14F-L), which suggests that proliferation is not reduced when Alk1 function is disrupted. In contrast, injecting *alk1* morpholino into *Tg*(*kdrl*:*dendra2*) embryos abated endothelial addition from AA1 into the OFT; whereas 3/3 uninjected controls demonstrated photoconverted cells in the OFT at 51 hpf, 0/5 *alk1* morphants had red cells in the OFT by 51 hpf (Fig. 2-18). When we synthesize these data with prior studies showing that *alk1* expression is reduced in *sih* (Corti et al., 2011), and our observations of decreased endothelial addition to the OFT in *sih* and *wea*, an intriguing model begins to emerge, which suggests that blood flow stimulates *alk1* expression to promote endothelial addition into the OFT, which shapes the overall OFT structure.

DISCUSSION

In this work, we provide new perspectives on the cellular, molecular and physical mechanisms by which the initial OFT attains its stereotypical morphology. By capturing the cellular dynamics underlying an understudied phase of OFT development, we begin to assemble a coherent picture of OFT morphogenesis with unprecedented detail. Our data identify a previously unappreciated role for cardiac function in modulating the precise interplay of cellular dynamics in the OFT endocardium. Specifically, we find that cardiac function promotes both proliferation and endothelial addition in the OFT. Consequently, in the absence of cardiac function, OFT endocardial growth and myocardial arrangement are severely disrupted. Our studies further uncover a novel function for the flow-responsive TGFβ type I receptor Alk1 in triggering cellular displacement, but not proliferation, in the OFT endocardium. Intriguingly, this phenotype is strikingly reminiscent of mutants where atrial function is specifically disrupted, indicating a potential role for blood flow in regulating Alk1 signaling to drive endothelial addition to the OFT. Overall, these findings suggest a model where cardiac function promotes both proliferation and Alk1-dependent endothelial addition to forge the inner endocardial wall of the OFT, which serves as a platform for myocardial organization to build a proper conduit for blood flow.

While our studies suggest that proliferation and addition collaboratively shape the OFT endocardium, we do not know if the two cellular behaviors are independent or molecularly coupled. In this regard, it is interesting to consider that while endothelial cells emanating from the aortic arches are routinely found in the distal OFT (Fig. 2-3),

BrdU+ cells are frequently observed in the proximal endocardium of the wild-type OFT (data not shown). Moreover, in *alk1* morphants, where endothelial addition is absent, the number of EdU+ cells appears unaltered (Fig. 2-14). These findings strongly imply that cells immigrating from the aortic arches are not dividing as they add to the OFT. In fact, a closer examination of OFT endocardial cell numbers in multiple conditions suggests that ~2-3 cells are added to the OFT endocardium as a result of proliferation, while ~10-15 cells come in from the bilateral aortic arches. Together, these data evoke a model where proliferation in the OFT endocardium determines the proximal diameter of the OFT, whereas cells from the aortic arches add to this emerging framework to facilitate distal expansion. Alternatively, endocardial cells from the ventricle, OFT and aortic arches could be undergoing significant rearrangement between 36 hpf and 51 hpf. To clarify this further, future studies could employ long-term live imaging of the OFT endocardium to visualize early OFT morphogenesis at high cellular resolution. Rigorous testing of this model awaits development of optogenetic tools to block proliferation specifically within the proximal endocardium.

If proliferation and displacement within the OFT endocardium are indeed uncoupled, it is likely that distinct molecular, and potentially physical, mechanisms govern the two cellular behaviors independently. As detailed above, a possible molecular mechanism regulating addition separately from proliferation is Alk1 signaling. Could different biomechanical cues lie upstream of such molecular pathways to orchestrate endocardial cell dynamics? Our findings suggest that inhibiting atrial function to reduce blood flow into the ventricle, as in *wea*, leads to dampened addition from the aortic arches, while proliferation in the OFT endocardium appears unaffected.

This is in contrast to *sih* and *haf* mutants, where OFT contractility is itself impaired, and both addition and proliferation are reduced. These results imply that blood flow acts independently to stimulate endothelial addition, while contractility promotes endocardial proliferation. Alternatively, the milder defect in *wea* mutants could be inadequate to depress proliferative capacity of OFT endocardial cells. How might blood flow and contractility, which are inextricably linked *in vivo*, prompt seemingly disparate cellular mechanisms towards a common goal of constructing the OFT? Although we do not yet have the tools to alter flow parameters without affecting contractility *in vivo*, a combination of three-dimensional tissue engineering in controlled flow environments will enable us to begin answering this question *ex vivo* (Lane et al., 2012; Qasim et al., 2019).

Our findings that *gata1* morphants do not exhibit a reduction in OFT endocardial cell number also beget the idea that even though blood flow is essential for endothelial addition to the OFT, shear forces from blood flow may not be the driving factor. This is in agreement with previous studies in the endothelium (Corti et al., 2011), atrioventricular canal (Heckel et al., 2015; Vermot et al., 2009) and ventricle (Dietrich et al., 2014), where loss of *gata1* was not found to influence flow-induced developmental mechanisms. What other flow-related parameters could be instigating endothelial addition to the OFT? In the atrioventricular canal, oscillatory flows are thought to stimulate valve development (Heckel et al., 2015). *wea* mutants indeed have reduced oscillatory flows at later stages (Vedula et al., 2017), so flow direction could be promoting endothelial addition to the OFT. Another possibility that has remained largely unexplored is the effect of stretch from blood pressure on developmental mechanisms

(Sidhwani & Yelon, 2019). Further work could employ spectroscopy techniques to directly manipulate flow direction or induce stretch to decipher the effects of such physical perturbations *in vivo* (Anton et al., 2013; Marjoram et al., 2016; Sidhwani & Yelon, 2019). Finally, blood may transport ligands to activate pathways promoting endothelial migration. In fact, previous studies have shown that, not only is *alk1* expression dependent upon function, but the Alk1 ligands *bmp10* and *bmp10-like* are expressed in the heart and brought to the site of *alk1* expression by blood flow (Laux et al., 2013). Therefore, in addition to flow-induced forces, it is important to consider blood as a carrier of vital molecules when analyzing functional mutants.

To support heightening blood flow, the cardiovascular system must continually adapt to increasing cardiac function. Alk1 is thought to play a central role in this process: it “senses” functional inputs to restrict lumen size of cranial vessels, while promoting expansion of vessels proximal to the heart (Corti et al., 2011; Laux et al., 2013; Rochon et al., 2016). In this work, we cue in a fundamental element to this model by showing that Alk1 also reinforces OFT size. Our findings are especially intriguing in light of prior studies showing that murine embryos lacking *bmp9* or *bmp10*, known ligands for Alk1, exhibit defects in cardiomyocyte proliferation and apoptosis, and consequently cardiac growth and maturation (Chen et al., 2013; Chen et al., 2004; Huang et al., 2012). Moreover, instances of cardiac failure are heightened in *alk1* knockout mice (Morine et al., 2017a; Morine et al., 2017b), as well as human patients of HHT2 (Cho et al., 2012; Goussous et al., 2009). Our results provide a renewed outlook on the pathogenesis of such cardiac abnormalities in HHT2 patients. Although further work is required to determine the relationship between the various effects of Alk1

signaling on the endocardium, endothelium and myocardium, our studies assert Alk1 as a key player in function-mediated synchronization of cardiovascular morphogenesis.

While OFT growth appears to be intertwined with vascular development via Alk1, we have little insight into how it might be integrated with chamber emergence. Previous work in zebrafish has indicated that, as in the OFT, endocardial cells within the ventricle proliferate and get smaller in response to functional influences (Dietrich et al., 2014). Could similar mechanotransducive pathways oversee endocardial proliferation in the OFT and ventricle, and if so, how might they modulate proliferation to build a ballooned chamber versus a cylindrical OFT? The Klf2 factors, which are differentially expressed in the OFT and ventricular endocardium, remain interesting candidates for one such mechanotransducive pathway. Although our work suggests that *klf2a* and *klf2b* are not reinforcing OFT endocardial cell number, the necessity of the Klf pathway in this process warrants further investigation. mRNA levels of *klf2b* and the related factor *klf4* (Clark et al., 2011; Goddard et al., 2017; Zhou et al., 2015) are increased in *klf2a* mutants (Rasouli et al., 2018), which suggests that the various Klf factors can compensate for each other. Therefore, as a first step, it is important for future studies to evaluate the contribution of the Klf homolog *klf4* in addition to *klf2a* and *klf2b* in OFT endocardial accumulation and proliferation.

Synthesizing our data with preceding studies promises to open additional avenues to grasp the etiology of, and design therapeutic strategies for congenital heart defects (CHD), a third of which include OFT abnormalities. For example, prior work has shown that defects in early OFT morphogenesis may lead to complications in OFT remodeling and septation, which often occur in patients with CHDs (El Robrini et al.,

2016; Neeb et al., 2013; Yelbuz et al., 2002). Given that many cardiac anomalies induce secondary errors in function, recognizing functional influences on early heart development is a key step towards circumventing subsequent issues. Finally, our findings also have major repercussions for cardiac tissue engineering approaches. Fabricating functional hearts has traditionally required a extracellular matrix scaffold (Ott et al., 2008); our studies underscore the usefulness of considering the endocardium as an additional yet crucial scaffold for myocardial assembly. Altogether, our studies bear multifaceted biomedical consequences, in addition to significantly advancing our understanding of the many ways in which “form follows function”.

MATERIALS AND METHODS

Zebrafish

Embryos were generated by intercrossing wild-type zebrafish or zebrafish heterozygous for the *tnnt2a* mutant allele *sih*^{b109} (Sehnert et al., 2002), *vmhc* mutant allele *haf*^{sk46} (Auman et al., 2007), *amhc* mutant allele *wea*^{m58} (Berdougo et al., 2003), *alk1* mutant allele *vbg*^{y6} (Roman et al., 2002) , *klf2a* mutant allele *klf2a*^{bns11} and *klf2b* mutant allele *klf2b*^{bns12} (Kwon et al., 2016), carrying the transgenes *Tg(fli1a:negfp)*^{y7} (Roman et al., 2002), *Tg*(*kdrl*:*grcfp*) (Cross et al., 2003),*Tg*(*kdrl*:*HsHRAS-mCherry*)^{s896} (Chi et al., 2008) , *Tg(kdrl:gfp)*^{la116} (Choi et al., 2007) and *Tg*(*myl7*:*H2A-mCherry*)^{sd12} (Schumacher et al., 2013). The *kdrl:ras-mCherry* construct was modified and injected into embryos for stable insertion to generate the *Tg*(*kdrl*:*dendra*)^{sd8} line for photoconversion experiments . Embryos homozygous for *sih*^{b109}, *haf*^{sk46} and *wea*^{m58} were selected based on visible contractility defects (Auman et al., 2007; Berdougo et al., 2003; Sehnert et al., 2002). *alk1* mutant embryos were identified based on their vascular phenotypes, including dilated cranial vessels and reduced blood flow in the tail (Roman et al., 2002). *klf2a* mutant embryos were genotyped using high-resolution melt analysis (HRMA) with the primers GACACCTACTGCCAACCGTCTC (F) and GGGAAAGCAGGCCTGACTAGGAAT (R) (Kwon et al., 2016; Rasouli et al., 2018). *klf2b* mutant embryos were also genotyped with HRMA using the primers CGTGGCACTGAACACAGAC (F) and GCTGAGATCCTCGTCATC (R) (Kwon et al., 2016; Rasouli et al., 2018).

Injections

For knockdown experiments, embryos were injected at the 1-4 cell stage with previously characterized morpholinos: 4 ng of anti-*tnnt2a* (ZFIN: MO1-*tnnt2a*) (Sehnert et al., 2002), 2.5 ng of anti-*amhc* (ZFIN: MO1-*amhc*) (Berdougo et al., 2003), or 2.5 ng of anti-*alk1* splice-blocking morpholino (5′-ATCGGTTTCACTCACCAACACACTC-3′) (Corti et al., 2011). In all cases, the morpholino phenotype was assessed qualitatively for severity, and was found to phenocopy mutants. No signs of toxicity were observed.

Immunofluorescence

Whole-mount immunostaining was modified from previously described protocols (Alexander et al., 1998; Cooke et al., 2005; Zeng & Yelon, 2014). Briefly, embryos were dechorionated and then fixed in 2% methanol-free formaldehyde for 10 minutes (Thermo Scientific, 28908), rinsed with 1x PBS and deyolked with a solution containing 0.2% saponin (Sigma, S4521) and 0.5% Triton X-100 (G Biosciences, 786513) in 1x PBS containing 0.1% Tween 20 (1x PBT) (Sigma, P9416). Embryos were then rinsed with 1x PBT and fixed overnight with fresh 4% paraformaldehyde (PFA) (Sigma, P6148). The next day, embryos were washed with 1x PBT, treated with 10 ug/mL proteinase K for 8 minutes (36 hpf embryos) or 13 minutes (51 hpf embryos) to facilitate antibody penetration, and fixed again for 20-30 minutes using 4% PFA. After washing with 1x PBT to remove fixative, embryos were blocked with 2 mg/mL Bovine Serum Albumin (Sigma, A9647) and 10% goat serum in 1x PBT overnight at 4°C. Embryos were incubated with primary antibody in block solution as follows: 1:50 dilution of mouse anti-Dm-grasp (Developmental Studies Hybridoma Bank, Zn-8 supernatant), 1:400

dilution of anti-GFP (Life Technologies, A11122 or A10262) or 1:1000 dilution of rabbit anti-dsRed (Clontech, 632496) overnight at 4°C. Embryos were then washed extensively with 1x PBT and incubated with the following secondary antibodies in 1x PBT: 1:150 dilution of goat anti-mouse AlexaFluor 594 (Life Technologies, A11012) or goat anti-mouse AlexaFluor 647 (Life Technologies, A21446), 1:400 dilution of goat anti-rabbit AlexaFluor 488 (Life Technologies, A11008) or goat anti-chick AlexaFluor 488 (Life Technologies, A11039) or goat anti-rabbit AlexaFluor 594 (Life Technologies, A11012) overnight at 4°C. After thorough washing with 1x PBT, embryos were mounted in 50% glycerol or SlowFade Gold anti-fade reagent (Invitrogen, S36936).

Proliferation assays

For BrdU treatments, embryos were soaked in freshly prepared 5 mg/mL BrdU in E3 from 36 hpf to 51 hpf, followed by fixation and detection (Dietrich et al., 2014). The EdU proliferation assay was adapted from previously described protocols (Hesselson et al., 2009), with slight modifications: embryos were injected pericardially or into the yolk with 1 nL EdU solution (200 uM EdU, 2% DMSO, 0.1% phenol red) at 36 hpf, followed by fixation at 51 hpf, whole-mount immunostaining as described above, and Click-iT detection as per manufacturer's guidelines (Invitrogen, C10339). Proliferation indices were calculated using the following formula: proliferation index (%) = (number of EdU+ or BrdU+ cells/total number of cells) x 100).

Imaging and photoconversion

Fixed samples were imaged from the left or left-ventral side on a Leica SP5 confocal laser-scanning microscope, using a 25x water objective and a slice thickness of 0.5 μm for all experiments except for those shown in Figure 4 and Figure S4-1, where the slice thickness was 0.29 μm. For live imaging, 36 hpf or 51 hpf embryos were anesthetized using 1 mg/mL tricaine and mounted in 1% low-melt agarose containing 1 mg/mL tricaine for imaging on a Zeiss Z.1 Light Sheet microscope. In some cases, relaxation buffer was used in accordance with previous guidelines (Huang et al., 2009); however, comparison of treated and untreated embryos yielded no difference in OFT measurements (data not shown). 36 hpf embryos were exposed to 0.5 mg/mL tricaine for 15-30 minutes prior to anesthesia to slow the heartrate, which leads to mild pericardial edema for optical access to the outflow tract. This strategy was also employed prior to photoconversion at 36 hpf, which was performed on embryos mounted in 2% methylcellulose containing 1 mg/mL tricaine, oriented with their left-ventral side towards a 25x water objective on a Leica SP5 confocal laser-scanning microscope. A region-of-interest (ROI) was selected for a 10-15 minute exposure to UV light at 25% laser intensity, until red signal was clearly visible in the ROI. Importantly, we determined that this UV exposure was not toxic and did not impair embryonic development. Embryos were imaged post-photoconversion with low Argon ion laser intensity (15%) to assess specificity: if regions beyond the intended ROI were photoconverted in an embryo, it was not analyzed further. Photoconverted embryos were then maintained until 51 hpf and imaged in 1 mg/mL tricaine.

Defining landmarks in the OFT

Although there is no known molecular marker that is specific for the OFT at the stages analyzed, we were able to define OFT boundaries in a rigorous and reproducible manner, as detailed below. The anatomical terminology used to define the OFT is as follows: proximal and distal, with respect to the arterial end of the ventricle, and inner vs. outer curvatures, where the inner curvature (IC) is the lesser, concave surface of the curved OFT (continuous with the ventricular outer curvature) and the outer curvature (OC) is the greater, convex curvature of the OFT (continuous with the ventricular inner curvature) (Fig. 2-1A-B).

The proximal boundary of the outflow tract was demarcated as the cross-sectional plane at the morphological constriction between the ventricle and the OFT, as visualized using anti-Dm-grasp in fixed embryos, and *Tg*(*myl7*:*H2A-mCherry*) in live embryos. At 36 hpf, this plane is perpendicular to the proximal-distal axis (Fig. 2-1A). However, by 51 hpf, due to the curved appearance of the OFT, this plane could be angled such that its IC edge is tilted distally compared to the OC edge (Fig. 2-1B). This constriction is easily observable along the entire circumference of the OFT myocardium. We also noted qualitative differences in cell morphologies anterior and posterior to this constriction: the ventricular CMs posterior to this constriction appear larger than the OFT CMs anterior to this constriction. To verify these guidelines, we analyzed the wild-type expression patterns of *klf2a* in the endocardium and of Isl1/2 and *nppa* in the myocardium. *klf2a* is highly expressed within the morphologicaly defined OFT at 48-51 hpf, and gradually diminishes towards the ventricle (Vermot et al., 2009). Isl1/2 extends into the ventricle at the OC side of the OFT but ends at the distinct morphological

constriction between the ventricle and the OFT on its IC side (Witzel et al., 2017). Conversely, *nppa* is excluded from the OFT, and its expression also ends at the ventricle/OFT boundary on the IC side (Auman et al., 2007; data not shown). Overall, this methodology allowed us to determine the proximal boundary in a consistent fashion.

The distal plane of the OFT was determined primarily using the bifurcation point of the aortic arches, but also considering the distal edge of Dm-grasp expression in fixed embryos or *Tg*(*myl7*:*H2A-mCherry*) expression in live embryos. At 36 hpf, Dm-grasp-expressing cells are routinely found around the aortic arches in addition to around the OFT (Fig. 2-1A). Therefore, the OFT distal boundary is defined as the plane through the bifurcation point of the aortic arches (AA), proximal to the distal edge of Dm-grasp expression. By 51 hpf, the distal end of Dm-grasp expression coincides with the AA bifurcation point, especially on the OC side, in a majority of embryos (in a typical batch of 10 embryos, 8 exhibited this characteristic) (Fig. 2-1B); in these cases, either can be considered as the distal plane of the OFT. However, in embryos where the distal edge of Dm-grasp expression is proximal to the AA bifurcation point, the former is considered the OFT distal boundary. As is the case for the OFT proximal plane, the distal plane is perpendicular to the proximal-distal axis at 36 hpf, but by 51 hpf, it is tilted such that the OFT OC ends more distally compared to the IC. These boundaries are highly reproducible and stereotypical, as suggested by the low SEM for OFT cellular and volumetric analyses in wild-type embryos (Figs. 2-1, 2-4) and are thus faithful landmarks for the OFT. Embryos in which these boundaries were not clear, due to poor staining or imaging angle, for example, were not analyzed further.

Morphometrics

All morphometric analyses were performed using Imaris (Bitplane) software unless mentioned otherwise. To perform OFT endocardial volumetric analysis, a smoothed surface (surfaces detail = 1) was created automatically using cytoplasmic GFP in *Tg*(*kdrl*:*grcfp*) embryos. The surface was then cut at the proximal and distal boundaries, as described above. We considered the volume of this surface to be the enclosed volume, since the surface "fills" the endocardial lumen of the OFT. For cross-sectional area analysis, areas of triangles formed by three points along the circumference of the cross-section were calculated using Heron's formula. A summation of the areas of all such triangles provides the total cross-sectional area of that plane.

For OFT myocardial volumes in fixed samples, a surface was created manually using the "contour surfaces" function in Imaris, so as to obtain the enclosed volume. In multiple cross-sections through the OFT, the apical boundary of Dm-grasp expression was drawn manually, and the three-dimensional surface was created by connecting these two-dimensional boundaries.

The medial cross-section (for cell counting and cross-sectional area measurements) is considered to be the plane through the central points in the OC and IC along the proximal-distal axis.

For cell counting, the "spots" function in Imaris was used to count endocardial or myocardial nuclei in the region demarcated as the OFT. All cell area and circularity measurements were performed using ImageJ (Fiji) software as described previously (Auman et al., 2007). Briefly, the OC and IC walls of the OFT were partially reconstructed (~5 um thick for the myocardium and ~0.5 um thick for the endocardium),

using the slices where lateral boundaries of cells are clearly visible, and then collapsed into maximum intensity projections. Cellular boundaries were traced using anti-Dm-grasp, a basolateral marker of cardiomyocytes, and anti-dsRed, which labels mCherry on endocardial cell surfaces in *Tg*(*kdrl*:*HsHRAS-mCherry*)-expressing embryos.

Statistics and replication

Statistical analysis was performed using GraphPad (Prism). First, a Shapiro-Wilk test was run to test normality of data. If data were normal, a Student's T-test (two-tailed) was performed. If the data were not normal, a Mann-Whitney U-test was performed instead. For all experiments, >= 2 technical replicates and >= 5 biological replicates were analyzed, unless mentioned otherwise, when alternative methodologies were used to confirm data.

Acknowledgements

Chapter 2, in full, is currently being prepared for submission to *eLife* for publication of the material. Sidhwani, Pragya; Boezio Giuilia; Yang, Hongbo; Chi, Neil; Roman, Beth; Stainier, Didier; Yelon, Deborah. "Cardiac function modulates endocardial cell dynamics to scuplt the cardiac outflow tract." *In preparation.* The dissertation author was the primary investigator and author of this material.

Figure 2-1: OFT development is characterized by endocardial and myocardial cell accumulation. (A-B) Cartoons illustrating prominent structural landmarks in frontal views of the OFT at 36 hpf (A) and 51 hpf (B). Eye and arrows demonstrate the angle of imaging. Note that at 36 hpf, second heart field cells are still differentiating, so the distal edge is defined using the point of aortic arch bifurcation (A). In all images, endocardial cells are shown in green and myocardial cells in red. Representative lateral slices (C, G) and medial sections (D, H) of the OFT in *Tg(fli1a:negfp)* embryos, where endocardial nuclei are marked by GFP fluorescence, labeled with an antibody against the myocardial marker Dm-grasp, demonstrate that the number of endocardial cells increases drastically between 36 hpf (C, D) and 51 hpf (I, J), as quantified in (S) and (T) (n = 12, 9 embryos; experimental replicates N = 3; asterisks mark significant difference from 36 hpf, $p<0.0001$, Student's T test). Partially reconstructed endocardial walls of the inner (E, I) and outer (F, J) curvatures of the Dm-grasp-labeled OFT carrying the transgene *Tg*(*kdrl*:*HsHRAS-mCherry*) to outline endocardial cells, illustrate that endocardial cells get smaller (U) and rounder (V) over time (n= 7, 9 embryos; 29, 59, 27, 43 cells; N= 3; asterisks mark significant difference from similar wall at 36 hpf, $p<0.001$, Mann Whitney test). Three-dimensional reconstructions (K, O) and medial sections (L, P) of the OFT myocardium labeled with *Tg*(*myl7*:*H2A-mCherry*) to visualize myocardial nuclei reveal a similar expansion of myocardial cell number between 36 hpf (K, L) and 51 hpf (O, P), which is graphically represented in (W) and (X) (n= 6,6 embryos; N=1; asterisks mark significant difference from 36 hpf, $p<0.01$, Student's T test). Partial reconstructions of the OFT myocardial walls immunostained with anti-Dm-grasp at 36 hpf (M, N) and 51 hpf (Q, R) show that, as myocardial cells accumulate, they get larger specifically in the OC, while also getting more circular, trends that are graphically represented in (Y) and (Z), respectively (n= 8,8 embryos; 57, 79, 45, 64 cells; N=2; asterisks mark significant difference from similar wall at 36 hpf, $p<0.05$, Mann Whitney test). White dots indicate GFP+ (D, J) or mCherry+ (P, V) nuclei. Bars in (S), (T), (W), (X) represent mean and SEM. Bars in (U), (V), (Y), (Z) represent median and interquartile range.
Scale bar: 5 μm

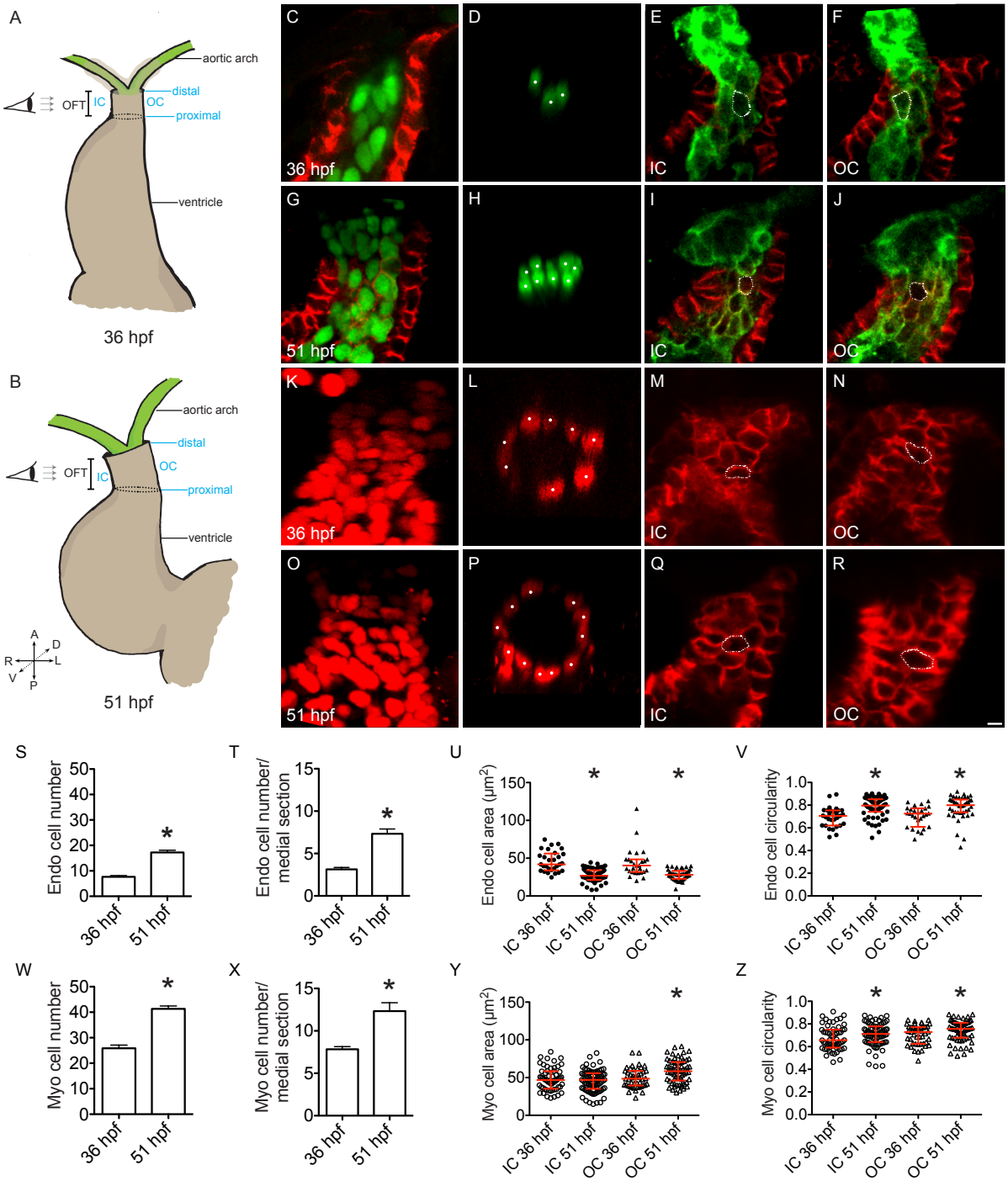
A
aortic arch
distal
OFT
IC
OC
proximal
ventricle
36 hpf
B
aortic arch
distal
OFT
IC
OC
proximal
ventricle
A
D
R
L
V
P
51 hpf
C
D
E
F
36 hpf
IC
OC
G
H
I
J
51 hpf
IC
OC
K
L
M
N
36 hpf
IC
OC
O
P
Q
R
51 hpf
IC
OC
S
Endo cell number
36 hpf
51 hpf
T
Endo cell number/ medial section
36 hpf
51 hpf
U
Endo cell area (μm²)
IC 36 hpf
IC 51 hpf
OC 36 hpf
OC 51 hpf
V
Endo cell circularity
IC 36 hpf
IC 51 hpf
OC 36 hpf
OC 51 hpf
W
Myo cell number
36 hpf
51 hpf
X
Myo cell number/ medial section
36 hpf
51 hpf
Y
Myo cell area (μm²)
IC 36 hpf
IC 51 hpf
OC 36 hpf
OC 51 hpf
Z
Myo cell circularity
IC 36 hpf
IC 51 hpf
OC 36 hpf
OC 51 hpf

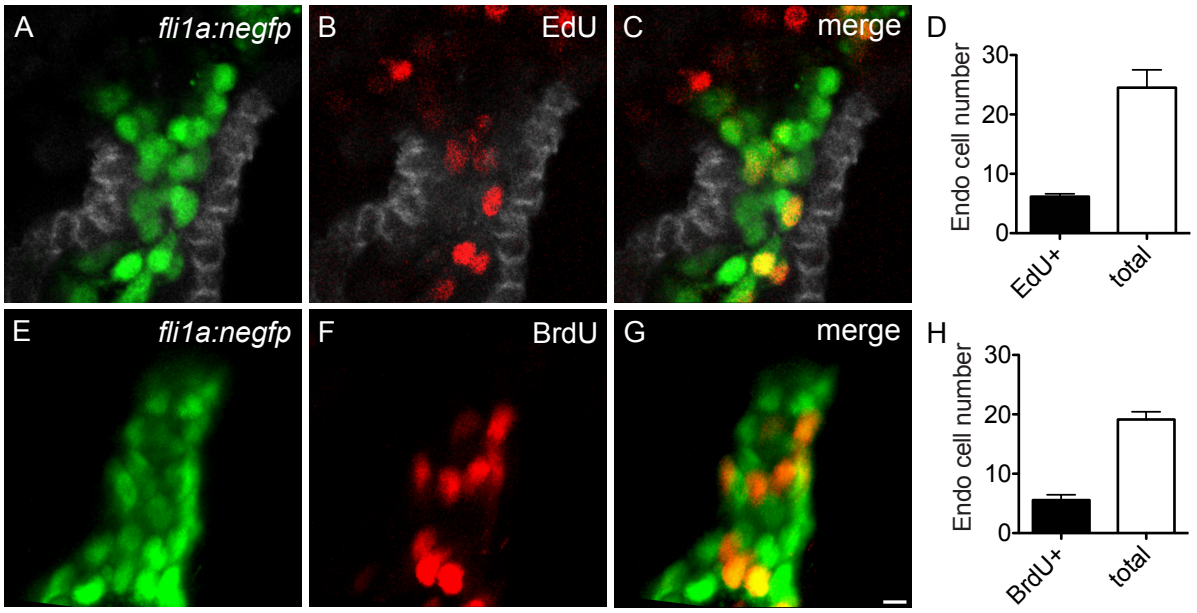

Figure 2-2: Endocardial proliferation supplements OFT endocardial growth. (A-D) (A-D) Representative lateral slices show that EdU (red) is incorporated into the OFT endocardium between 36 hpf and 51 hpf in *Tg(fli1a:negfp)* (green) embryos marked with anti-Dm-grasp (grey), suggesting that OFT endocardial cells also proliferate with a proliferation index (PI) of 25.8 ± 1.2 % during this period of OFT expansion (n=6 embryos, N=1). (E - H) BrdU assay confirms the EdU assay, since BrdU+ cells (red) are observed in *Tg(fli1a:negfp)* embryos when embryos are exposed to BrdU from 36 hpf to 51 hpf, with a PI of 28.9 ± 4.2 % (n= 14 embryos; N= 2). Bars represent mean and SEM.
Scale bar: 5 μm

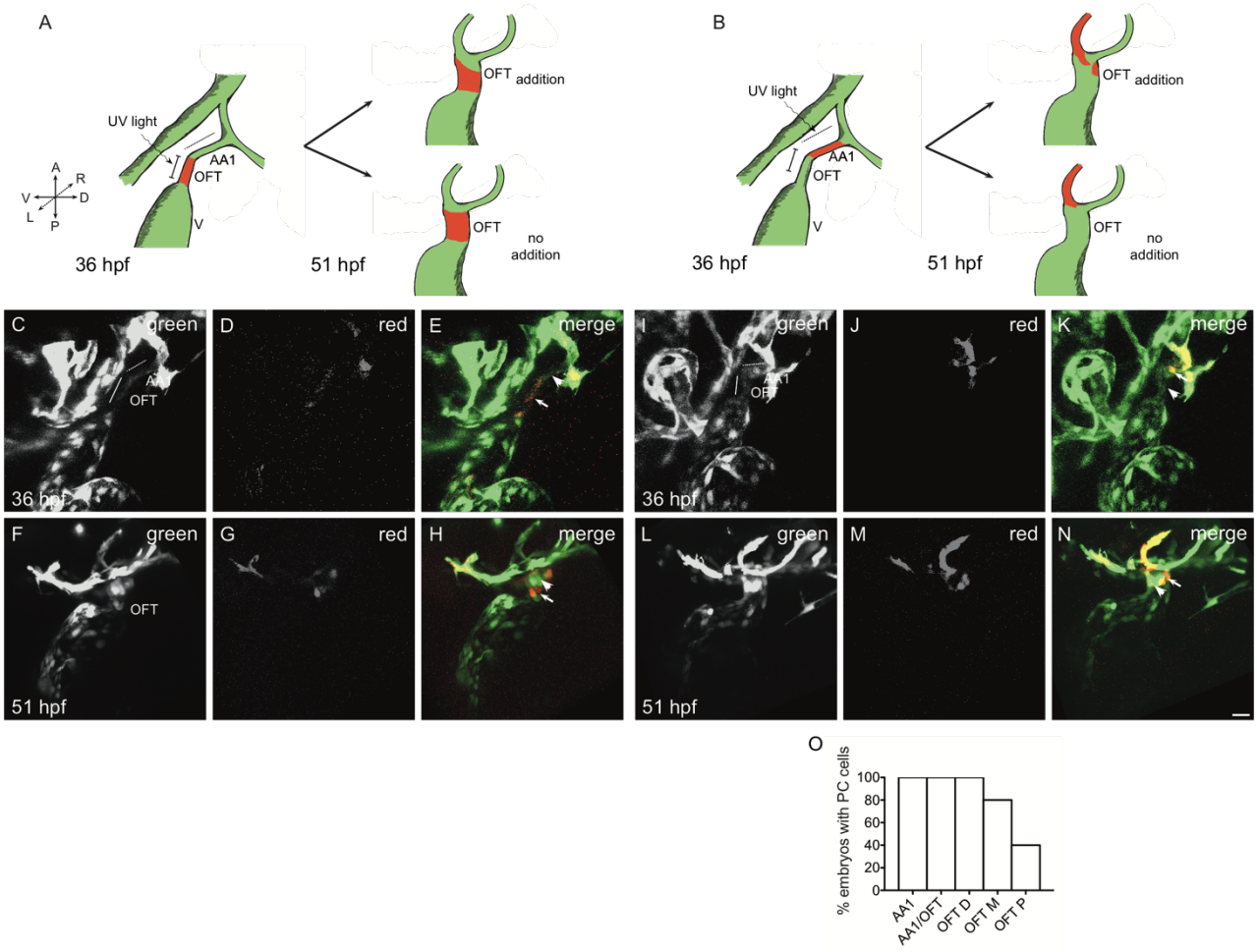

Figure 2-3: Endothelial cells from the aortic arches contribute to OFT endocardium. (A-B) Lateral view of the heart and aortic arches is depicted in cartoons outlining the scheme of photoconversion labeling experiments to assess contribution of external sources (A) or endothelial cells from aortic arch I (AA1) (B) to the OFT endocardium. (C-H) At 36 hpf, either the OFT endocardium (C- E) or the AA1 endothelium (I-K) were specifically photoconverted in *Tg*(*kdrl*:*dendra*) embryos, where the green-to-red photoconvertible protein is expressed under a pan-endothelial promoter. (F-H) In embryos where the OFT was photoconverted at 36 hpf, green-only cells were observed in the OFT at 51 hpf, indicating that extrinsic cells facilitate OFT growth between 36 and 51 hpf (n=3 embryos; N=2). (L-N) These cells appear to originate from the AA1, since red cells are found in the OFT at 51 hpf in embryos where the AA1 was photoconverted at 36 hpf. (O) Furthermore, these additional cells from the AA1 are frequently found in the distal region of the OFT (n=5 embryos; N=2). Dotted lines mark the AA1 and solid line indicates OFT endocardium. Arrowheads point to unphotoconverted cells and arrows indicate photoconverted cells in three-dimensional reconstructions.
Scale bar: 20 μm

Figure 2-4: Cardiac function is necessary to promote OFT growth. Lateral views of three-dimensional reconstructions demonstrate the wild-type OFT and ventricle (A, K) and *sih* OFT and ventricle (F, P) marked with anti-Dm-grasp (red) and *Tg(fli1a:negfp)* (green). Since Dm-grasp marks the basolateral boundaries of myocardial cells and not the cytoplasm, the endocardium is visible through the myocardial layer. Zoomed in views of the OFT region show that at 36 hpf, the overall OFT appears similar in wild-type (B) and *sih* mutants (G), which lack cardiac function (n= 5,4 embryos; N=2). However, by 51 hpf, whereas OFT endocardial and myocardial volumes have expanded significantly ($p<0.0005$, Student's T test) in wild-type (L), the *sih* OFT endocardium (Q) fails to develop, as quantified in (U) and (V) respectively, resulting in a significantly higher ratio of myocardial to endocardial volume in *sih* by 51 hpf (W) (n= 7,6 embryos; N=2; asterisks depict significant difference from wild-type at similar stage, $p<0.005$, Student's T test). Lateral (B′, G′, L′, Q′) and frontal (B″, G″, L″, Q″) views of smoothed OFT endocardial surfaces created using cytoplasmic GFP expression in *Tg*(*kdrl*:*grcfp*) clearly display these differences. Of note, the lateral side of the WT OFT at 36 hpf (B′) appears to transition into the frontal side at 51 hpf (L″), suggesting that the OFT rotates 90° during this time. Additionally, while the OFT endocardium broadens distally in wild-type (compare C-E, 36 hpf to M-O, 51 hpf; $p<0.05$, Student's T test), it collapses substantially in *sih* (H-J, 36 hpf; R-T, 51 hpf), as seen in medial sections of *Tg*(*fli1a*:*negfp*)-expressing embryos (C, H, M, R) as well as proximal (D, I, N, S), medial (C′, H′, M′, R′) and distal (E, J, O, T) surfaces of *Tg*(*kdrl*:*grcfp*)-expressing embryos, and quantified in (X) and (Y) (n= 6, 4 for 36 hpf; 5, 5 embryos for 51 hpf; N=2; asterisks depict significant differences from wild-type at similar positions, $p<0.005$, Student's T test). Lateral and frontal surfaces are oriented with the proximal end to the bottom. Proximal, medial and distal sections are oriented with the OFT outer curvature to the left. Bars represent mean and SEM.
Scale bar: 5 μm

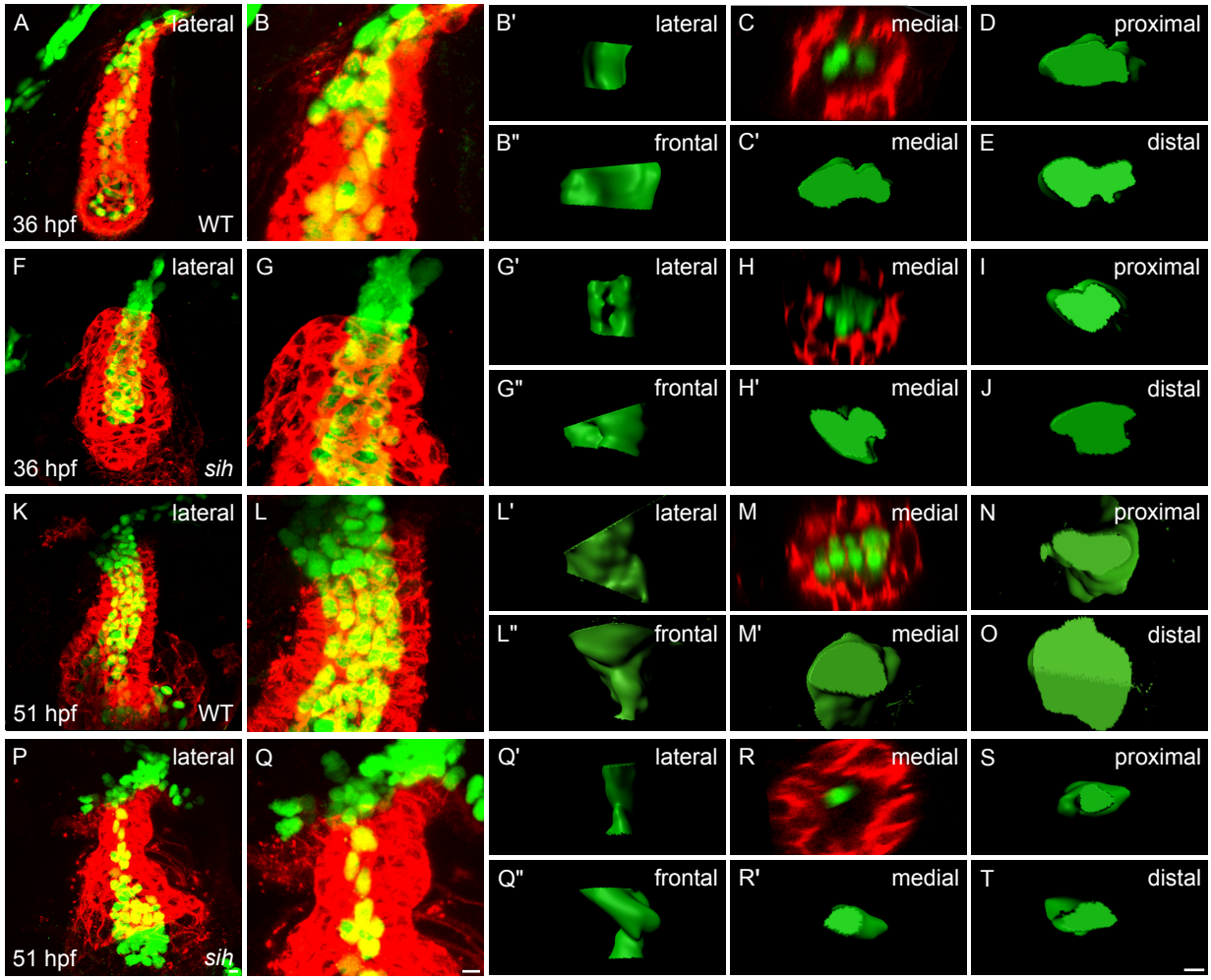
A
lateral
36 hpf
WT
B
B'
lateral
C
medial
D
proximal
B"
frontal
C'
medial
E
distal
F
lateral
36 hpf
sih
G
G'
lateral
H
medial
I
proximal
G"
frontal
H'
medial
J
distal
K
lateral
51 hpf
WT
L
L'
lateral
M
medial
N
proximal
L"
frontal
M'
medial
O
distal
P
lateral
51 hpf
sih
Q
Q'
lateral
R
medial
S
proximal
Q"
frontal
R'
medial
T
distal
U
Endo volume (μm3)
10000
8000
6000
4000
2000
0
WT
sih
WT
sih
36 hpf
51 hpf
*
V
Myo volume (μm3)
40000
30000
20000
10000
0
WT
sih
WT
sih
36 hpf
51 hpf
W
Myo:endo volume
20
15
10
5
0
WT
sih
WT
sih
36 hpf
51 hpf
*
X
Endo sectional area (μm2)
600
400
200
0
36 hpf WT
36 hpf sih
Proximal
Medial
Distal
Y
Endo sectional area (μm2)
600
400
200
0
51 hpf WT
51 hpf sih
*
*
*
Proximal
Medial
Distal

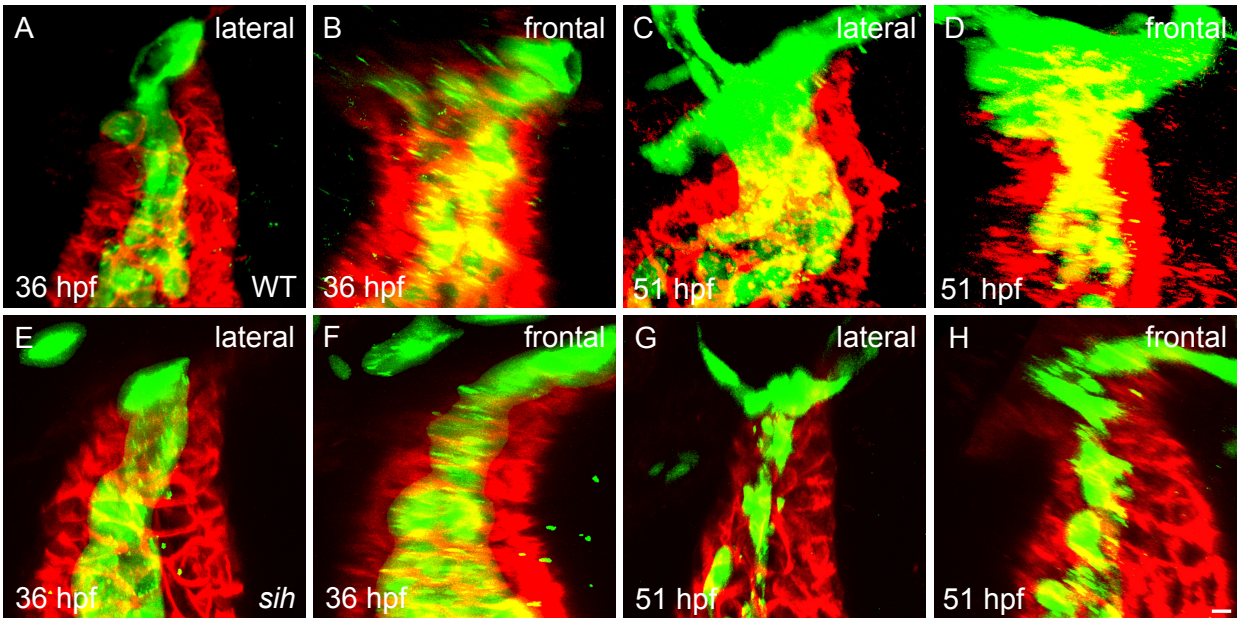

Figure 2-5: Function influences OFT endocardial growth. Three-dimensional reconstructions of lateral (A, C, E, G) and frontal (B, D, F, H) views of the OFT in wild-type (A-D) and *sih* (E-H) embryos labeled with *Tg*(*kdrl*:*grcfp*) (green) and anti-Dm-grasp (red), the surface representations of which are displayed in Fig. 2-4. Z-slices were captured in the lateral orientation at low sampling intervals and rotated in the Bitplane (Imaris) software to generate frontal views.

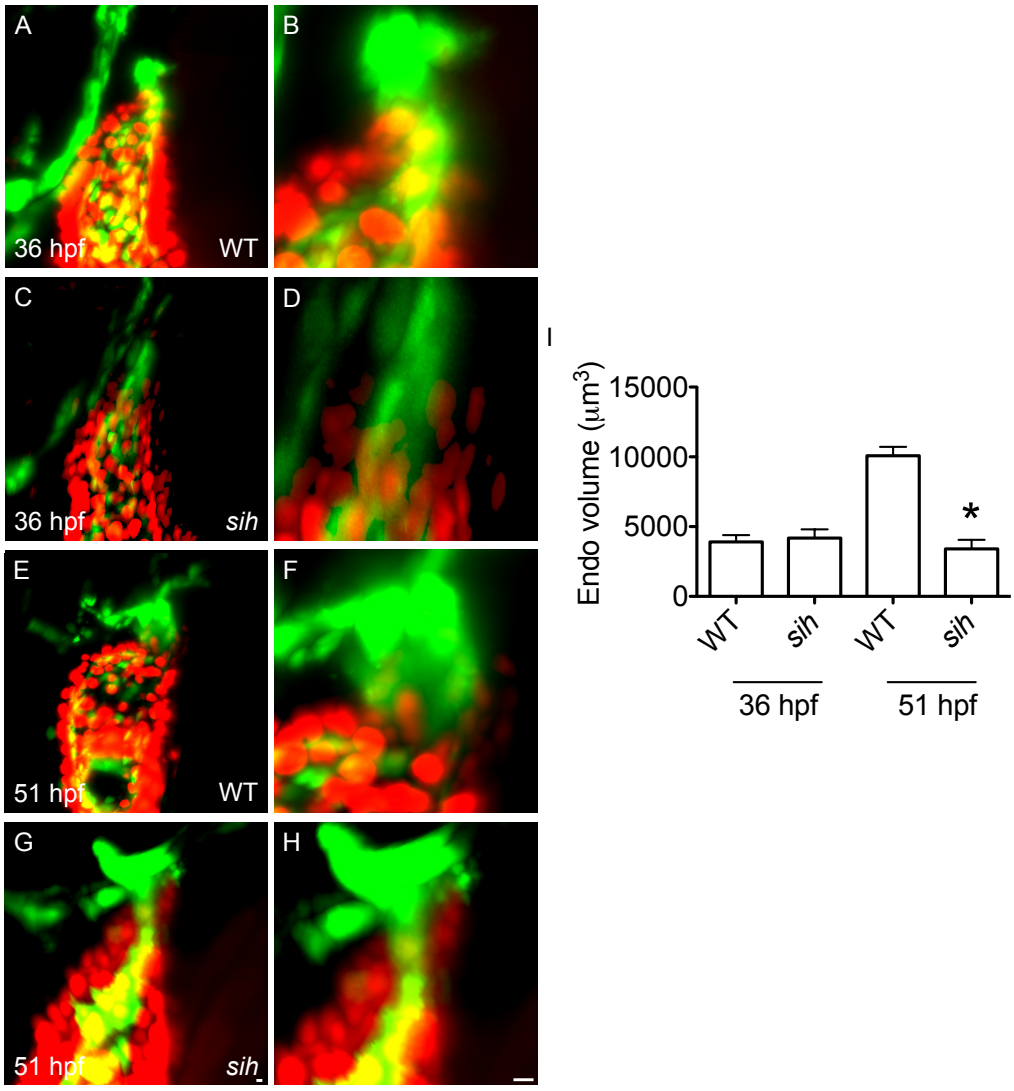

Figure 2-6: Live imaging confirms that OFT endocardial growth depends upon function. Lateral views of *Tg*(*kdrl*:*grcfp*);*Tg*(*myl7*:*h2a-mCherry*) embryos, where the endocardium is marked in green and myocardial nuclei in red. Left panel (A, C, E, G) shows views of the OFT on top of the ventricle; right panel (B, D, F, H) are zoomed in views of the OFT. At 36 hpf, the OFT appears similar in wild-type (A, B) and *sih* (C, D). However, by 51 hpf, the *sih* OFT endocardium (G, H) is markedly smaller in volume compared to wild-type (E, F), as quantified in (I). Note that while endocardial volume of each group is higher than its fixed counterpart (Fig. 4), the differences in endocardial volume between 36 hpf and 51 hpf embryos ($p<0.0001$, Student's T test) as well as wild-type and *sih* at 51 hpf (asterisks indicate significant difference from wild-type at similar stage, $p<0.0001$, Student's T test) are proportionately similar between fixed and live embryos. n=7, 3 embryos; N=1 for 36 hpf. n=6, 5 embryos; N=2 for 51 hpf. Bars represent mean and SEM.

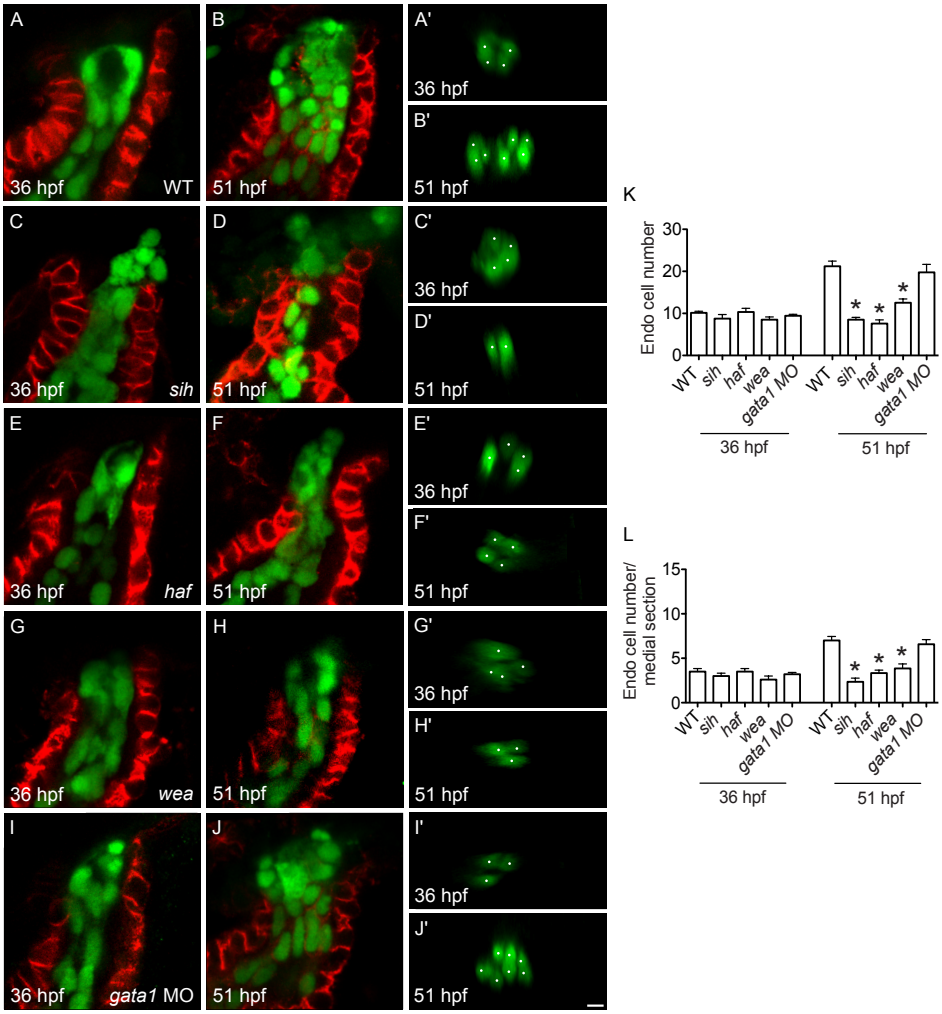

Figure 2-7: Function is essential for OFT endocardial accumulation in the OFT. Lateral slices (A-J) and medial sections (A′-J′) of *Tg*(*fli1a*:*negfp*) (green) embryos marked with anti-Dm-grasp (red) demonstrate that in wild-type embryos, the number of endocardial cells increases from 36 hpf (A, A′) to 51 hpf (B, B′) ($p<0.0001$, Student's T test). However, in the absence of cardiac function, as in *sih* mutants, endocardial cells fail to accrue in the OFT between 36 hpf (C, C′) and 51 hpf (D, D′). (E, E′, F, F′) *haf* (*vmhc*) mutants that lack ventricular function present with similar endocardial defects by 51 hpf, confirming that the phenotype is associated with functional defects and not particularly Tnnt2. (G, G′, H, H′) *wea* (*amhc*) mutants, which have non-contractile atria, and consequently reduced blood flow into the OFT, also exhibit a reduction in OFT endocardial cell number by 51 hpf. (I, I′, J, J′) However, *gata1* morphants that have fewer erythrocytes and therefore reduced shear forces, have a normal number of OFT endocardial cells. These differences are depicted in (K) and (L). n = 15, 8, 6, 6, 7 embryos for 36 hpf, 24, 6, 10, 13, 8 embryos for 51 hpf; N=2; asterisks represent significant differences from wild-type at similar stages, $p<0.05$, Student's T test. White dots indicate GFP+ nuclei. Bars represent mean and SEM.
Scale bar: 5 μm

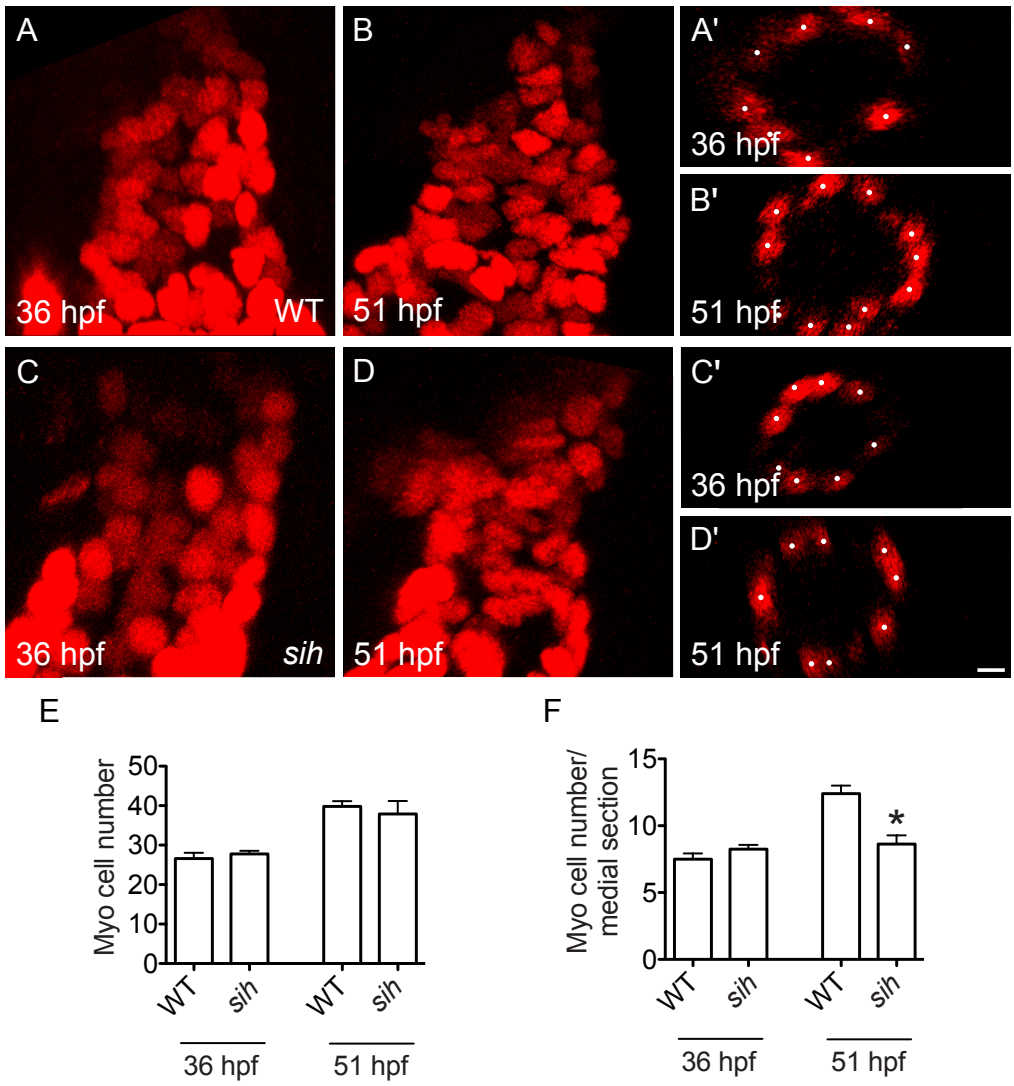

Figure 2-8: Function influences myocardial arrangement in the OFT. Three-dimensional reconstructions of *Tg*(*myl7*:*h2a-mCherry*) embryos at 36 hpf (A, C) and 51 hpf (B, D) show that at both stages, the total number of myocardial cells is similar between wild-type embryos (A-B) and *sih* embryos (C-D). However, whereas the number of cells in a medial section is comparable between wild-type (A′) and *sih* (C′) at 36 hpf, it is significantly reduced in *sih* by 51 hpf (D′) compared to wild-type (B′). These trends, which are quantified in (E) and (F), suggest that cardiomyocyte arrangement in the OFT is dependent on cardiac function. n= 6,8 embryos for 36 hpf; 5,8 embryos for 51 hpf; N=2; asterisks indicate significant difference from wild-type at similar stage; $p<0.05$, Student's T test. White dots represent cell counts. Bars depict mean and SEM. Scale bar: 5 μm

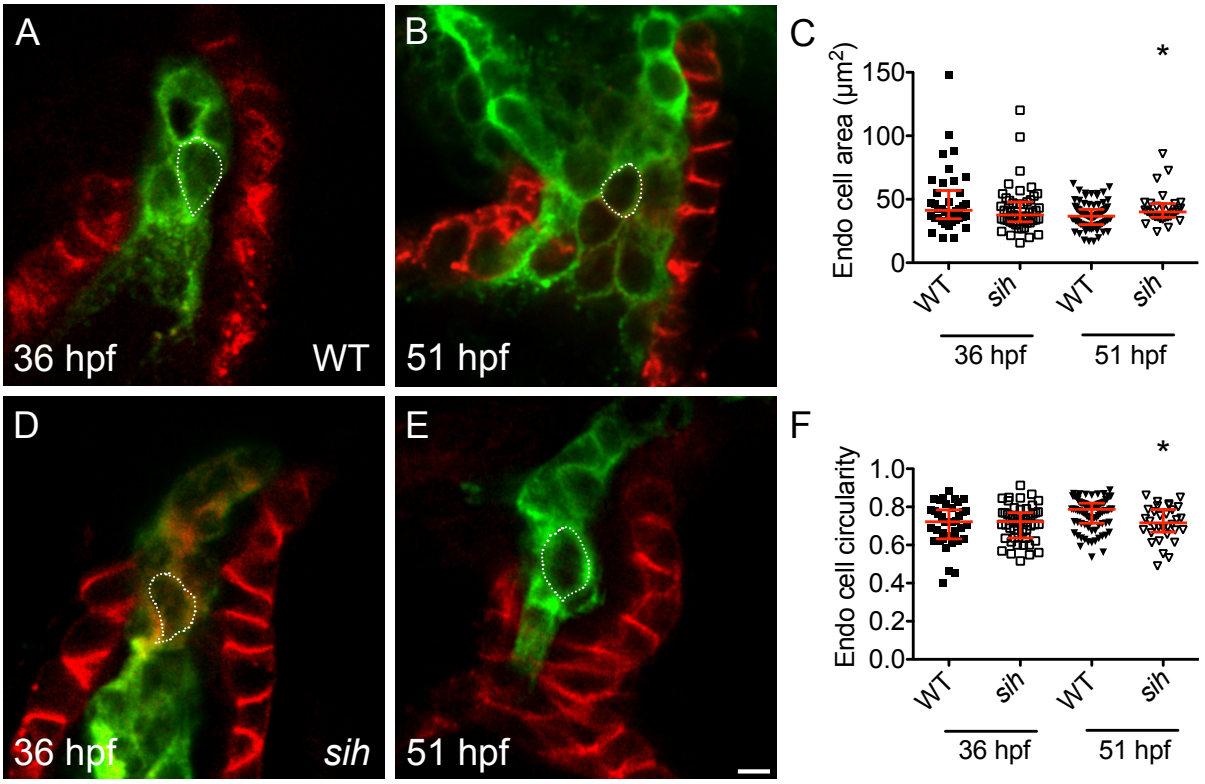

Figure 2-9: Function influences OFT endocardial cell size and shape. Lateral slices of *Tg*(*kdrl*:*mcherry-ras*) (green) marked with an antibody against Dm-grasp (red). OC and IC cells are grouped together due to technical challenges associated with isolating the walls within the collapsed endocardium in *sih*. At 36 hpf, endocardial cells are similar in area (C) and circularity (F) in wild-type (A) and *sih* mutants (C). However, by 51 hpf, whereas OFT endocardial cells become smaller (C) ($p<0.05$, Mann-Whitney test) and rounder (F) ($p<0.005$, Mann Whitney test) in wild-type (D), they remain large and long in *sih* (E) (n= 9, 8, 9, 5 embryos; 38, 51, 87, 30 cells; N= 3; asterisks indicate significant difference from wild-type at similar stage, $p<0.05$, Mann Whitney test). Red bars depict median and interquartile ranges.
Scale bar: 5 μm

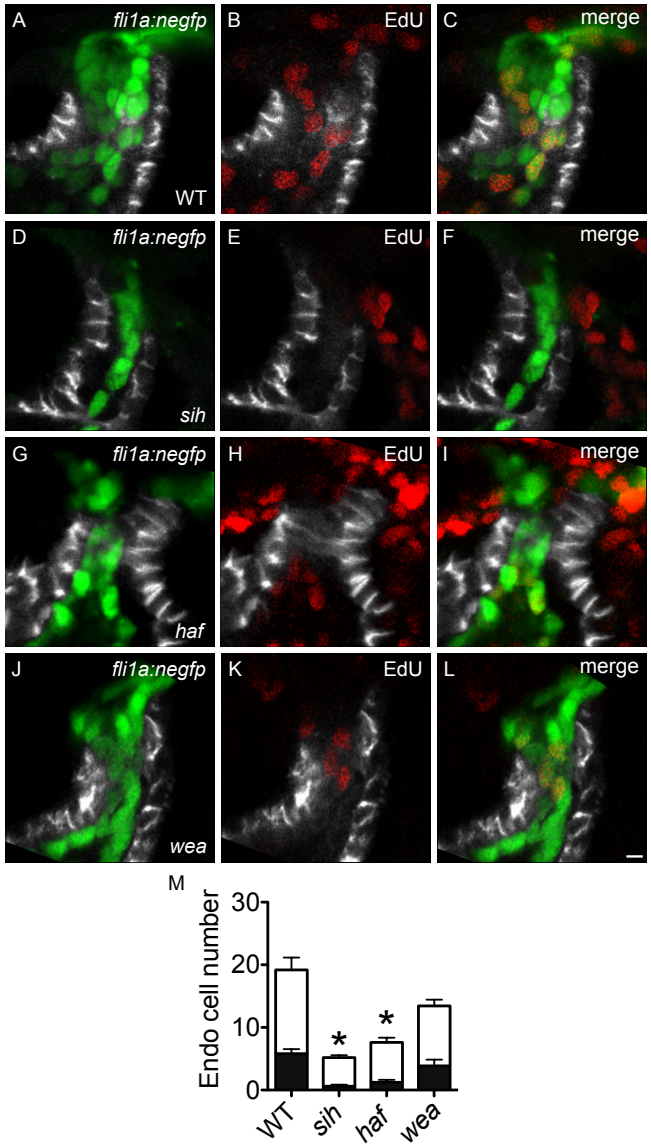

Figure 2-10: OFT endocardial proliferation depends upon functional inputs. Representative lateral slices of 51 hpf embryos labeled with *Tg*(*fli1a*:*negfp*) (green), anti-Dm-grasp (gray) and EdU (red). When wild-type (A-C), *sih* mutants (D-F), *haf* mutants (G-I) and *wea* mutants (J-L) are injected with EdU at 36 hpf, EdU incorporation is drastically reduced in *sih* (proliferation index = 10.2 ± 4.3 %) and *haf* (proliferation index = 15.6 ± 4.9 %) but not in *wea* (proliferation index = 27.8 ± 6.3 %) compared to wild-type (proliferation index = 29.6 ± 3.7 %) by 51 hpf (n=17, 10, 13, 7 embryos; N=2; asterisks signify significant difference in proliferation indices compared to wild-type, $p<0.05$, Student's T test). Black and white bars represent mean EdU+ and EdU- cells with SEM, respectively.
Scale bar: 5 μm

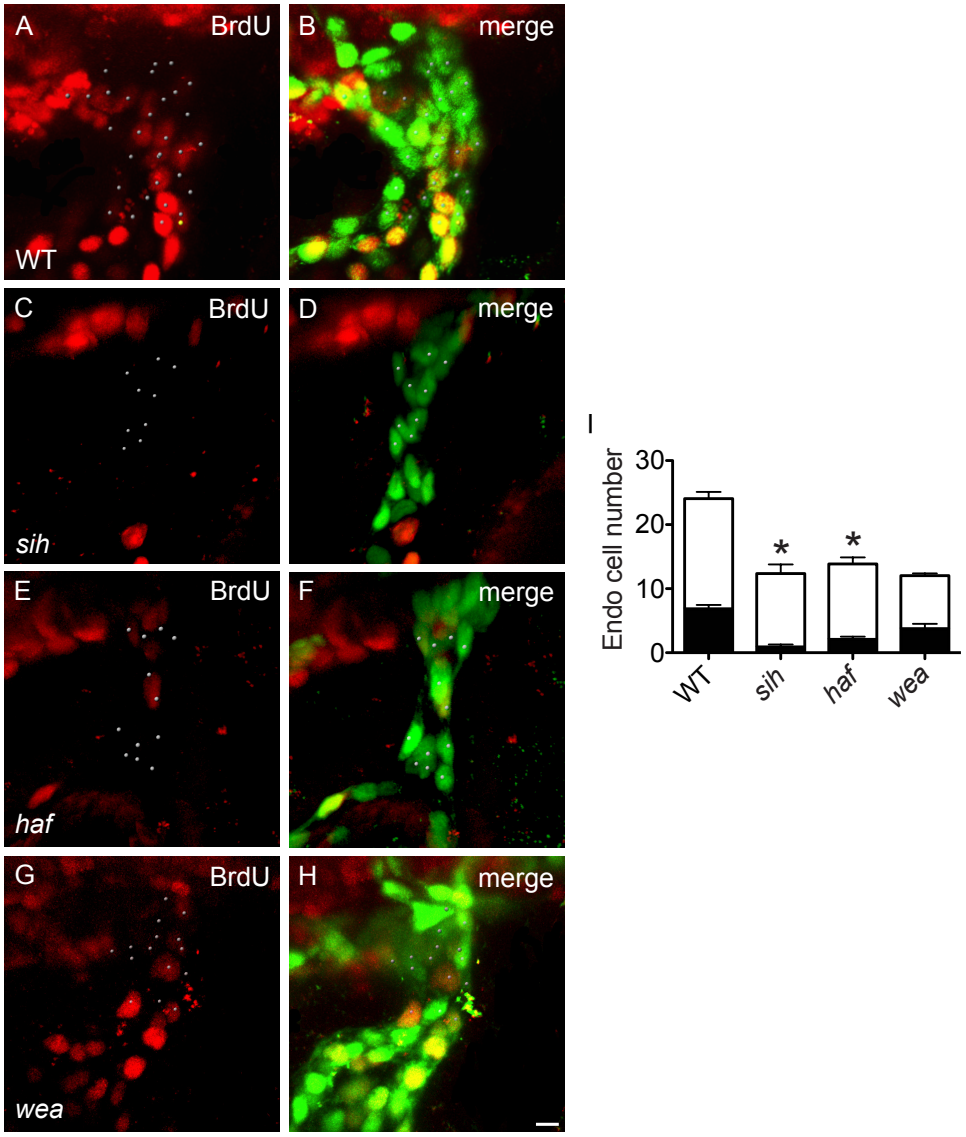

Figure 2-11: BrdU assay confirms that functional mutants have reduced OFT endocardial proliferation. (A-B) Three-dimensional reconstructions of *Tg*(*fli1a*:*negfp*) embryos (green) show that when wild-type embryos are incubated with BrdU (red) from 36 hpf to 51 hpf, the OFT endocardium contains BrdU+ cells at 51 hpf, resulting in a proliferation index of 28.5 ± 2.2 %. However, when *sih* (C-D) and *haf* (E-F) mutants are exposed to BrdU in a similar timeframe, fewer BrdU+ cells are present in the OFT by 51 hpf (proliferation index of *sih* = 8.2 ± 3.8 %; *haf* = 13.8 ± 2.7 %). (G-H) *wea* mutants have a proliferation index that is comparable to wild-type (proliferation index = 29.1 ± 4.4 %), as quantified in (I) (n= 21, 12, 12, 12; N=2; asterisks mark significant difference in PI from wild-type; $p<0.001$, Student's T test). Bars depict mean and SEM of BrdU+ cells (black) and BrdU- cells (white). Scale bar: 5 μm

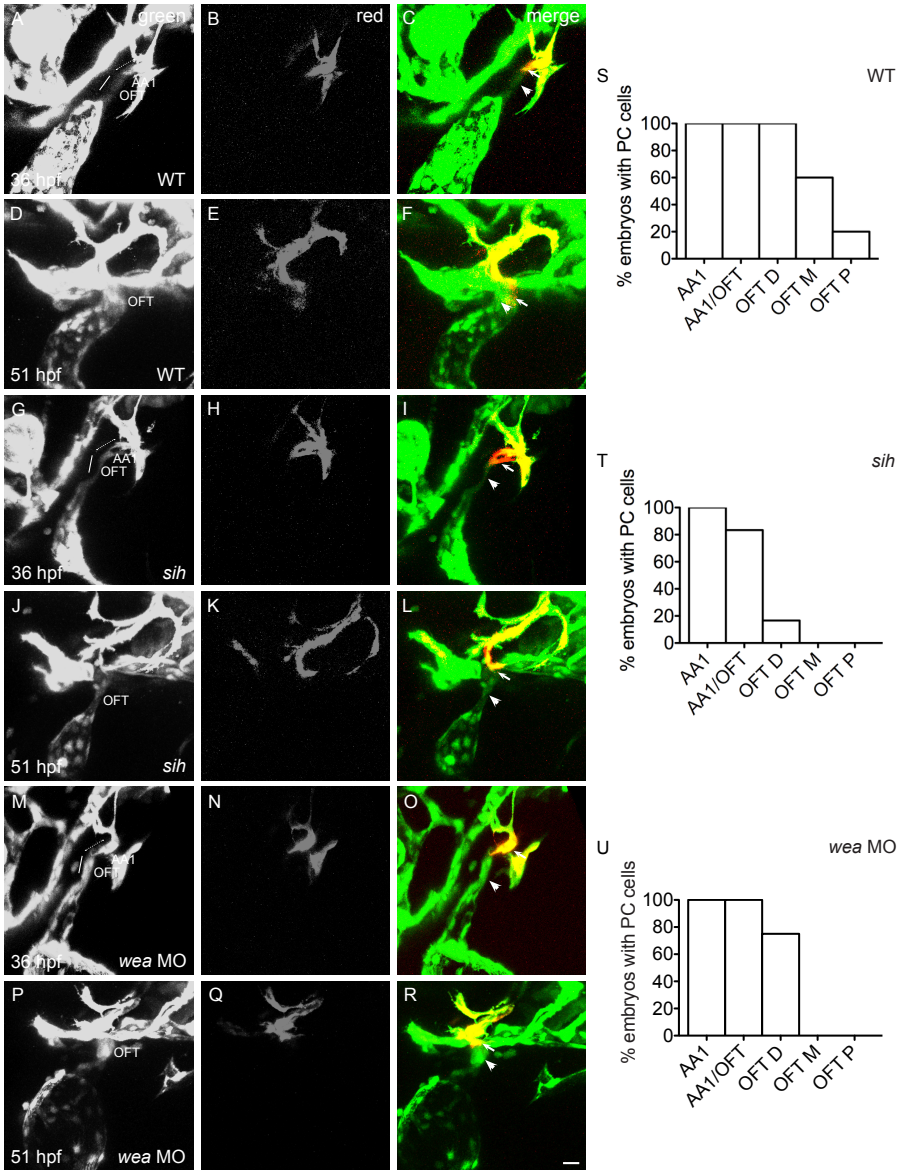

Figure 2-12: Cardiac function promotes endothelial addition from the aortic arches. Lateral views of three-dimensional reconstructions depict the AA1 photoconverted at 36 hpf in wild-type (A-C), *sih* (G-I) or *wea* morphants (M-O) expressing *Tg*(*kdrl*:*dendra*). (D-F) By 51 hpf, photoconverted cells are routinely found in the distal, medial and proximal regions of the wild-type OFT (n= 5 embryos; N=2). In contrast, in *sih* mutants (J-L) and *wea* morphants (P-R), photoconverted cells are less often present in the distal OFT and entirely absent from medial and distal regions by 51 hpf. These differences are represented graphically in S-U. n=6 embryos for *sih*, 5 embryos for *wea* MO; N=2. Arrowheads and arrows point to unphotoconverted and photoconverted cells, respectively. Dotted lines mark AA1 and solid lines mark OFT.
Scale bar: 20 μm

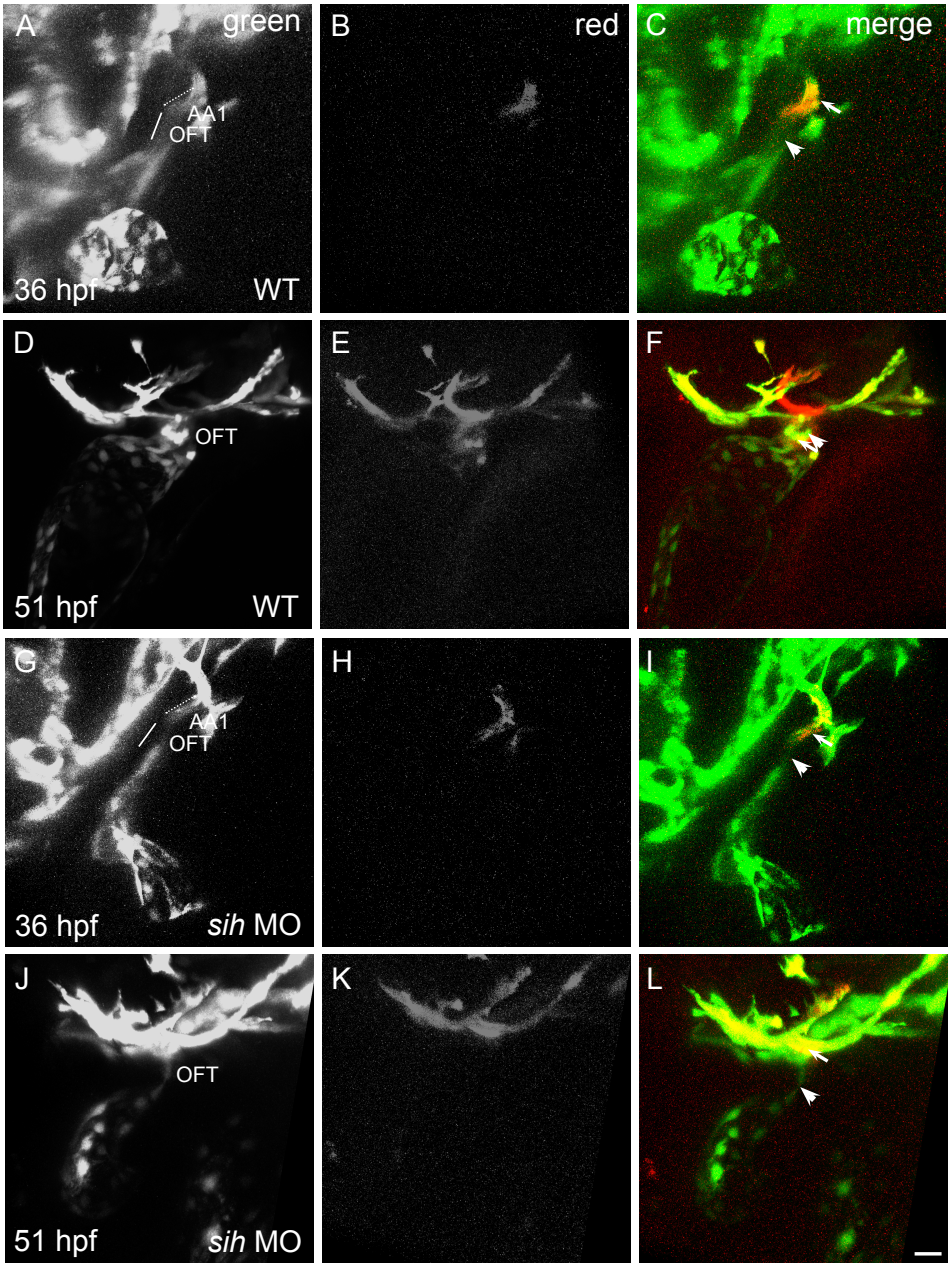

Figure 2-13: *sih* morphants recapitulate defects in OFT endothelial addition observed in *sih* mutants. In wild-type controls expressing the transgene *Tg*(*kdrl*:*dendra*), photoconversion of the AA1 at 36 hpf (A-C) leads to photoconverted cells being present in the OFT by 51 hpf (D-F). This is not the case in *sih* morphants, where photoconverted cells are not present in the OFT at 51 hpf (J-L) when the AA1 is photoconverted at 36 hpf (G-I). Arrowheads and arrows indicate unphotoconverted and photoconverted cells, respectively. Solid line and dotted line mark OFT and AA1, respectively. n= 5, 5 embryos; N=2.
Scale bar: 20 μm

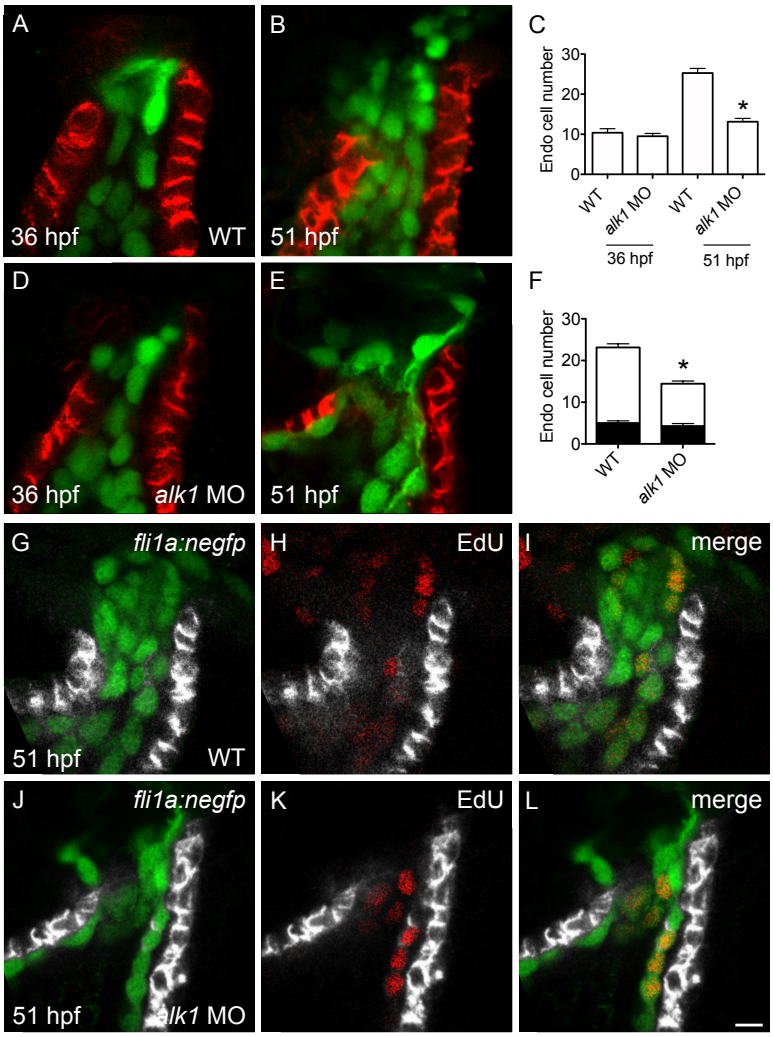

Figure 2-14: Alk1 is required for endocardial accumulation but not proliferation in the OFT. Representative lateral slices of *Tg*(*fli1a*:*negfp*) (green) embryos immunostained with an antibody against Dm-grasp (red in A-B, D-E; gray in G-L) illustrate that at 36 hpf, wild-type controls (A) and *alk1* morphants (D) have similar number of endocardial cells in the OFT (n= 5,8; N=2). However, by 51 hpf, *alk1* morphants (E) have strikingly fewer OFT endocardial cells compared to wild-type (B), as quantified in (C) (n=14, 16; N=2; asterisks mark significant difference from controls, $p<0.0001$, Student's T test). This reduction is not a consequence of defective proliferation, as the number of EdU+ cells (red) in the *alk1* morphant OFT (J-L) is similar to wild-type (G-I), resulting in a proliferation index (PI) of 29.1 ± 2.7 %, which is significantly higher than that of wild-type (PI = 21.5 ± 1.9 %), as seen in (F) (n= 8, 7 embryos; N=2; asterisk represents significant difference in PI from control, $p<0.05$, Student's T test. Bars in (C) represent mean endocardial cell number and SEM; bars in (F) represent mean and SEM of EdU+ (black) and EdU- cells (Zhou et al.), respectively.

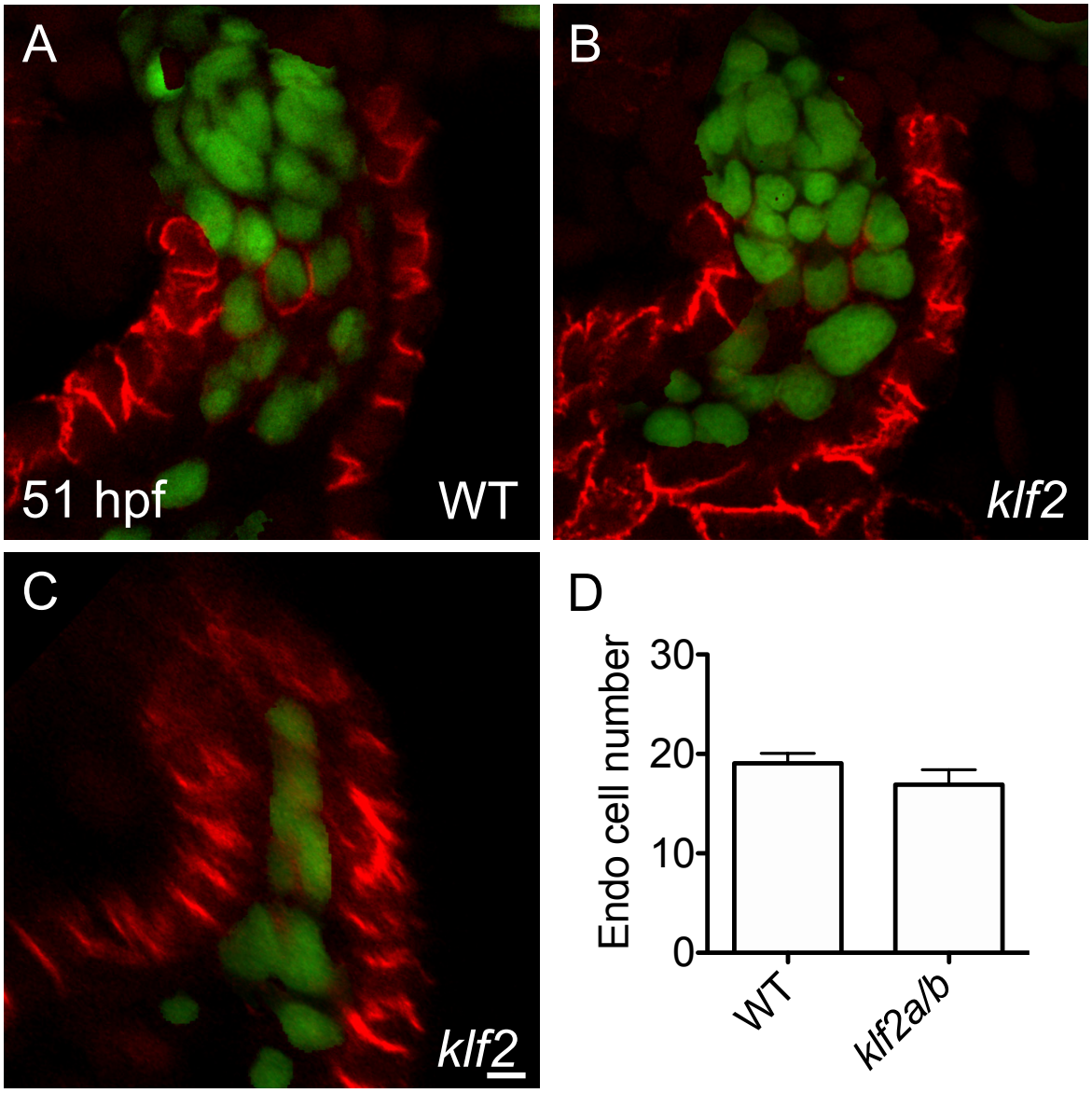

Figure 2-15: Mechanically induced transcription factor Klf2 partially regulates OFT endocardial accumulation. Representative lateral slices of *Tg(fli1a:negfp)* embryos labeled with anti-Dm-grasp (red) and the nuclear marker DAPI, where DAPI is masked using GFP fluorescence (green) show that at 51 hpf, whereas the wild-type embryo has ~20 endocardial cells in the OFT, *klf2* mutants can exhibit normal number of cells (B) or fewer cells (C). *klf2* mutants with fewer OFT endocardial cells demonstrate thinned and elongated OFTs, as in (C). However, since the phenotype is incompletely penetrant, the difference in total number of OFT endocardial cells is not significant, as seen in (D). n= 18, 11 embryos; N=3. Graphs display mean and SEM.
Scale bar: 5 μm

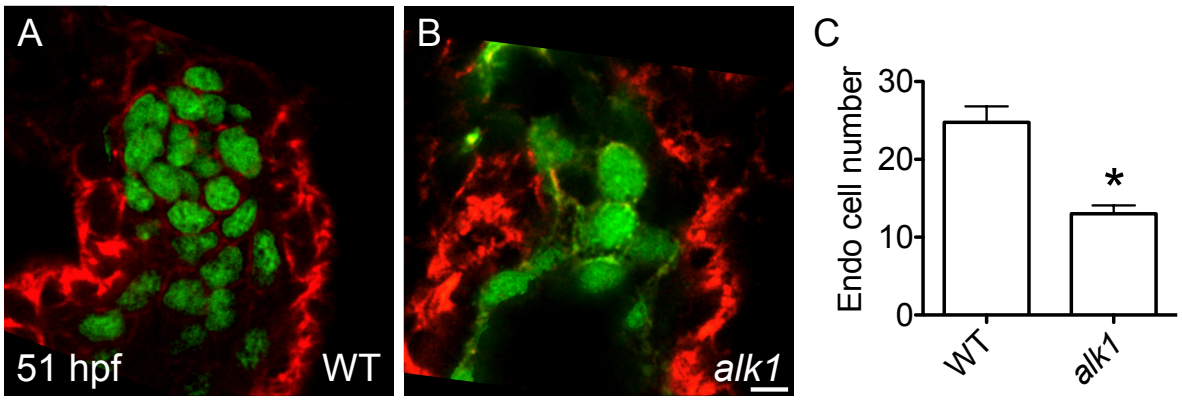

Figure 2-16: *alk1* mutants phenocopy *alk1* morphants with respect to the OFT phenotype. Representative slices of *Tg(kdrl:GFP)* embryos marked with phalloidin (red) and the nuclear marker TO-PRO-3, where TO-PRO-3 is masked using green fluorescence (green) show that, similar to *alk1* morphants, *alk1* mutants have a significant reduction in OFT endocardial cells, as quantified in (C). n=4, 4 embryos; N=1; $p<0.01$, Student's T test. Graphs show mean and SEM.
Scale bar: 5 μm

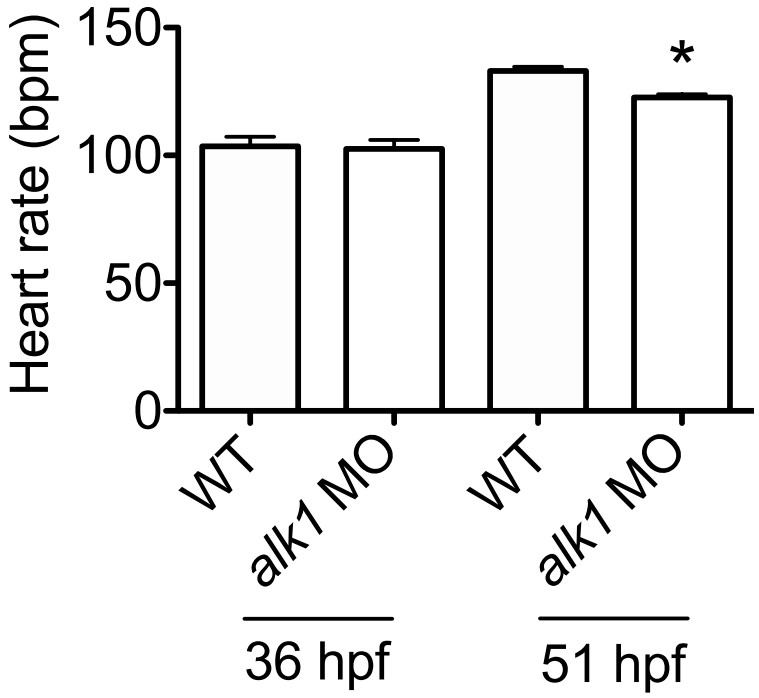

Figure 2-17: *alk1* morphants have reduced heart rate by 51 hpf. Heart rate was calculated by counting beats for 30 seconds under a stereoscope. At 36 hpf, the heart rate is comparable between wild-type and *alk1* morphants. However, by 51 hpf, *alk1* morphants have a small but significant reduction in heart rate (n= 4, 4, 11, 11 embryos; N=3; asterisks depict significant difference from wild-type at similar stage, $p<0.0001$, Student's T test). Mean and SEM are shown.

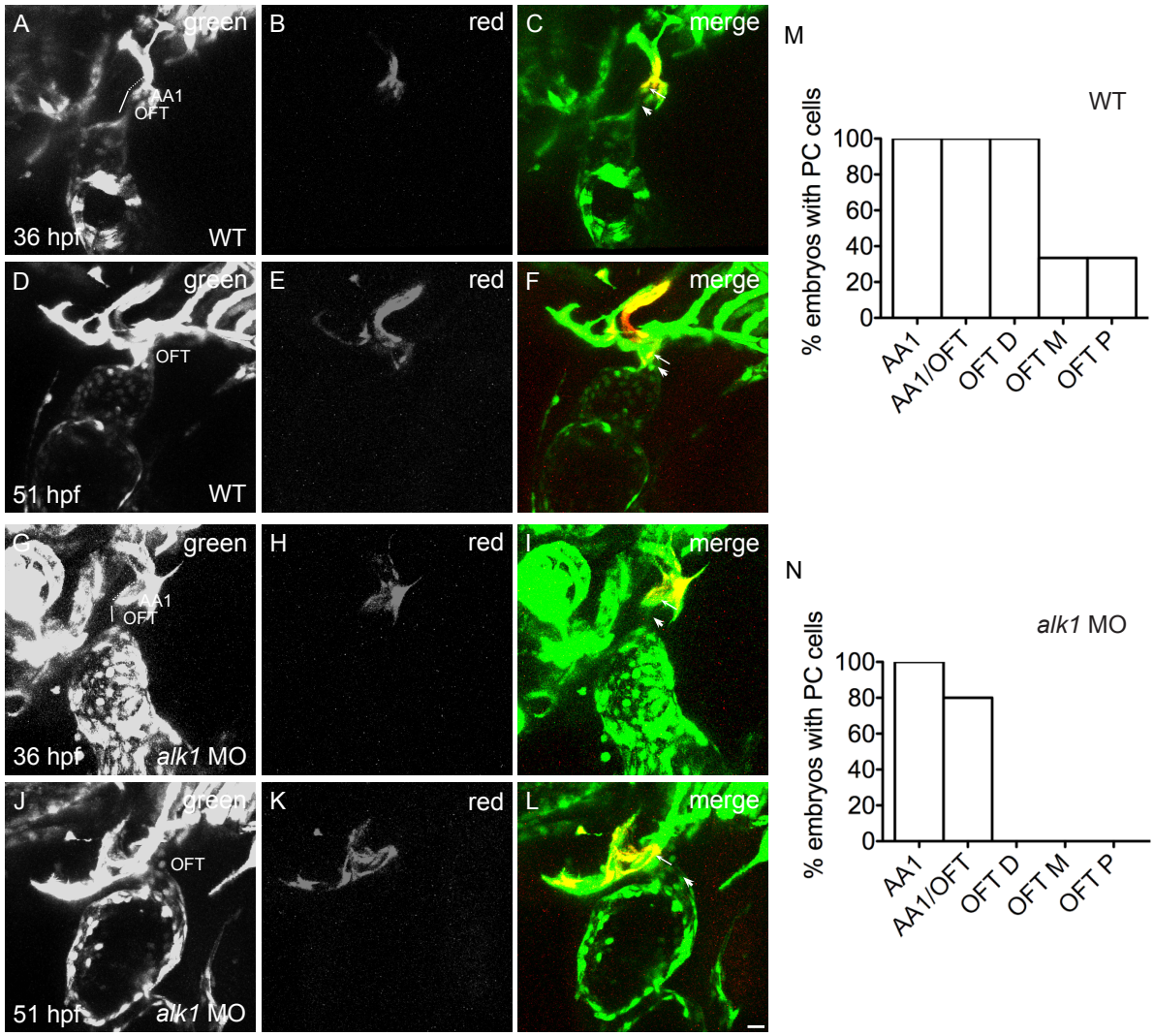

Figure 2-18: Alk1 is necessary for endothelial addition for OFT growth. In wild-type embryos, when the AA1 is photoconverted at 36 hpf (A-C), photoconverted cells are present in the distal, medial and proximal OFT by 51 hpf (D-F) (n= 3; N=2). However, in *alk1* morphants, AA1 cells photoconverted at 36 hpf (G-I) fail to accrete to the OFT by 51 hpf (J-L) (n=5; N=2). These differences are represented in (M) and (N). Arrowheads and arrows point to unphotoconverted and photoconverted cells, respectively. Dotted lines mark AA1 and solid lines mark OFT.
Scale bar: 20 μm

References

Alexander, J., Stainier, D.Y., Yelon, D. (1998). Screening Mosaic F1 Females for Mutations Affecting Zebrafish Heart Induction and Patterning. *Dev Genet*, *22*, 288-299.

Anton, H., Harlepp, S., Ramspacher, C., Wu, D., Monduc, F., Bhat, S., Liebling, M., Paoletti, C., Charvin, G., Freund, J.B., Vermot, J. (2013). Pulse Propagation by a Capacitive Mechanism Drives Embryonic Blood Flow. *Development*, *140*, 4426-4434.

Auman, H.J., Coleman, H., Riley, H.E., Olale, F., Tsai, H.J., Yelon, D. (2007). Functional Modulation of Cardiac Form through Regionally Confined Cell Shape Changes. *PLoS Biol*, *5*, e53.

Berdougo, E., Coleman, H., Lee, D.H., Stainier, D.Y., Yelon, D. (2003). Mutation of Weak Atrium/Atrial Myosin Heavy Chain Disrupts Atrial Function and Influences Ventricular Morphogenesis in Zebrafish. *Development*, *130*, 6121-6129.

Biechler, S.V., Junor, L., Evans, A.N., Eberth, J.F., Price, R.L., Potts, J.D., Yost, M.J., Goodwin, R.L. (2014). The Impact of Flow-Induced Forces on the Morphogenesis of the Outflow Tract. *Front Physiol*, *5*, 225.

Chen, H., Brady Ridgway, J., Sai, T., Lai, J., Warming, S., Chen, H., Roose-Girma, M., Zhang, G., Shou, W., Yan, M. (2013). Context-Dependent Signaling Defines Roles of Bmp9 and Bmp10 in Embryonic and Postnatal Development. *Proc Natl Acad Sci U S A*, *110*, 11887-11892.

Chen, H., Shi, S., Acosta, L., Li, W., Lu, J., Bao, S., Chen, Z., Yang, Z., Schneider, M.D., Chien, K.R., Conway, S.J., Yoder, M.C., Haneline, L.S., Franco, D., Shou, W. (2004). Bmp10 Is Essential for Maintaining Cardiac Growth During Murine Cardiogenesis. *Development*, *131*, 2219-2231.

Chi, N.C., Shaw, R.M., De Val, S., Kang, G., Jan, L.Y., Black, B.L., Stainier, D.Y. (2008). Foxn4 Directly Regulates Tbx2b Expression and Atrioventricular Canal Formation. *Genes Dev*, *22*, 734-739.

Cho, D., Kim, S., Kim, M., Seo, Y.H., Kim, W., Kang, S.H., Park, S.M., Shim, W. (2012). Two Cases of High Output Heart Failure Caused by Hereditary Hemorrhagic Telangiectasia. *Korean Circ J*, *42*, 861-865.

Choi, J., Dong, L., Ahn, J., Dao, D., Hammerschmidt, M., Chen, J.N. (2007). Foxh1 Negatively Modulates Flk1 Gene Expression and Vascular Formation in Zebrafish. *Dev Biol*, *304*, 735-744.

Clark, P.R., Jensen, T.J., Kluger, M.S., Morelock, M., Hanidu, A., Qi, Z., Tatake, R.J., Pober, J.S. (2011). Mek5 Is Activated by Shear Stress, Activates Erk5 and Induces Klf4 to Modulate Tnf Responses in Human Dermal Microvascular Endothelial Cells. *Microcirculation*, *18*, 102-117.

Cohen, E.D., Wang, Z., Lepore, J.J., Lu, M.M., Taketo, M.M., Epstein, D.J., Morrisey, E.E. (2007). Wnt/Beta-Catenin Signaling Promotes Expansion of Isl-1-Positive Cardiac Progenitor Cells through Regulation of Fgf Signaling. *J Clin Invest*, *117*, 1794-1804.

Collins, M.M., Stainier, D.Y. (2016). Organ Function as a Modulator of Organ Formation: Lessons from Zebrafish. *Curr Top Dev Biol*, *117*, 417-433.

Cooke, J.E., Kemp, H.A., Moens, C.B. (2005). Epha4 Is Required for Cell Adhesion and Rhombomere-Boundary Formation in the Zebrafish. *Curr Biol*, *15*, 536-542.

Cortes, C., Francou, A., De Bono, C., Kelly, R.G. (2018). Epithelial Properties of the Second Heart Field. *Circ Res*, *122*, 142-154.

Corti, P., Young, S., Chen, C.Y., Patrick, M.J., Rochon, E.R., Pekkan, K., Roman, B.L. (2011). Interaction between Alk1 and Blood Flow in the Development of Arteriovenous Malformations. *Development*, *138*, 1573-1582.

Cross, L.M., Cook, M.A., Lin, S., Chen, J.N., Rubinstein, A.L. (2003). Rapid Analysis of Angiogenesis Drugs in a Live Fluorescent Zebrafish Assay. *Arterioscler Thromb Vasc Biol*, *23*, 911-912.

de Pater, E., Clijsters, L., Marques, S.R., Lin, Y.F., Garavito-Aguilar, Z.V., Yelon, D., Bakkers, J. (2009). Distinct Phases of Cardiomyocyte Differentiation Regulate Growth of the Zebrafish Heart. *Development*, *136*, 1633-1641.

Dietrich, A.C., Lombardo, V.A., Veerkamp, J., Priller, F., Abdelilah-Seyfried, S. (2014). Blood Flow and Bmp Signaling Control Endocardial Chamber Morphogenesis. *Dev Cell*, *30*, 367-377.

Eder, D., Aegerter, C., Basler, K. (2017). Forces Controlling Organ Growth and Size. *Mech Dev*, *144*, 53-61.

El Robrini, N., Etchevers, H.C., Ryckebusch, L., Faure, E., Eudes, N., Niederreither, K., Zaffran, S., Bertrand, N. (2016). Cardiac Outflow Morphogenesis Depends on Effects of Retinoic Acid Signaling on Multiple Cell Lineages. *Dev Dyn*, *245*, 388-401.

Felker, A., Prummel, K.D., Merks, A.M., Mickoleit, M., Brombacher, E.C., Huisken, J., Panakova, D., Mosimann, C. (2018). Continuous Addition of Progenitors Forms the Cardiac Ventricle in Zebrafish. *Nat Commun*, *9*, 2001.

Francou, A., De Bono, C., Kelly, R.G. (2017). Epithelial Tension in the Second Heart Field Promotes Mouse Heart Tube Elongation. *Nat Commun*, *8*, 14770.

Francou, A., Kelly, R.G., 2016. Properties of Cardiac Progenitor Cells in the Second Heart Field, in: Nakanishi, T., Markwald, R.R., Baldwin, H.S., Keller, B.B., Srivastava, D., Yamagishi, H. (Eds.), Etiology and Morphogenesis of Congenital Heart Disease: From Gene Function and Cellular Interaction to Morphology, Tokyo, pp. 177-182.

Francou, A., Saint-Michel, E., Mesbah, K., Kelly, R.G. (2014). Tbx1 Regulates Epithelial Polarity and Dynamic Basal Filopodia in the Second Heart Field. *Development*, *141*, 4320-4331.

Galvez-Santisteban, M., Chen, D., Zhang, R., Serrano, R., Nguyen, C., Zhao, L., Nerb, L., Masutani, E.M., Vermot, J., Burns, C.G., Burns, C.E., Del Alamo, J.C., Chi, N.C. (2019). Hemodynamic-Mediated Endocardial Signaling Controls in Vivo Myocardial Reprogramming. *Elife*, *8*.

Goddard, L.M., Duchemin, A.L., Ramalingan, H., Wu, B., Chen, M., Bamezai, S., Yang, J., Li, L., Morley, M.P., Wang, T., Scherrer-Crosbie, M., Frank, D.B., Engleka, K.A., Jameson, S.C., Morrisey, E.E., Carroll, T.J., Zhou, B., Vermot, J., Kahn, M.L. (2017). Hemodynamic Forces Sculpt Developing Heart Valves through a Klf2-Wnt9b Paracrine Signaling Axis. *Dev Cell*, *43*, 274-289 e275.

Goussous, T., Haynes, A., Najarian, K., Daccarett, M., David, S. (2009). Hereditary Hemorrhagic Telangiectasia Presenting as High Output Cardiac Failure During Pregnancy. *Cardiol Res Pract*, *2009*, 437237.

Guner-Ataman, B., Paffett-Lugassy, N., Adams, M.S., Nevis, K.R., Jahangiri, L., Obregon, P., Kikuchi, K., Poss, K.D., Burns, C.E., Burns, C.G. (2013). Zebrafish Second Heart Field Development Relies on Progenitor Specification in Anterior Lateral Plate Mesoderm and Nkx2.5 Function. *Development*, *140*, 1353-1363.

Heckel, E., Boselli, F., Roth, S., Krudewig, A., Belting, H.G., Charvin, G., Vermot, J. (2015). Oscillatory Flow Modulates Mechanosensitive Klf2a Expression through Trpv4 and Trpp2 During Heart Valve Development. *Curr Biol*, *25*, 1354-1361.

Heisenberg, C.P., Bellaiche, Y. (2013). Forces in Tissue Morphogenesis and Patterning. *Cell*, *153*, 948-962.

Hesselson, D., Anderson, R.M., Beinat, M., Stainier, D.Y. (2009). Distinct Populations of Quiescent and Proliferative Pancreatic Beta-Cells Identified by Hotcre Mediated Labeling. *Proc Natl Acad Sci U S A*, *106*, 14896-14901.

Hinton, R.B., Yutzey, K.E. (2011). Heart Valve Structure and Function in Development and Disease. *Annu Rev Physiol*, *73*, 29-46.

Hogers, B., DeRuiter, M.C., Gittenberger-de Groot, A.C., Poelmann, R.E. (1999). Extraembryonic Venous Obstructions Lead to Cardiovascular Malformations and Can Be Embryolethal. *Cardiovasc Res*, *41*, 87-99.

Hsu, J.J., Vedula, V., Baek, K.I., Chen, C., Chen, J., Chou, M.I., Lam, J., Subhedar, S., Wang, J., Ding, Y., Chang, C.C., Lee, J., Demer, L.L., Tintut, Y., Marsden, A.L., Hsiai, T.K. (2019). Contractile and Hemodynamic Forces Coordinate Notch1b-Mediated Outflow Tract Valve Formation. *JCI Insight*, *5*.

Huang, J., Elicker, J., Bowens, N., Liu, X., Cheng, L., Cappola, T.P., Zhu, X., Parmacek, M.S. (2012). Myocardin Regulates Bmp10 Expression and Is Required for Heart Development. *J Clin Invest*, *122*, 3678-3691.

Huang, W., Zhang, R., Xu, X. (2009). Myofibrillogenesis in the Developing Zebrafish Heart: A Functional Study of Tnnt2. *Dev Biol*, *331*, 237-249.

Jahangiri, L., Sharpe, M., Novikov, N., Gonzalez-Rosa, J.M., Borikova, A., Nevis, K., Paffett-Lugassy, N., Zhao, L., Adams, M., Guner-Ataman, B., Burns, C.E., Burns, C.G. (2016). The Ap-1 Transcription Factor Component Fosl2 Potentiates the Rate of Myocardial Differentiation from the Zebrafish Second Heart Field. *Development*, *143*, 113-122.

Knight, H.G., Yelon, D., 2016. Utilizing Zebrafish to Understand Second Heart Field Development, in: Nakanishi, T., Markwald, R.R., Baldwin, H.S., Keller, B.B., Srivastava, D., Yamagishi, H. (Eds.), Etiology and Morphogenesis of Congenital Heart Disease: From Gene Function and Cellular Interaction to Morphology, Tokyo, pp. 193-199.

Kwon, H.B., Wang, S., Helker, C.S., Rasouli, S.J., Maischein, H.M., Offermanns, S., Herzog, W., Stainier, D.Y. (2016). In Vivo Modulation of Endothelial Polarization by Apelin Receptor Signalling. *Nat Commun*, *7*, 11805.

Lane, W.O., Jantzen, A.E., Carlon, T.A., Jamiolkowski, R.M., Grenet, J.E., Ley, M.M., Haseltine, J.M., Galinat, L.J., Lin, F.H., Allen, J.D., Truskey, G.A., Achneck, H.E. (2012). Parallel-Plate Flow Chamber and Continuous Flow Circuit to Evaluate Endothelial Progenitor Cells under Laminar Flow Shear Stress. *J Vis Exp*.

Laux, D.W., Young, S., Donovan, J.P., Mansfield, C.J., Upton, P.D., Roman, B.L. (2013). Circulating Bmp10 Acts through Endothelial Alk1 to Mediate Flow-Dependent Arterial Quiescence. *Development*, *140*, 3403-3412.

Lazic, S., Scott, I.C. (2011). Mef2cb Regulates Late Myocardial Cell Addition from a Second Heart Field-Like Population of Progenitors in Zebrafish. *Dev Biol*, *354*, 123-133.

Letteboer, T.G., Mager, J.J., Snijder, R.J., Koeleman, B.P., Lindhout, D., Ploos van Amstel, J.K., Westermann, C.J. (2006). Genotype-Phenotype Relationship in Hereditary Haemorrhagic Telangiectasia. *J Med Genet*, *43*, 371-377.

Lin, L., Cui, L., Zhou, W., Dufort, D., Zhang, X., Cai, C.L., Bu, L., Yang, L., Martin, J., Kemler, R., Rosenfeld, M.G., Chen, J., Evans, S.M. (2007). Beta-Catenin Directly Regulates Islet1 Expression in Cardiovascular Progenitors and Is Required for Multiple Aspects of Cardiogenesis. *Proc Natl Acad Sci U S A*, *104*, 9313-9318.

Lin, Y.F., Swinburne, I., Yelon, D. (2012). Multiple Influences of Blood Flow on Cardiomyocyte Hypertrophy in the Embryonic Zebrafish Heart. *Dev Biol*, *362*, 242-253.

Marjoram, R.J., Guilluy, C., Burridge, K. (2016). Using Magnets and Magnetic Beads to Dissect Signaling Pathways Activated by Mechanical Tension Applied to Cells. *Methods*, *94*, 19-26.

Morine, K.J., Qiao, X., Paruchuri, V., Aronovitz, M.J., Mackey, E.E., Buiten, L., Levine, J., Ughreja, K., Nepali, P., Blanton, R.M., Karas, R.H., Oh, S.P., Kapur, N.K. (2017a). Conditional Knockout of Activin Like Kinase-1 (Alk-1) Leads to Heart Failure without Maladaptive Remodeling. *Heart Vessels*, *32*, 628-636.

Morine, K.J., Qiao, X., Paruchuri, V., Aronovitz, M.J., Mackey, E.E., Buiten, L., Levine, J., Ughreja, K., Nepali, P., Blanton, R.M., Oh, S.P., Karas, R.H., Kapur, N.K. (2017b). Reduced Activin Receptor-Like Kinase 1 Activity Promotes Cardiac Fibrosis in Heart Failure. *Cardiovasc Pathol*, *31*, 26-33.

Neeb, Z., Lajiness, J.D., Bolanis, E., Conway, S.J. (2013). Cardiac Outflow Tract Anomalies. *Wiley Interdiscip Rev Dev Biol*, *2*, 499-530.

Ott, H.C., Matthiesen, T.S., Goh, S.K., Black, L.D., Kren, S.M., Netoff, T.I., Taylor, D.A. (2008). Perfusion-Decellularized Matrix: Using Nature's Platform to Engineer a Bioartificial Heart. *Nat Med*, *14*, 213-221.

Qasim, M., Haq, F., Kang, M.H., Kim, J.H. (2019). 3d Printing Approaches for Cardiac Tissue Engineering and Role of Immune Modulation in Tissue Regeneration. *Int J Nanomedicine*, *14*, 1311-1333.

Rasouli, S.J., El-Brolosy, M., Tsedeke, A.T., Bensimon-Brito, A., Ghanbari, P., Maischein, H.M., Kuenne, C., Stainier, D.Y. (2018). The Flow Responsive Transcription Factor Klf2 Is Required for Myocardial Wall Integrity by Modulating Fgf Signaling. *Elife*, *7*.

Rochon, E.R., Menon, P.G., Roman, B.L. (2016). Alk1 Controls Arterial Endothelial Cell Migration in Lumenized Vessels. *Development*, *143*, 2593-2602.

Roman, B.L., Hinck, A.P. (2017). Alk1 Signaling in Development and Disease: New Paradigms. *Cell Mol Life Sci*, *74*, 4539-4560.

Roman, B.L., Pham, V.N., Lawson, N.D., Kulik, M., Childs, S., Lekven, A.C., Garrity, D.M., Moon, R.T., Fishman, M.C., Lechleider, R.J., Weinstein, B.M. (2002). Disruption of Acvrl1 Increases Endothelial Cell Number in Zebrafish Cranial Vessels. *Development*, *129*, 3009-3019.

Schumacher, J.A., Bloomekatz, J., Garavito-Aguilar, Z.V., Yelon, D. (2013). Tal1 Regulates the Formation of Intercellular Junctions and the Maintenance of Identity in the Endocardium. *Dev Biol*, *383*, 214-226.

Sehnert, A.J., Huq, A., Weinstein, B.M., Walker, C., Fishman, M., Stainier, D.Y. (2002). Cardiac Troponin T Is Essential in Sarcomere Assembly and Cardiac Contractility. *Nat Genet*, *31*, 106-110.

Sidhwani, P., Yelon, D. (2019). Fluid Forces Shape the Embryonic Heart: Insights from Zebrafish. *Curr Top Dev Biol*, *132*, 395-416.

Steed, E., Boselli, F., Vermot, J. (2016). Hemodynamics Driven Cardiac Valve Morphogenesis. *Biochim Biophys Acta*, *1863*, 1760-1766.

Vedula, V., Lee, J., Xu, H., Kuo, C.J., Hsiai, T.K., Marsden, A.L. (2017). A Method to Quantify Mechanobiologic Forces During Zebrafish Cardiac Development Using 4-D Light Sheet Imaging and Computational Modeling. *PLoS Comput Biol*, *13*, e1005828.

Vermot, J., Forouhar, A.S., Liebling, M., Wu, D., Plummer, D., Gharib, M., Fraser, S.E. (2009). Reversing Blood Flows Act through Klf2a to Ensure Normal Valvulogenesis in the Developing Heart. *PLoS Biol*, *7*, e1000246.

Watkins, S.C., Maniar, S., Mosher, M., Roman, B.L., Tsang, M., St Croix, C.M. (2012). High Resolution Imaging of Vascular Function in Zebrafish. *PLoS One*, *7*, e44018.

Witzel, H.R., Cheedipudi, S., Gao, R., Stainier, D.Y., Dobreva, G.D. (2017). Isl2b Regulates Anterior Second Heart Field Development in Zebrafish. *Sci Rep*, *7*, 41043.

Yelbuz, T.M., Waldo, K.L., Kumiski, D.H., Stadt, H.A., Wolfe, R.R., Leatherbury, L., Kirby, M.L. (2002). Shortened Outflow Tract Leads to Altered Cardiac Looping after Neural Crest Ablation. *Circulation*, *106*, 504-510.

Zeng, X.X., Yelon, D. (2014). Cadm4 Restricts the Production of Cardiac Outflow Tract Progenitor Cells. *Cell Rep*, *7*, 951-960.

Zhou, Y., Cashman, T.J., Nevis, K.R., Obregon, P., Carney, S.A., Liu, Y., Gu, A., Mosimann, C., Sondalle, S., Peterson, R.E., Heideman, W., Burns, C.E., Burns, C.G. (2011). Latent Tgf-Beta Binding Protein 3 Identifies a Second Heart Field in Zebrafish. *Nature*, *474*, 645-648.

Zhou, Z., Rawnsley, D.R., Goddard, L.M., Pan, W., Cao, X.J., Jakus, Z., Zheng, H., Yang, J., Arthur, J.S., Whitehead, K.J., Li, D., Zhou, B., Garcia, B.A., Zheng, X., Kahn, M.L. (2015). The Cerebral Cavernous Malformation Pathway Controls Cardiac Development Via Regulation of Endocardial Mekk3 Signaling and Klf Expression. *Dev Cell*, *32*, 168-180.

CHAPTER 3

Future directions towards understanding functional influences on outflow tract morphogenesis

Abstract

In this dissertation, we have revealed key cellular behaviors underlying early steps of OFT morphogenesis. Furthermore, we have identified essential roles for cardiac function in choreographing these cellular dynamics. Finally, we have demonstrated that Alk1 is an important player in OFT development. Although our work provides a coherent picture of certain aspects of OFT development, many questions remain unanswered. For example, do endocardial proliferation and addition independently regulate OFT shape? What are the precise mechanisms by which Alk1 regulates endocardial displacement in the OFT? This chapter will discuss future directions towards tackling such questions.

Do proliferation and addition independently regulate OFT shape?

While our studies suggest that proliferation and addition collaboratively shape the OFT endocardium, it remains unknown if these two cellular behaviors are independent or molecularly coupled. To address this question, we could begin by comparing the location of proliferating cells to the location of those being added from the endothelium: are these cells frequently colocalizing within the OFT endocardium, or do they appear as distinct clusters? Our studies suggest that endothelial cells emanating from the aortic arches are routinely found in the distal OFT (Fig. 2-3).

While we did not observe an obvious pattern of localization for EdU+ cells, preliminary data suggest that BrdU+ cells are frequently detected in the proximal endocardium of the wild-type OFT (Fig. 3-1). Moreover, in *alk1* morphants, where endothelial addition is absent, the number of EdU+ cells appears unaltered (Fig. 2-14, Fig. 2-18). These findings strongly imply that cells immigrating from the aortic arches are not dividing as they add to the OFT, and that proliferation is not dependent on addition. In fact, a closer examination of OFT endocardial cell numbers in wild-type suggests that more cells come in from the aortic arches than are added as a result of proliferation. In wild-type, a proliferation index of ~25% suggests that ~2-3 cells are added to the OFT endocardium due to proliferation. Therefore, the remaining ~10-15 cells might be annexing from the bilateral aortic arches. Interestingly, *sih* mutants, which have defects in both proliferation and addition have ~10 cells, while *wea* and *alk1* morphants, which lack addition specifically, have ~13 endocardial cells in the OFT. Comparing these conditions to wild-type, which have ~25 cells, again suggests that proliferation contributes ~2-3 cells while addition contributes ~10-15 cells.

Altogether, our current observations favor a model in which proliferation in the OFT endocardium determines the proximal diameter of the OFT, whereas cells from the aortic arches add to this emerging framework to facilitate distal expansion. Alternatively, endocardial cells from the ventricle, OFT and aortic arches could be undergoing significant rearrangement between 36 hpf and 51 hpf. To clarify this further, future studies could employ long-term live imaging of the OFT endocardium to visualize early OFT morphogenesis at high cellular resolution. Conclusively

addressing this model would require development of optogenetic tools to block proliferation specifically within the proximal endocardium, which would allow us to test whether proliferation could impact addition.

What are the physical and cellular mechanisms balancing overall OFT dimensions?

As discussed in previous chapters, the OFT is situated in a complex mechanical milieu: in addition to contractility and fluid forces associated with cardiac function, the OFT might also experience epithelial tension due to SHF deployment (Francou et al., 2017). In summary, the many forces the OFT is exposed to between 36 hpf and 51 hpf presumably include stretch in a direction perpendicular to blood flow, due to myocardial contractility and blood pressure; shear specifically in endocardial cells, in a direction parallel to flow due to the viscosity of blood; and tension in the direction parallel to flow due to the attachment of the arterial pole to the dorsal pericardial wall. Finally, the direction of blood flow can itself administer distinct mechanical cues to cells: reversing or retrograde flows, for instance, are thought to activate specific downstream pathways. If the OFT is indeed constantly pulled and squeezed in various directions, how does it finally achieve a homeostatic morphology?

Our findings in multiple mutant scenarios allow us to derive testable hypotheses towards addressing this question. First, our studies suggest that inhibiting atrial function to reduce blood flow into the ventricle, as in *wea*, leads to dampened addition from the aortic arches, while proliferation in the OFT

endocardium appears unaffected. This is in contrast to *sih* and *haf* mutants, where OFT contractility is itself impaired, and both addition and proliferation are reduced. These results imply that blood flow acts independently to stimulate endothelial addition, while contractility promotes endocardial proliferation. Alternatively, the milder defect in *wea* mutants could be inadequate to depress proliferative capacity of OFT endocardial cells. How might blood flow and contractility, which are inextricably linked *in vivo*, prompt seemingly disparate cellular mechanisms towards a common goal of constructing the OFT? Although we do not yet have the tools to alter flow parameters without affecting contractility *in vivo*, a combination of three-dimensional tissue engineering in controlled flow environments will enable us to begin answering this question *ex vivo* (Lane et al., 2012; Qasim et al., 2019).

So, which fluid parameters might instigate endothelial addition in response to blood flow? Since *gata1* morphants have normal OFT endocardial cell number, shear forces are unlikely to be relevant, especially considering that *gata1* knockdown reduces blood viscosity by 90% (Vermot et al., 2009). Could stretch from blood pressure be influencing OFT shape? Given the atrial dysfunction in *wea*, it's likely that stretch from blood pressure is reduced in the *wea* OFT. However, one would need to quantify stretch in the endocardium, and then disrupt it to rigorously evaluate its effects to confirm this hypothesis. For the former, it will be exciting for future studies to employ tools like tissue-specific, FRET-based tension sensors (Lagendijk et al., 2017) or tissue-embedded, force-sensitive oil microdroplets (Campas et al., 2014) to elucidate the precise spatiotemporal dynamics of endocardial tension. Then,

tension in the endocardium could be disrupted by wounding endocardial cells to infer epithelial tension, as has been described previously (Francou et al., 2017).

Finally, *wea* mutants are also known to have reduced retrograde flow at later stages (Vedula et al., 2017), so flow direction could also be a factor promoting endothelial addition to the OFT. Evaluating *gata2* morphants, which have reduced retrograde flows, has been the method of choice to address this (Vermot et al., 2009); however, *gata2* morphants have reduced heart rates (Dietrich et al., 2014), so it is challenging to uncouple effects of retrograde flows from those related to cardiac function. Applications of single molecule spectroscopy could be adapted to test this model definitively: optical tweezing, for instance, could be used to manipulate erythrocyte velocity or direction in a confined region (Anton et al., 2013). Finally, although this is unrelated to fluid forces, it is important to consider blood as a carrier of vital molecules. In fact, previous studies have shown that the Alk1 ligands *bmp10* and *bmp10-like* are expressed in the heart and have suggested that they are brought to the site of *alk1* in the aortic arches by blood flow (Laux et al., 2013). However, *alk1* expression is also dependent on function (Corti et al., 2011), adding a second layer of mechanical regulation of Alk1 signaling. Overall, our results suggest that stretch from blood pressure or flow direction could be relevant to OFT morphology. However, further work is required to test this in a specific and stringent manner.

If stretch from contractility induces proliferation within the endocardium, future studies will need to address if proliferation is caused by stretch within the endocardium itself, or contractility within the myocardium relaying signals to the endocardium. Cyclic stretch indeed induces specific gene expression profiles in

cultured endothelial cells, in support of the former possibility (Sumpio et al., 1990). Alternatively, a crosstalk between the myocardial and endocardial layers, potentially mediated by the intermediary layer of extracellular matrix (ECM) or “cardiac jelly”, could be crucial for endocardial proliferation, as well as for coordinating endocardial growth with that of the myocardium. In support of this, the mechanoresponsive transcription factor Klf2, which is expressed in the endocardium, regulates fibronectin deposition in the ECM while also maintaining myocardial integrity (Rasouli et al., 2018; Steed et al., 2016).

If the ECM is an essential mediator of mechanical crosstalk could we potentially rescue OFT proliferation in *sih* by altering ECM deposition? To begin investigating this, one could inject the enzyme hyaluronidase into *sih* to degrade hyaluronic acid, an important “space-filling” component of the ECM (De Angelis et al., 2017). Additionally, future studies could evaluate OFT endocardial cell number in zebrafish mutants that have too much ECM deposition, like *tmem2* mutants (Totong et al., 2011), or too little ECM, like *fbn2b* mutants (Mellman et al., 2012). A significant drawback of these approaches, however, is that ECM mutants have many other cardiac defects that will be challenging to tease apart from the effects of ECM disruption itself. To circumvent this, another approach could involve a thorough investigation of myocardial-endocardial signaling pathways, especially within the context of functional mutants, and perturbing those directly. For example, Bmp ligands produced by the myocardium are thought to influence endocardial proliferation, albeit independently of function (Dietrich et al., 2014). Discovery of other

such pathways will undoubtedly advance our understanding of mechanically-driven intercommunication between the two layers.

Since the endocardium and myocardium are closely apposed during OFT morphogenesis, epithelial tension between the DPW and the developing myocardium is yet another biomechanical cue that could influence overall OFT morphology. Another factor that potentially influences tension in this direction is the developmental straightening of the embryonic head, which could pull on the arterial pole of the heart. Curiously, in *sih*, the endocardium appears stretched in the proximal-distal direction at 51 hpf, which would suggest that in the absence of sufficient number of cells to support OFT broadening, tension in the proximal-distal direction overwhelms OFT structure. To evaluate mechanical anisotropy in this direction, wound assays can be utilized in the OFT endocardium, as has been done previously in mice (Francou et al., 2017).

How does Alk1 regulate endothelial displacement into the OFT?

In our studies, we employed photoconversion labeling techniques to demonstrate that cells within the aortic arches at 36 hpf enter the OFT by 51 hpf. However, since our experiments are essentially end-point analyses, they do not divulge the precise cellular basis for this displacement. Are cells from the aortic arches actively migrating into the OFT endocardium between 36 hpf and 51 hpf, or are they passively rearranging between the endothelium and OFT endocardium? In support of the former model, prior studies in zebrafish have suggested that cells from distal sections of the arterial vasculature, such as the aortic arches or internal carotid

artery, actively migrate against blood flow into the heart (Rochon et al., 2016). However, rigorous testing of this model awaits high-resolution live imaging of OFT endocardial development.

Another possibility for endothelial addition to the OFT is passive rearrangement of endothelial cells between the endothelium and endocardium. Such rearrangement could be driven by modifications in cell-cell contacts, where endocardial cells are being displaced by endothelial cells. Alternatively, this could be a consequence of tissue-level restructuring of the endothelium-endocardium boundary, where endothelial cells in the aortic arches zipper together to construct the distal portion of the OFT endocardium. Coupling live imaging with an approach where endothelial cells are distinctly labeled, such as multicolor labeling with Brainbow (Pan et al., 2011), could be useful to assess whether such a rearrangement, if it exists, is on a cellular or tissue level.

Since endothelial cells displace OFT endocardial cells, and endocardial cells are in fact specialized endothelial cells, does the OFT endocardium consist of two molecularly distinct populations of cells by 51 hpf? However, single-cell RNA sequencing of endocardial cells is required to address this conclusively. I hypothesize that in the scRNA-seq analysis of the endocardium, we will be able to pull out two clusters that highly expresses *klf2a* in wild-type embryos by 51 hpf, which likely represent OFT endocardial cells and AVC endocardial cells. Resolving the OFT cluster even further might yield insights into the existence and molecular characteristics of endothelial and endocardial populations within the OFT.

What are the ligands activating Alk1 signaling to regulate endocardial displacement? In many contexts, Bmp9 and Bmp10 have been determined as ligands for Alk1 (Li et al., 2016). Prior studies suggest that the heart is a source of Bmp10 and Bmp10-like for Alk1 activation in zebrafish (Laux et al., 2013). Accordingly, *bmp10* mutants phenocopy *alk1* mutants in that they have dilated cranial vessels and reduced endothelial migration (Laux et al., 2013). Moreover, simply overexpressing *alk1* is not sufficient to rescue endothelial migration against blood flow in *sih*, but injecting Bmp10 in this context does rescue endothelial cell number in the internal carotid artery. These experiments support a model where blood carries Bmp10 to the source of Alk1. It remains unclear, however, if this mechanism also facilitates OFT growth. As a first step towards addressing this, it is essential to evaluate OFT endocardial cell number and endothelial addition in mutants for *bmp10* and *bmp10-like*. However, it remains unclear how such a mechanism would promote directed migration against blood flow. Perhaps endothelial cells are able to sense a gradient of Bmp expression emanating from the heart, or perhaps other mechanisms exist to ensure unidirectional migration. Ectopically expressing Bmp10 at distal locations in an attempt to force migration in the opposite direction i.e. parallel to blood flow, might shed light on the existence of supplemental pathways for navigating cells.

What are the molecular mechanisms governing OFT endocardial proliferation in response to function?

In our studies, we identified Alk1 as an important mediator of function-driven OFT expansion. However, we were unable to characterize a pathway governing

proliferation in response to functional influences. In an attempt to identify such pathways, we performed preliminary evaluations of many known mechanotransducive entities. For example, we quantified OFT endocardial cell number in embryos lacking the calcium mechanosensitive channel Trpv4, which is thought to play a role in zebrafish AVC development (Heckel et al., 2015). However, these mutants displayed no obvious phenotype in the OFT endocardium (Fig. 3-2). We did observe a fascinating phenotype when we exposed embryos to Yoda1, an antagonist for a recently discovered calcium mechanosensitive channel Piezo1 (Syeda et al., 2015), from 24 hpf to 51 hpf: these embryos had a wider OFT (measured at the proximal edge of the OFT endocardium) (Fig. 3-3), and some of the embryos in the treated cohort displayed a significant increase in endocardial cell number (data not shown). In one experiment, Yoda1-treated embryos were also determined to have upregulated Notch activity in the heart, visualized using the report *Tg*(*tp1*:*GFP*) (data not shown). However, we were unable to reproduce these results in a rigorous manner. Moreover, from preliminary examinations of *piezo1* mutants (Shmukler et al., 2015), we did not spot an obvious heart phenotype (data not shown). Therefore, although Piezo1 might be important for endocardial accumulation in the OFT, our results from preliminary studies remain inconclusive.

The Klf2 factors, which are highly expressed in the OFT endocardium, remain interesting candidates for a mechanotransducive pathway regulating OFT endocardial proliferation. Although our work suggests that *klf2a* and *klf2b* are not playing a major role in reinforcing OFT endocardial cell number, the necessity of the Klf pathway in this process warrants further investigation. mRNA levels of *klf2b* and

the related factor *klf4* (Clark et al., 2011; Goddard et al., 2017; Zhou et al., 2015) are increased in *klf2a* mutants (Rasouli et al., 2018), which suggests that the various Klf factors can compensate for each other. Therefore, as a first step, it is important for future studies to evaluate the contribution of the Klf homolog *klf4* in addition to *klf2a* and *klf2b* in OFT endocardial accumulation and proliferation.

Finally, it might be informative to employ RNA-sequencing approaches to determine if there are any differences at the transcriptomic level in the endocardium of wild-type, *sih*, *haf* and *wea*. Since isolating cells for RNA-sequencing potentially mechanically perturbs them, it might be useful to get a transcriptomic "snapshot" of cells prior to isolation. For this purpose, RNA-sequencing could be performed in flash-frozen tissue collected using laser-capture microdissection techniques. Alternatively, RNAs could be tagged *in vivo* with thiouracil, as has been described previously (Erickson & Nicolson, 2015), so RNAs synthesized during isolation do not interfere with the analysis. Although such an approach might not allow us to identify mechanonsensitive channels, whose activity and not expression is regulated by forces, it might aid characterization of downstream effectors for a "bottom up" approach.

Do morphological demarcations of the OFT correspond with molecular distinctions between the ventricle and OFT?

One considerable challenge for our studies was the dearth of molecular markers specific to the OFT. Previous studies employed a combination of myocardial GFP and dsRed reporters to pinpoint SHF-derived cells: since dsRed takes 24 hours

to mature, unlike GFP that has fast maturation dynamics, late-differentiating SHF-derived myocardial cells are specifically GFP+/dsRed- at 48 hpf (de Pater et al., 2009). Similarly, transgenes like Draculin, and Cre-labeling approaches to mark the Ltbp3 lineage are alternative approaches to mark SHF-derived myocardial cells (Mosimann et al., 2015; Zhou et al., 2011). Since SHF-derived cells also append to the distal ventricle, however, they do not mark the OFT specifically, and hence were not particularly useful for our analyses. Interestingly, recent studies reported that an antibody against Isl1/2 marks the OFT and inner curvature of the ventricular IC (Witzel et al., 2017). Although our preliminary studies confirmed this expression pattern, Isl1/2 levels appear reduced in *sih* mutants (data not shown). Given that our studies required OFT demarcation in *sih* as well, we could not employ Isl1/2 as reproducible markers for the OFT. Due to similar reasons, we were also unable to employ OFT endocardial markers like *klf2a*, *notch1b* and *wnt9b,* and myocardial markers like *nppa*.

Since we lacked an OFT marker, it remains possible that, in mutants like *sih*, the morphological constriction between the ventricle and OFT is shifted, thereby influencing our assessment of endocardial cell number. In this regard, it is important to note that our preliminary data suggest that the SHF progenitor pool is not affected in *sih* (Fig. 3-4). Moreover, previous studies have shown that SHF differentiation is also normal in *sih* (de Pater et al., 2009). Given these observations, it is reassuring that, per our definition of the OFT, myocardial cell number in the *sih* OFT seems normal. Ultimately, though, it will be crucial to confirm our analysis using an alternate marker for the OFT.

To pursue discovery of novel markers for the OFT, we reanalyzed the microarray dataset we had previously generated, comparing wild-type embryos to embryos treated with the Fgf inhibitor SU5402 between 24 hpf and 48 hpf (Zeng & Yelon, 2014); since this treatment results in the downregulation of SHF progenitor markers, followed by a diminished ventricle and absent OFT, we speculated that potential OFT markers would be reduced in the SU5402-treated cohort. Although we were able to formulate a list of possible markers, we were limited by the paucity of commercially available antibodies to visualize their expression patterns. However, this remains a credible approach towards identifying OFT-specific markers. Additionally, our lab has recently generated single-cell RNA-sequencing datasets of myocardial cells in collaboration with the Yost lab. At higher resolution in the t-SNE plots, there is a cluster of myocardial cells that could be representative of the OFT (data not shown). Perhaps deeper analysis of this cluster will reveal novel markers for the OFT, whose expression patterns could be tested using *in situ* hybridization and immunostaining. Until then, our rigorous approach for demarcating the OFT morphologically can be employed to mark the OFT in a consistent fashion.

What is the broader significance of our studies?

Our studies have important ramifications for the field of developmental biology, as well broader consequences for influencing our understanding of congenital heart diseases and hereditary hemorrhagic telangiectasia type 2 (HHT2). Within the realm of developmental biology, our work has progressed our knowledge of the multiple cellular and molecular mechanisms by which forces inform form. Our studies suggest

that multiple forces, engendered by linked processes of blood flow and contractility, can essentially choreograph independent molecular pathways to build a composite organ. This isn't entirely new information: we have long known that cells in a developing organism integrate diverse physical and molecular mechanisms to construct a tissue. However, by leveraging the precisely quantifiable dimensions and junctional location of the OFT, we have been able to garner an "organ-level" understanding of how this happens. Further, our work inserts a key element of OFT development: we now understand the mechanical and cellular means by which the OFT attains its stereotypical morphology, which is a crucial step towards ensuring proper valve development, and, in higher vertebrates, OFT remodeling and septation. We find that cardiac function actively participates in building a broad OFT; in this way, function appears to "feed back" into the cardiovascular system, to continuously adjust lumen dimensions in order to maintain systemic blood pressure.

Synthesizing our data with preceding studies promises to open additional avenues to grasp the etiology of, and design therapeutic strategies for, congenital heart defects (CHD), a third of which include OFT abnormalities. For example, prior work has shown that defects in early OFT morphogenesis may lead to complications in OFT remodeling and septation, which often occur in patients with CHDs (El Robrini et al., 2016; Neeb et al., 2013; Yelbuz et al., 2002). Given that many cardiac anomalies induce secondary errors in function, recognizing functional influences on early heart development is a key step towards circumventing subsequent issues. Further, our discovery of a fundamental role for the HHT2-causative gene Alk1 (Letteboer et al., 2006) in OFT development suggests an additional type of cardiac

defect that could occur in HHT2 patients. Our findings are especially intriguing in light of prior studies showing that murine embryos lacking *bmp9* or *bmp10*, known ligands for Alk1, exhibit defects in cardiomyocyte proliferation and apoptosis, and consequently cardiac growth and maturation (Chen et al., 2013; Chen et al., 2004; Huang et al., 2012). Moreover, instances of cardiac failure are heightened in *alk1* knockout mice (Morine et al., 2017a; Morine et al., 2017b), as well as human patients of HHT2 (Cho et al., 2012; Goussous et al., 2009). Our results provide a renewed outlook on the pathogenesis of such cardiac abnormalities in HHT2 patients. Finally, our findings also have major repercussions for cardiac tissue engineering approaches. Fabricating functional hearts has traditionally required a protein scaffold (Ott et al., 2008); our studies highlight the usefulness of considering the endocardium as an additional yet crucial scaffold for myocardial assembly. Altogether, our studies bear multifaceted biomedical consequences, in addition to significantly advancing our understanding of the many ways in which “form follows function”.

Acknowledgements

Preliminary experiments in Chapter 3 were designed and performed by the dissertation author. Please note that a portion of material presented in Chapter 3 is adapted from Chapter 2.

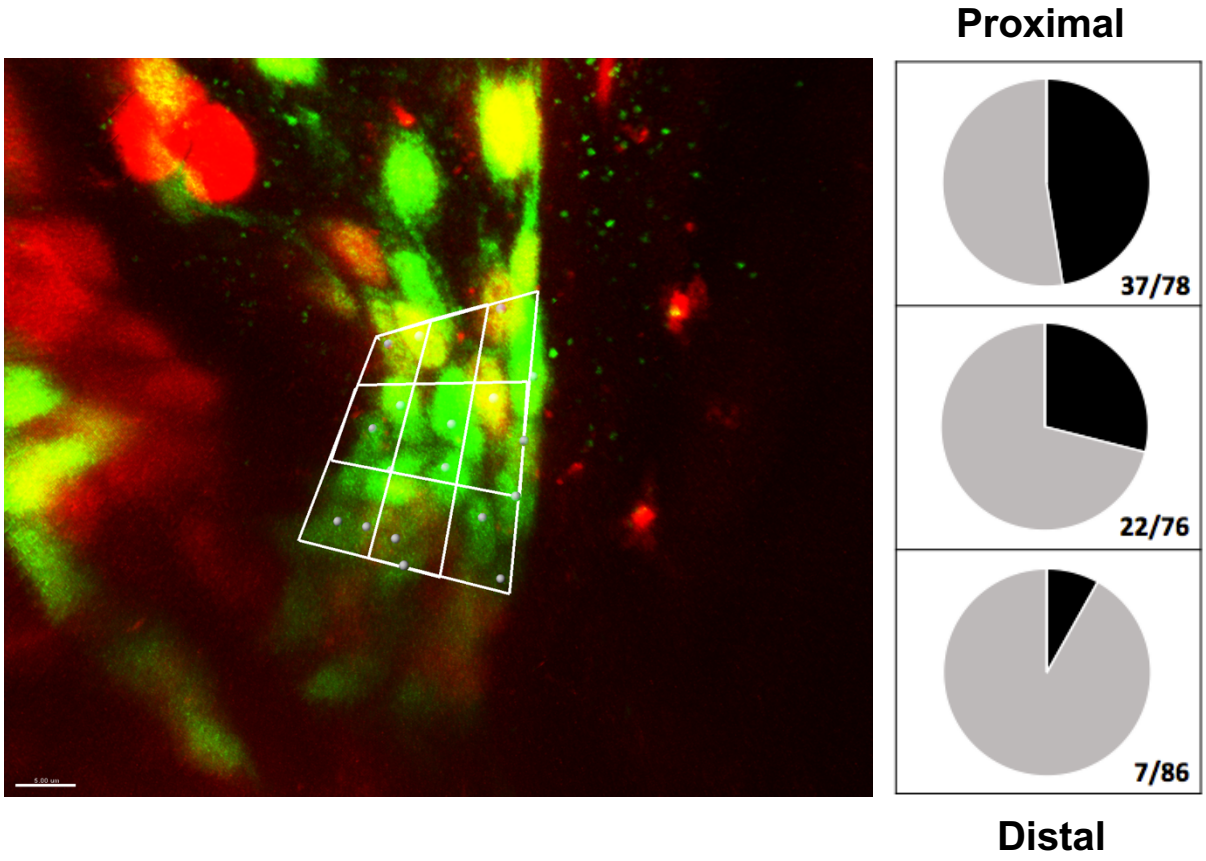

Figure 3-1: BrdU+ cells are frequently located in the proximal OFT. A preliminary assessment was performed by orienting the OFT in a consistent manner and dividing it in a 3 x 3 grid, where each row represents proximal, medial and distal cells, respectively. BrdU+ cells (black) were frequently found in the proximal region, and gradually diminished towards the distal region. Fractions represent BrdU+ cells/ BrdU- cells in a total of 14 embryos.

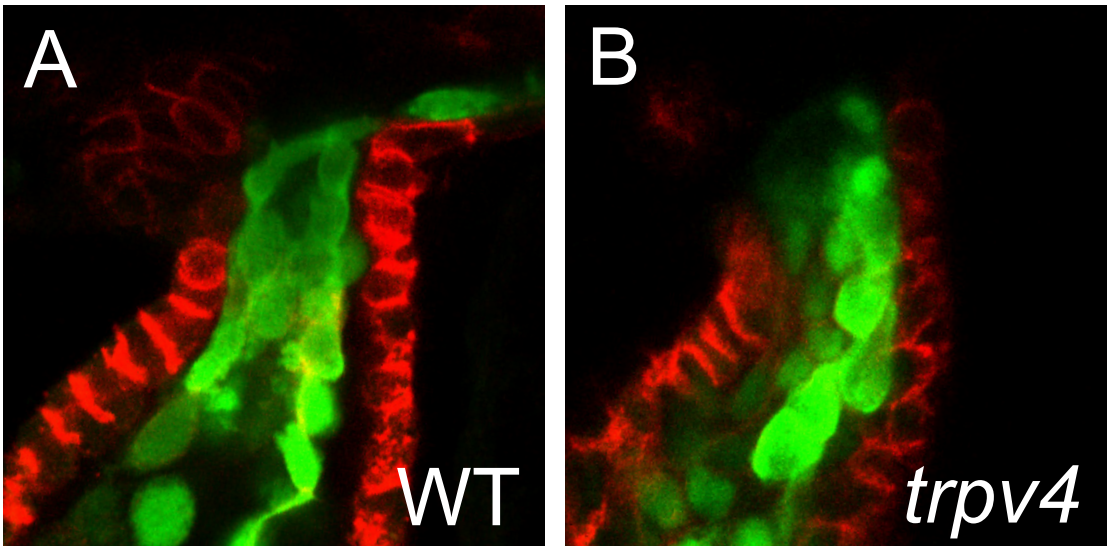

Figure 3-2: *trpv4* mutants do not have an obvious OFT phenotype. Comparing wild-type (A) embryos to *trpv4* mutants (B) marked with *Tg*(*fli1a*:*negfp*) (green) and an antibody against Dm-grasp (red) does not reveal and obvious OFT defect at 51 hpf. n= 11, 5. N=1.

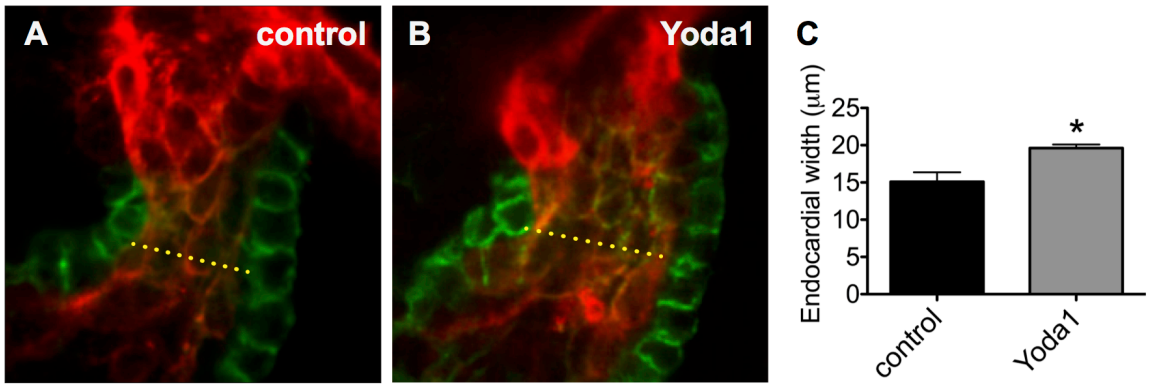

Figure 3-3: Treatment with a pharmacological activator of Piezo1 influences the OFT endocardium (A,B) *Tg*(*kdrl*:*ras*-mCherry) embryos, where mCherry labels the endocardial cell membranes, are immunostained with anti-DmGrasp to mark the myocardium (green) and anti-dsRed to label the endocardium (red). The OFT endocardial width of an untreated control is ~15 um (A), as quantified in (C) (n=6). Treatment with Yoda1 causes a significant increase in endocardial width (B), as quantified in (C) (n=6, p=0.0077). OFT width was measured at the proximal end od the OFT as endocardium, as determined by the morphological constriction between the ventricle and the OFT. Analyses performed using Student's T test.

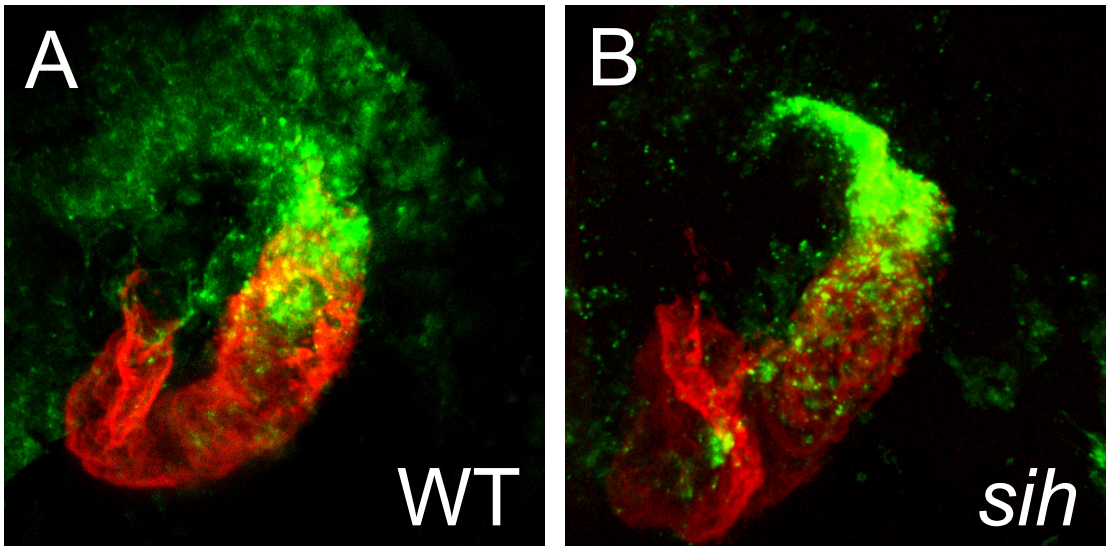

Figure 3-4: The SHF progenitor pool is unaltered in *sih*. Wild-type (A) and *sih* mutant (B) heart tubes labeled with the myocardial marker MF20 (red) and the SHF progenitor marker *ltbp3* (green) at 30 hpf. Fluorescence intensity of the green signal at the arterial pole of the heart is not qualitatively different between wild-type and *sih*, suggesting that the SHF progenitor pool is not disrupted by lack of cardiac function.

References

Anton, H., Harlepp, S., Ramspacher, C., Wu, D., Monduc, F., Bhat, S., Liebling, M., Paoletti, C., Charvin, G., Freund, J.B., Vermot, J. (2013). Pulse Propagation by a Capacitive Mechanism Drives Embryonic Blood Flow. *Development*, *140*, 4426-4434.

Campas, O., Mammoto, T., Hasso, S., Sperling, R.A., O'Connell, D., Bischof, A.G., Maas, R., Weitz, D.A., Mahadevan, L., Ingber, D.E. (2014). Quantifying Cell-Generated Mechanical Forces within Living Embryonic Tissues. *Nat Methods*, *11*, 183-189.

Cho, D., Kim, S., Kim, M., Seo, Y.H., Kim, W., Kang, S.H., Park, S.M., Shim, W. (2012). Two Cases of High Output Heart Failure Caused by Hereditary Hemorrhagic Telangiectasia. *Korean Circ J*, *42*, 861-865.

Clark, P.R., Jensen, T.J., Kluger, M.S., Morelock, M., Hanidu, A., Qi, Z., Tatake, R.J., Pober, J.S. (2011). Mek5 Is Activated by Shear Stress, Activates Erk5 and Induces Klf4 to Modulate Tnf Responses in Human Dermal Microvascular Endothelial Cells. *Microcirculation*, *18*, 102-117.

Corti, P., Young, S., Chen, C.Y., Patrick, M.J., Rochon, E.R., Pekkan, K., Roman, B.L. (2011). Interaction between Alk1 and Blood Flow in the Development of Arteriovenous Malformations. *Development*, *138*, 1573-1582.

Crest, J., Diz-Munoz, A., Chen, D.Y., Fletcher, D.A., Bilder, D. (2017). Organ Sculpting by Patterned Extracellular Matrix Stiffness. *Elife*, *6*.

De Angelis, J.E., Lagendijk, A.K., Chen, H., Tromp, A., Bower, N.I., Tunny, K.A., Brooks, A.J., Bakkers, J., Francois, M., Yap, A.S., Simons, C., Wicking, C., Hogan, B.M., Smith, K.A. (2017). Tmem2 Regulates Embryonic Vegf Signaling by Controlling Hyaluronic Acid Turnover. *Dev Cell*, *40*, 421.

de Pater, E., Clijsters, L., Marques, S.R., Lin, Y.F., Garavito-Aguilar, Z.V., Yelon, D., Bakkers, J. (2009). Distinct Phases of Cardiomyocyte Differentiation Regulate Growth of the Zebrafish Heart. *Development*, *136*, 1633-1641.

Dietrich, A.C., Lombardo, V.A., Veerkamp, J., Priller, F., Abdelilah-Seyfried, S. (2014). Blood Flow and Bmp Signaling Control Endocardial Chamber Morphogenesis. *Dev Cell*, *30*, 367-377.

El Robrini, N., Etchevers, H.C., Ryckebusch, L., Faure, E., Eudes, N., Niederreither, K., Zaffran, S., Bertrand, N. (2016). Cardiac Outflow Morphogenesis Depends on Effects of Retinoic Acid Signaling on Multiple Cell Lineages. *Dev Dyn*, *245*, 388-401.

Erickson, T., Nicolson, T. (2015). Identification of Sensory Hair-Cell Transcripts by Thiouracil-Tagging in Zebrafish. *BMC Genomics*, *16*, 842.

Francou, A., De Bono, C., Kelly, R.G. (2017). Epithelial Tension in the Second Heart Field Promotes Mouse Heart Tube Elongation. *Nat Commun*, *8*, 14770.

Goddard, L.M., Duchemin, A.L., Ramalingan, H., Wu, B., Chen, M., Bamezai, S., Yang, J., Li, L., Morley, M.P., Wang, T., Scherrer-Crosbie, M., Frank, D.B., Engleka, K.A., Jameson, S.C., Morrisey, E.E., Carroll, T.J., Zhou, B., Vermot, J., Kahn, M.L. (2017). Hemodynamic Forces Sculpt Developing Heart Valves through a Klf2-Wnt9b Paracrine Signaling Axis. *Dev Cell*, *43*, 274-289 e275.

Goussous, T., Haynes, A., Najarian, K., Daccarett, M., David, S. (2009). Hereditary Hemorrhagic Telangiectasia Presenting as High Output Cardiac Failure During Pregnancy. *Cardiol Res Pract*, *2009*, 437237.

Lagendijk, A.K., Gomez, G.A., Baek, S., Hesselson, D., Hughes, W.E., Paterson, S., Conway, D.E., Belting, H.G., Affolter, M., Smith, K.A., Schwartz, M.A., Yap, A.S., Hogan, B.M. (2017). Live Imaging Molecular Changes in Junctional Tension Upon Ve-Cadherin in Zebrafish. *Nat Commun*, *8*, 1402.

Lane, W.O., Jantzen, A.E., Carlon, T.A., Jamiolkowski, R.M., Grenet, J.E., Ley, M.M., Haseltine, J.M., Galinat, L.J., Lin, F.H., Allen, J.D., Truskey, G.A., Achneck, H.E. (2012). Parallel-Plate Flow Chamber and Continuous Flow Circuit to Evaluate Endothelial Progenitor Cells under Laminar Flow Shear Stress. *J Vis Exp*.

Laux, D.W., Young, S., Donovan, J.P., Mansfield, C.J., Upton, P.D., Roman, B.L. (2013). Circulating Bmp10 Acts through Endothelial Alk1 to Mediate Flow-Dependent Arterial Quiescence. *Development*, *140*, 3403-3412.

Letteboer, T. G., Mager, J. J., Snijder, R. J., Koeleman, B. P., Lindhout, D., Ploos van Amstel, J. K., & Westermann, C. J. (2006). Genotype-phenotype relationship in hereditary haemorrhagic telangiectasia. *Journal of medical genetics*, *43*(4), 371–377.

Li, W., Salmon, R.M., Jiang, H., Morrell, N.W. (2016). Regulation of the Alk1 Ligands, Bmp9 and Bmp10. *Biochem Soc Trans*, *44*, 1135-1141.

Marjoram, R.J., Guilluy, C., Burridge, K. (2016). Using Magnets and Magnetic Beads to Dissect Signaling Pathways Activated by Mechanical Tension Applied to Cells. *Methods*, *94*, 19-26.

Mellman, K., Huisken, J., Dinsmore, C., Hoppe, C., Stainier, D.Y. (2012). Fibrillin-2b Regulates Endocardial Morphogenesis in Zebrafish. *Dev Biol*, *372*, 111-119.

Mosimann, C., Panakova, D., Werdich, A.A., Musso, G., Burger, A., Lawson, K.L., Carr, L.A., Nevis, K.R., Sabeh, M.K., Zhou, Y., Davidson, A.J., DiBiase, A., Burns, C.E., Burns, C.G., MacRae, C.A., Zon, L.I. (2015). Chamber Identity Programs Drive Early Functional Partitioning of the Heart. *Nat Commun*, *6*, 8146.

Neeb, Z., Lajiness, J.D., Bolanis, E., Conway, S.J. (2013). Cardiac Outflow Tract Anomalies. *Wiley Interdiscip Rev Dev Biol*, *2*, 499-530.

Ott, H.C., Matthiesen, T.S., Goh, S.K., Black, L.D., Kren, S.M., Netoff, T.I., Taylor, D.A. (2008). Perfusion-Decellularized Matrix: Using Nature's Platform to Engineer a Bioartificial Heart. *Nat Med*, *14*, 213-221.

Pan, Y.A., Livet, J., Sanes, J.R., Lichtman, J.W., Schier, A.F. (2011). Multicolor Brainbow Imaging in Zebrafish. *Cold Spring Harb Protoc*, *2011*, pdb prot5546.

Qasim, M., Haq, F., Kang, M.H., Kim, J.H. (2019). 3d Printing Approaches for Cardiac Tissue Engineering and Role of Immune Modulation in Tissue Regeneration. *Int J Nanomedicine*, *14*, 1311-1333.

Rasouli, S.J., El-Brolosy, M., Tsedeke, A.T., Bensimon-Brito, A., Ghanbari, P., Maischein, H.M., Kuenne, C., Stainier, D.Y. (2018). The Flow Responsive Transcription Factor Klf2 Is Required for Myocardial Wall Integrity by Modulating Fgf Signaling. *Elife*, *7*.

Reischauer, S., Stone, O.A., Villasenor, A., Chi, N., Jin, S.W., Martin, M., Lee, M.T., Fukuda, N., Marass, M., Witty, A., Fiddes, I., Kuo, T., Chung, W.S., Salek, S., Lerrigo, R., Alsio, J., Luo, S., Tworus, D., Augustine, S.M., Mucenieks, S., Nystedt, B., Giraldez, A.J., Schroth, G.P., Andersson, O., Stainier, D.Y. (2016). Cloche Is a Bhlh-Pas Transcription Factor That Drives Haemato-Vascular Specification. *Nature*, *535*, 294-298.

Rochon, E.R., Menon, P.G., Roman, B.L. (2016). Alk1 Controls Arterial Endothelial Cell Migration in Lumenized Vessels. *Development*, *143*, 2593-2602.

Sehnert, A.J., Huq, A., Weinstein, B.M., Walker, C., Fishman, M., Stainier, D.Y. (2002). Cardiac Troponin T Is Essential in Sarcomere Assembly and Cardiac Contractility. *Nat Genet*, *31*, 106-110.

Shmukler, B.E., Huston, N.C., Thon, J.N., Ni, C.W., Kourkoulis, G., Lawson, N.D., Paw, B.H., and Alper, S.L. (2015). Homozygous knockout of the piezo1 gene in the zebrafish is not associated with anemia. Haematologica *100*, e483-485.

Steed, E., Boselli, F., Vermot, J. (2016). Hemodynamics Driven Cardiac Valve Morphogenesis. *Biochim Biophys Acta*, *1863*, 1760-1766.

Sumpio, B.E., Banes, A.J., Link, G.W., Iba, T. (1990). Modulation of Endothelial Cell Phenotype by Cyclic Stretch: Inhibition of Collagen Production. *J Surg Res*, *48*, 415-420.

Syeda, R., Xu, J., Dubin, A.E., Coste, B., Mathur, J., Huynh, T., Matzen, J., Lao, J., Tully, D.C., Engels, I.H., Petrassi, M., Schumacher, A.M., Montal, M., Bandell, M., Patapoutian, A. (2015). Chemical activation of the mechanotransduction channel Piezo1. eLife *4*.

Totong, R., Schell, T., Lescroart, F., Ryckebusch, L., Lin, Y.F., Zygmunt, T., Herwig, L., Krudewig, A., Gershoony, D., Belting, H.G., Affolter, M., Torres-Vazquez, J., Yelon, D. (2011). The Novel Transmembrane Protein Tmem2 Is Essential for Coordination of Myocardial and Endocardial Morphogenesis. *Development*, *138*, 4199-4205.

Vedula, V., Lee, J., Xu, H., Kuo, C.J., Hsiai, T.K., Marsden, A.L. (2017). A Method to Quantify Mechanobiologic Forces During Zebrafish Cardiac Development Using 4-D Light Sheet Imaging and Computational Modeling. *PLoS Comput Biol*, *13*, e1005828.

Vermot, J., Forouhar, A.S., Liebling, M., Wu, D., Plummer, D., Gharib, M., Fraser, S.E. (2009). Reversing Blood Flows Act through Klf2a to Ensure Normal Valvulogenesis in the Developing Heart. *PLoS Biol*, *7*, e1000246.

Witzel, H.R., Cheedipudi, S., Gao, R., Stainier, D.Y., Dobreva, G.D. (2017). Isl2b Regulates Anterior Second Heart Field Development in Zebrafish. *Sci Rep*, *7*, 41043.

Yelbuz, T.M., Waldo, K.L., Kumiski, D.H., Stadt, H.A., Wolfe, R.R., Leatherbury, L., Kirby, M.L. (2002). Shortened Outflow Tract Leads to Altered Cardiac Looping after Neural Crest Ablation. *Circulation*, *106*, 504-510.

Zeng, X.X., Yelon, D. (2014). Cadm4 Restricts the Production of Cardiac Outflow Tract Progenitor Cells. *Cell Rep*, *7*, 951-960.

Zhou, Y., Cashman, T.J., Nevis, K.R., Obregon, P., Carney, S.A., Liu, Y., Gu, A., Mosimann, C., Sondalle, S., Peterson, R.E., Heideman, W., Burns, C.E.,

Burns, C.G. (2011). Latent Tgf-Beta Binding Protein 3 Identifies a Second Heart Field in Zebrafish. *Nature*, *474*, 645-648.

Zhou, Z., Rawnsley, D.R., Goddard, L.M., Pan, W., Cao, X.J., Jakus, Z., Zheng, H., Yang, J., Arthur, J.S., Whitehead, K.J., Li, D., Zhou, B., Garcia, B.A., Zheng, X., Kahn, M.L. (2015). The Cerebral Cavernous Malformation Pathway Controls Cardiac Development Via Regulation of Endocardial Mekk3 Signaling and Klf Expression. *Dev Cell*, *32*, 168-180.

Appendix: Forces shape the embryonic heart: insights from zebrafish

Reprinted from: Sidhwani, P., Yelon, D., 2019. Fluid forces shape the embryonic heart: insights from zebrafish. *Current Topics in Developmental Biology* 2019; 132: 395-416

Fluid forces shape the embryonic heart: insights from zebrafish

Pragya Sidhwani and Deborah Yelon*

Division of Biological Sciences

University of California, San Diego

La Jolla, CA, 92093, USA

*Correspondence: email: dyelon@ucsd.edu; phone: (858) 534-1822

Running Title: Fluid forces in cardiac morphogenesis

Key Words: heart development, blood flow, cardiac chambers, atrioventricular canal, trabeculation

Abstract

Heart formation involves a complex series of tissue rearrangements, during which regions of the developing organ expand, bend, converge, and protrude in order to create the specific shapes of important cardiac components. Much of this morphogenesis takes place while cardiac function is underway, with blood flowing through the rapidly contracting chambers. Fluid forces are therefore likely to influence the regulation of cardiac morphogenesis, but it is not yet clear how these biomechanical cues direct specific cellular behaviors. In recent years, the optical accessibility and genetic amenability of zebrafish embryos have facilitated unique opportunities to integrate the analysis of flow parameters with the molecular and cellular dynamics underlying cardiogenesis. Consequently, we are making progress toward a comprehensive view of the biomechanical regulation of cardiac chamber emergence, atrioventricular canal differentiation, and ventricular trabeculation. In this review, we highlight a series of studies in zebrafish that have provided new insight into how cardiac function can shape cardiac morphology, with a particular focus on how hemodynamics can impact cardiac cell behavior. Over the long term, this knowledge will undoubtedly guide our consideration of the potential causes of congenital heart disease.

1. Introduction

Biomechanical forces are important regulators of embryonic morphogenesis. As early as gastrulation, circumferential contractions and flow-frictional mechanisms drive the spreading of the enveloping cell layer over the zebrafish yolk (Behrndt et al., 2012). Compressing and stretching the apical surface of cells induces apoptosis and proliferation, respectively, to shape the overall structure of the Drosophila wing (Diaz de la Loza & Thompson, 2017). The periodic spacing of feather follicles in chick is governed by competing interactions between cellular contractility and substrate stiffness (Shyer et al., 2017). In many contexts, physical cues provoke specific cellular behaviors that ultimately give rise to tissue morphology.

Forces are especially crucial during cardiac development, since blood flow and cardiac contractility produce distinct physical inputs while heart formation is underway (Freund et al., 2012; Haack & Abdelilah-Seyfried, 2016). It is particularly interesting to consider how flow-induced forces create spatiotemporally heterogeneous patterns that provide regionalized cues within the developing organ. Fluid frictional forces, for example, induce shear stress that deforms cells in the direction of blood flow. Blood pressure, on the other hand, causes cells to stretch circumferentially. Finally, the direction of blood flow can itself administer distinct mechanical cues to cells: reversing or retrograde flows, for instance, are thought to activate specific downstream pathways. Together, these fluid forces sculpt the heart, in a biological manifestation of “form follows function”.

How do fluid forces prompt cardiac cells to enlarge, elongate, divide, converge, and protrude as they create the specific architecture of the embryonic heart? Despite awareness of several mechanosensitive pathways that operate in endothelial cells (Baratchi et al., 2017), we do not yet fully understand the cellular and molecular mechanisms that drive cardiac morphogenesis in response to hemodynamic cues. To gain insights into these mechanisms, we need to be able to integrate *in vivo* assessment of fluid forces, high-resolution analysis of cell behaviors, and precise manipulation of mechanosensitive genes. The zebrafish embryo serves as an ideal model organism in this regard: its optical clarity allows real-time visualization of fluid dynamics as well as live imaging of morphogenesis at cellular resolution, and its genetic tractability permits both classical genetic screens and cutting-edge genome editing (Collins & Stainier, 2016; Li et al., 2016). Importantly, zebrafish offer the unique advantage that they can survive throughout embryogenesis without convective oxygen, allowing the analysis of cardiovascular defects without confounding lethality. Finally, although the zebrafish heart is anatomically simpler than the mammalian heart, the mechanosensory pathways operating during cardiac development appear to be highly conserved (Goddard et al., 2017). Together, these benefits of zebrafish have facilitated a number of investigations into the ways in which function influences form in the developing heart.

Here, we review a number of recent advances in our understanding of the impact of fluid forces on cardiac morphogenesis, with a particular focus on work performed in zebrafish. We first outline several commonly used techniques for quantification of flow parameters in the zebrafish vasculature and heart. We then

highlight a series of studies that have illuminated how biomechanical inputs regulate the characteristic curvatures of the cardiac chambers, the distinctive features of the atrioventricular canal, and the elaborate network of the ventricular trabeculae. Overall, these insights emphasize the important connections between the mechanical, cellular, and molecular pathways that collaborate to construct the embryonic heart. Importantly, these studies may provide guidance for understanding the etiology of cardiac birth defects in humans, since they imply that fluctuations in blood flow *in utero* could have significant consequences on cardiac morphogenesis.

2. Examination of fluid forces in zebrafish

2.1 Techniques for quantification of fluid forces in the vasculature

To evaluate the influence of fluid forces on cardiac development, it is essential to be able to quantify these forces *in vivo*. Parameters such as shear stress and retrograde flow can then be correlated with patterns of cell behavior in order to create models for how mechanics instruct morphology. A number of techniques have been found to be useful for the assessment of fluid forces in the zebrafish heart, and several of these were first developed in the context of the zebrafish vasculature, where the size and simplicity of the major vessels facilitate live imaging of blood flow.

Digital motion analysis was an initial approach employed to visualize blood flow in zebrafish vessels (Schwerte & Pelster, 2000). Using a simple dissecting microscope and a CCD camera for video imaging, “difference images” can be created to track the motion of erythrocytes in consecutive video frames. Analysis of these images allows assessment of erythrocyte distribution, erythrocyte velocity and

vessel diameter (Schwerte et al., 2003). Although easy to perform, a drawback of two-dimensional video microscopy is that slight variations in embryo orientation can significantly affect results; to some extent, this can be overcome by embedding larvae in tubular molds that are rotated to allow imaging from multiple angles (Bagatto & Burggren, 2006). Additionally, the use of high-speed cameras to follow erythrocytes expressing fluorescent reporter transgenes can substantially enhance the accuracy of cell tracking techniques (Fig. 1A-C) (Watkins et al., 2012).

With the advent of particle image velocimetry (PIV), methods for evaluating flow parameters became even more rigorous. Unlike cell tracking techniques that follow only individual features, PIV averages velocity fields of sub-regions or “interrogation windows” within an image with a high signal-to-noise ratio (Yalcin et al., 2017). This information can be translated into estimates of wall shear stress when coupled with local area measurements, which can be obtained by simultaneously imaging vessel wall motion (Chen et al., 2011). PIV can be performed with both bright-field and fluorescent images, although confocal imaging of fluorescent dyes or transgene-expressing erythrocytes greatly facilitates subsequent image segmentation.

While PIV measurements can be used to estimate the distribution of physical forces, methods such as optical tweezing can directly measure the forces experienced by erythrocytes *in vivo* (Anton et al., 2013). In this technique, forces administered by a focused laser beam are used to hold an erythrocyte in position, such that the amount of force necessary allows assessment of the cell's mechanical milieu. Optical tweezing can be especially useful at branch points in the vasculature,

where sudden changes in the direction of erythrocyte movement can be difficult to track.

Additional techniques have been utilized to image blood flow in the zebrafish vasculature, including fluorescence correlation microscopy (Pan et al., 2007) and optical coherent tomography (Iftimia et al., 2008). Fluorescence correlation microscopy utilizes the inherent autofluorescence of erythrocytes and blood vessels to determine erythrocyte velocity, sidestepping the need to introduce fluorescent tracers. Similarly, optical coherent tomography measures backscattered and back-reflected light to image fluid flow in real time. Although these techniques are beneficial, they require specialized instruments that may not be readily accessible at all research institutions. Consequently, video imaging and confocal imaging, followed by cell tracking or PIV, remain the prevalent methods for assessing flow parameters in zebrafish vessels.

2.2 Techniques for analysis of flow parameters in the heart

The embryonic zebrafish heart is a morphologically elaborate structure that functions to propel blood from the atrium into the ventricle before finally supplying circulation to the aortic vessels. Owing to its particular architecture, imaging blood flow in the heart presents unique technical challenges distinct from those encountered in the vasculature. For example, the dimensions of the cardiac chambers provide many opportunities for erythrocytes to move in and out of the plane of focus. The motion of the chambers creates further complexity, since the chamber wall has to be properly segmented during image analysis. Moreover, the

structure of the heart, coupled with the sequential contraction of the chambers, produces complex flow patterns featuring vortical and reversing flows. Nevertheless, techniques developed for the zebrafish vasculature have been successfully adapted for use in the embryonic heart.

As in the vasculature, PIV has been the method of choice to quantify wall shear stress and other flow parameters during cardiac development. Early applications of this technique used a fluorescent contrast agent to visualize serum motion and demonstrated vortical patterns of flow within the heart (Hove et al., 2003). Although still used widely, PIV has certain drawbacks when applied in the heart. For example, when utilizing video imaging to collect data for PIV analysis, three-dimensional information has to be projected in two dimensions, which results in underestimation of the distance traveled by erythrocytes (Hove et al., 2003). Techniques such as defocusing digital particle image velocimetry, which employ microscopes with two or more apertures to detect out-of-focus particles, can enable more precise tracking of intracardiac flows (Lu et al., 2008). More recently, the depth sectioning capabilities of light sheet microscopy have also been exploited for PIV analysis (Zickus & Taylor, 2018). Another complication associated with PIV measurements in the heart is the interference of cardiac wall motion with erythrocyte tracking, especially in bright-field images. To overcome this, a local signal-to-noise ratio can be used to achieve “cardiac-phase filtering”, which effectively removes artifacts from cardiac wall motion post-image acquisition (Jamison et al., 2013). Since this method identifies the position of the cardiac wall, it enables assessment of wall shear stress in addition to more accurate PIV calculations.

The development of faster imaging techniques has also been valuable for following the complex patterns of erythrocyte motion within the heart. Using a confocal laser slit scanning system, which executes line-wise illumination for faster imaging, significant retrograde flows were observed in the zebrafish heart, both during atrial contraction back into the sinus venosus, and during ventricular contraction back into the atrium (Liebling et al., 2006). Subsequent analysis with high-speed bright-field video microscopy confirmed that the region between the ventricle and the atrium, the atrioventricular canal, experiences a heightened retrograde flow fraction, which is defined as the fraction of the cardiac cycle exhibiting flow reversal (Vermot et al., 2009). These studies have motivated an interest in retrograde flow as a critical signal for atrioventricular canal differentiation, which we will discuss further in a subsequent section.

The emergence of additional strategies for image analysis, such as computational fluid dynamics (CFD), marks a new era for assessment of fluid forces in the zebrafish heart (Yalcin et al., 2017). In computational fluid dynamics, flow parameters are inferred from tracking both chamber wall motions and inlet velocities, which bypasses the requirement for high-resolution imaging as in PIV. Use of computational fluid dynamics in the zebrafish heart has allowed correlation of certain flow characteristics with specific morphogenetic processes (Lee et al., 2013). For example, mean peak shear stress increases significantly during chamber emergence and atrioventricular canal differentiation, suggesting an influence of shear forces on these steps of heart morphogenesis.

Altogether, several options are readily available for analysis of flow parameters in the zebrafish heart (Fig. 1D). Using video, confocal, or light sheet imaging to track erythrocytes, serum, or chamber walls, investigators can use cell tracking, PIV, or computational fluid dynamics approaches to assess erythrocyte velocity, wall shear stress, and retrograde flow fraction. This variety of strategies opens the door to connecting fluid forces to the regulation of a number of specific processes during cardiac morphogenesis, as discussed in the following sections.

3. Hemodynamics and cardiovascular morphogenesis

3.1 Fluid forces regulate multiple aspects of vessel development

When considering how fluid forces influence cardiac morphology, it is instructive to reflect upon our understanding of the influence of flow on vessel development. The impact of physical forces on endothelial cells in the vasculature is especially relevant to the potential roles of such forces on the endocardium, the specialized inner layer of endothelium that lines the muscular myocardial layer of the heart. Since the biomechanical regulation of vascular morphogenesis has been reviewed elsewhere (Baratchi et al., 2017; Boselli et al., 2015), this section will simply provide a few recent perspectives on how processes like lumen growth and vessel remodeling respond to fluid forces in zebrafish.

Blood flow has been shown to regulate vessel diameter through its influence on several types of endothelial cell behaviors. For example, Endoglin, a TGF-β receptor, modulates endothelial cell shape in response to hemodynamic cues,

thereby restricting the diameters of the dorsal aorta and posterior cardinal vein (Sugden et al., 2017). In the caudal vein, shear forces lead to an increase in endothelial cell number via mechanosensation by Pkd2/Trpp2, a calcium channel present on endothelial cilia (Goetz et al., 2014). In the cranial vasculature, flow-induced expression of the TGF-β receptor Alk1 regulates the migration of endothelial cells in the direction opposite to blood flow, thereby limiting vessel caliber (Corti et al., 2011; Rochon et al., 2016). Finally, Yap1, a Hippo pathway effector, localizes to the nucleus in a flow-dependent manner in the dorsal longitudinal anastomotic vessel, where it regulates the maintenance of lumen size (Nakajima et al., 2017).

Fluid forces are also critical for the morphogenetic processes that are involved in vessel remodeling. For instance, flow regulates the apical membrane invagination that is required for successful tube formation during vessel fusion (Herwig et al., 2011). Blood flow is also important for the establishment of planar cell polarity in endothelial cells (Kwon et al., 2016), which could influence vessel regression, as has been predicted in mice (Franco et al., 2015). Indeed, vessel regression in the zebrafish eye (Kochhan et al., 2013) and midbrain (Chen et al., 2012) have been shown to occur in response to blood flow, potentially via flow-mediated cell rearrangement and migration.

Together, these studies underscore the importance of fluid forces during multiple aspects of vascular morphogenesis and provide inspiration for the ways in which blood flow could influence cell shape, cell number, migration, and polarity during heart development. In the following sections, we will examine the impact of cardiac function and fluid forces on cell behavior during three essential phases of

cardiac morphogenesis: chamber emergence, atrioventricular canal differentiation, and ventricular trabeculation.

3.2 Chamber emergence requires hemodynamic inputs

In the early embryo, the primitive heart is a simple, relatively linear cylinder positioned at the embryonic midline. As development proceeds, the heart tube enlarges and transforms into a morphologically distinct series of cardiac chambers, each expanding into its characteristic curvatures (Collins & Stainier, 2016). Since chamber emergence takes place while the heart is beating and the blood is flowing, biomechanical inputs generated by cardiac function have the potential to influence this process. Indeed, surgical obstruction of blood flow into the embryonic chick heart results in aberrant chamber morphology (Broekhuizen et al., 1999). Mouse mutants lacking atrial contractility due to a mutation in *atrial myosin light chain 2a* exhibit abnormal ventricular morphogenesis (Huang et al., 2003), further supporting a connection between blood flow and cardiac chamber development. Taking advantage of the opportunities for examining chamber emergence in the context of the zebrafish embryo, a number of studies have delved deeper into the cell behaviors that shape the chambers in response to biomechanical cues.

In zebrafish, as the ventricle and atrium emerge from the linear heart tube, distinct convex and concave surfaces form the outer and inner curvatures of each chamber. These tissue shape changes are associated with regional patterns of cell shape change: in the ventricle, for example, outer curvature cardiomocytes enlarge and elongate during chamber emergence, while inner curvature cardiomyocytes

remain relatively small and round (Auman et al., 2007). Analysis of cardiomyocyte morphology in mutant embryos has suggested that cell shape change at the ventricular outer curvature depends upon inputs generated by cardiac function. In *weak atrium* (*amhc*) mutants, which lack atrial contractility and therefore have reduced blood flow into the ventricle, outer curvature cardiomyocytes are smaller and rounder than in the wild-type ventricle (Fig. 2A,B) (Auman et al., 2007); these cells also exhibit diminished myofibril maturation (Lin et al., 2012). In contrast, *half-hearted* (*vmhc*) mutants, which lack ventricular contractility, display excessively enlarged and elongated cells in the ventricular outer curvature (Fig. 2C,D) (Auman et al., 2007). These studies suggest that forces produced by both blood flow and contractility modulate cardiomyocyte shape and size and therefore contribute to the regulation of chamber emergence.

In conjunction with the outward expansion of the myocardium, the inner endocardial layer of the heart also grows as the chambers emerge. Cellular proliferation drives this endocardial expansion (Fig. 3A,E,F), while local differences in endocardial cell morphologies correlate with the curved chamber contours (Dietrich et al., 2014). Interestingly, in conditions where fluid forces are reduced, proliferation of the ventricular endocardium is markedly decreased (Fig. 3B-F) (Dietrich et al., 2014). Endocardial cells also fail to acquire normal morphologies under these circumstances. Together, these results suggest a model in which fluid forces trigger proliferation of endocardial cells, causing an overall enlargement of the endocardium that provokes cell shape changes within the myocardium, thereby facilitating synchronous expansion of both cardiac layers.

Which molecular pathways might drive chamber emergence in response to fluid forces? Exposure of endothelial cells to shear stress *in vitro* induces the expression of *KLF2*, which encodes a mechanoresponsive transcription factor (Dekker et al., 2002), and the expression of the zebrafish homolog *klf2a* also appears to be flow-responsive (Vermot et al., 2009). The *klf2* pathway is thought to contribute to the regulation of chamber emergence, since *klf2a* morphants exhibit aberrant endocardial morphology in the ventricle (Dietrich et al., 2014). Micro-RNAs are also interesting candidates for mechanoresponsive functions, since they can be regulated rapidly in response to flow (Banjo et al., 2013). Indeed, function-dependent expression of *miR-143* in both the myocardium and the endocardium impacts the process of ventricular emergence (Miyasaka et al., 2011). In the myocardium, *miR-143* targets *adducin3*, which regulates cytoskeletal actin dynamics and can thereby influence cardiomyocyte morphology (Deacon et al., 2010). In the endocardium, *miR-143* limits retinoic acid signaling by directly targeting *raldh2* and *rxrab* (Miyasaka et al., 2011). Intriguingly, *miR-143* morphants exhibit gaps in the ventricular endocardium (Miyasaka et al., 2011), hinting at defects in endocardial cell number. In future studies, it will be valuable to identify not only additional mechanosensitive genes that are relevant to chamber emergence but also additional downstream effectors responsible for executing the patterns of proliferation in the endocardium and cell shape change in the myocardium.

3.3 Retrograde flow drives atrioventricular canal differentiation

As the cardiac chambers emerge, the junction between the atrium and the ventricle constricts to form the atrioventricular canal (AVC). Within this region, distinct differentiation pathways create the endocardial cushions, specialized structures that will subsequently remodel to create the atrioventricular valve. Endocardial cushion formation has been examined with cellular precision in zebrafish, owing to the optical accessibility of the embryo. At early stages, endocardial cells accumulate both through proliferation and via convergence to the AVC region (Fig. 4A-C) (Boselli et al., 2017; Steed et al., 2016), while also acquiring distinctive cuboidal morphologies (Beis et al., 2005; Steed et al., 2016). Following this, the endocardial cells invaginate as a sheet into the extracellular matrix, ultimately forming valve leaflets (Pestel et al., 2016).

Early work in chick had shown that impediment of mechanical forces in the heart, via surgical alteration, can result in abnormal morphology of the atrioventricular valve (Sedmera et al., 1999). Following this, several studies in zebrafish have indicated that cardiac function provides essential cues for endocardial cushion formation. Endocardial cushions fail to form in *silent heart* mutants and *cardiofunk* mutants, both of which have defects in cardiac contractility (Bartman et al., 2004; Beis et al., 2005). Similarly, physical occlusion of blood flow into the zebrafish heart impairs atrioventricular valve development (Hove et al., 2003).

The oscillatory component of wall shear stress, or retrograde flow, is known to be particularly elevated within the AVC (Heckel et al., 2015), suggesting that the magnitude and the direction of fluid forces could influence AVC differentiation. To examine the effects of these types of mechanical inputs, the phenotypes generated

by knocking down *gata1* and *gata2*, genes involved in hematopoiesis, were examined (Vermot et al., 2009). Since both genes contribute to erythrocyte development, knockdown of either should reduce shear forces in the heart. In addition, *gata2* morphants display a reduction in retrograde flow fraction (RFF) in the AVC, whereas *gata1* morphants display an increased RFF. Furthermore, *gata2* morphants fail to develop valve leaflets, whereas *gata1* morphants appear strikingly normal. Likewise, valve formation fails in *weak atrium* mutants, which also exhibit a reduced RFF in the AVC (Kalogirou et al., 2014). Notably, the valve defects in *gata2* morphants are preceded by a failure to accumulate endocardial cells at the AVC, as well as irregular cellular morphologies (Vermot et al., 2009). The former is consistent with the observation that endocardial convergence at the AVC fails in *silent heart* mutants (Fig. 4B-E) (Boselli et al., 2017). Together, these findings imply that retrograde flow, and not shear, is the driving force for atrioventricular valve formation, potentially through its influence on cellular rearrangement during AVC differentiation.

Investigation of the molecular pathways triggered by retrograde flow in the AVC has primarily centered on *klf2a*. Expression of *klf2a* in the AVC endocardium is reduced in *gata2* morphants (Heckel et al., 2015; Vermot et al., 2009), and *klf2a* morphants resemble *gata2* morphants in that their AVC endocardial cells are reduced in number as well as abnormally elongated and flat (Vermot et al., 2009). Moreover, the calcium channels Trpp2 and Trpv4 appear to regulate *klf2a* expression in response to oscillatory flow patterns within the AVC endocardium (Heckel et al., 2015). Downstream effectors of Klf2 in the AVC endocardium include the extracellular matrix component Fibronectin: *fibronectin1b* morphants have defective

cell clustering at the AVC, similar to *klf2a* morphants and *gata2* morphants (Steed et al., 2016). In addition, *wnt9b* acts a paracrine factor downstream of *klf2a* during AVC differentiation (Goddard et al., 2017).

Given the importance of *klf2a* to mechanosensation at the AVC, it is reasonable to imagine that the levels of *klf2a* expression must be carefully controlled. In accordance with this, the cerebral cavernous malformation (CCM) proteins Ccm1 and Ccm2 have been shown to restrict *klf2a* expression, with Ccm2 acting in a manner independent of cardiac function (Renz et al., 2015). Interestingly, the expression of Heg1, which acts to stabilize Ccm1, appears to be dependent on both cardiac function and *klf2a*, suggesting that *klf2a* acts in a negative feedback loop to influence its own expression (Donat et al., 2018). Altogether, studies of the factors upstream and downstream of *klf2a* place it as a key node in a retrograde flow-regulated pathway that drives AVC differentiation.

When considering additional factors that may act in or parallel to the *klf2a* pathway in this context, it is again interesting to examine the possible roles of micro-RNAs. For example, *miR-21* is expressed in the AVC in a function-dependent manner, and *miR-21* morphants fail to exhibit normal atrioventricular valve formation (Banjo et al., 2013). *miR-21* is thought to activate the MAP kinase cascade by targeting *sprouty2*, suggesting a possible mechanism for its influence on endocardial cell behavior during AVC differentiation. Further work will be necessary to evaluate whether these and/or other players interface with the *klf2a* pathway in executing the biomechanical regulation of AVC differentiation by retrograde flow.

3.4 Functional regulation of ventricular trabeculation

Following cardiac chamber emergence, the architecture of the ventricle becomes more elaborate through the formation of trabeculae – myocardial ridges that extend into the ventricular lumen. Analyses in zebrafish have shown that trabeculation is driven by the directional migration of cells that delaminate from the compact layer of the myocardium (Liu et al., 2010; Staudt et al., 2014). This delamination process involves constriction of the abluminal cardiomyocyte surface and is dependent upon the proper apicobasal polarization of the myocardial tissue (Jimenez-Amilburu et al., 2016; Staudt et al., 2014). In a noncontractile zebrafish heart, trabeculation fails: in *silent heart* morphants, for example, cardiomyocytes still extend protrusions into the ventricular lumen, but these protrusions frequently retract and stable trabeculae do not form (Staudt et al., 2014). These findings indicate that cardiac function is important for regulating trabeculation, consistent with prior observations in chick, where ventricular afterload has been implicated in regulating the thickening of the compact and trabecular layers (Sedmera et al., 1999).

Do fluid forces play a key role in controlling the cell behaviors that underlie trabeculation? Indeed, reduction of blood flow in both *weak atrium* mutants and *gata1* morphants inhibits trabeculation (Fig. 5A,C,D) (Lee et al., 2016; Peshkovsky et al., 2011; Staudt et al., 2014; Vedula et al., 2017). Furthermore, studies in *weak atrium* mutants and morphants suggest that both the initial formation of luminal protrusions and their progression into stable trabeculae could be sensitive to the patterns of blood flow through the ventricle (Peshkovsky et al., 2011; Staudt et al., 2014). Flow parameters at the onset of ventricular trabeculation have not yet been carefully

examined; however, the oscillatory shear index has been shown to be higher in trabecular grooves and lower in trabecular ridges at 4 days post-fertilization, after mature trabeculae are in place, and this distinct pattern is perturbed when trabeculation is inhibited (Fig. 5) (Vedula et al., 2017). In future studies, it will be valuable to investigate flow patterns in the ventricle at earlier stages in order to discern whether parameters like the oscillatory shear index can predict where trabecular protrusions will form.

Several signaling pathways that are known to be important regulators of trabeculation are also responsive to biomechanical cues. For example, the Neuregulin signaling pathway, operating through the Erbb2 receptor tyrosine kinase, is required for trabeculation (Liu et al., 2010), and expression of both *erbb2* (Lee et al., 2016) and its ligand *nrg2a* (Rasouli & Stainier, 2017) have been shown to be dependent on cardiac function. Function-mediated Notch signaling activity in the endocardium has also been implicated in trabeculation, potentially via its role in regulating expression of the Erbb2 ligand *nrg1* (Samsa et al., 2015), as has been suggested in mice (Grego-Bessa et al., 2007). Wwtr1, a Hippo pathway effector that localizes to the nucleus in response to function, is an essential regulator of the compact wall architecture supporting trabeculation, where it can also influence myocardial Notch signaling (Lai et al., 2018). Furthermore, Erbb2 signaling can direct Wwtr1 localization (Lai et al., 2018) and Notch signaling in the myocardium (Jimenez-Amilburu et al., 2016). Finally, cardiac function, Erbb2, Wwtr1, and Notch have all independently been shown to be important for the relocalization of N-cadherin in delaminating cardiomyocytes (Cherian et al., 2016; Han et al., 2016; Lai et al., 2018).

Collectively, these data signify complex spatiotemporal interactions between cardiac function and the Erbb2, Notch, and Hippo signaling pathways during the modulation of trabeculation. Ongoing studies will continue to illuminate the precise nature of these interactions, while also deciphering how these pathways instruct cell behaviors as trabeculae form.

4. Summary and future directions

Recent studies in zebrafish have amply demonstrated the broad utility of this model organism for analysis of the biomechanical regulation of cardiac development. The exceptional optical access to the developing heart, coupled with a variety of options for manipulation of gene function, has illuminated multiple morphogenetic processes that are dependent upon cardiac function. Moreover, scenarios in which blood flow is altered have provided intriguing evidence linking fluid forces to several key steps in cardiac maturation. Finally, further genetic analyses have created an emerging framework of the mechanoresponsive pathways that orchestrate important patterns of cell behavior in the embryonic heart (Fig. 6).

Despite these recent advances, there are still substantial challenges inherent to studying the relationship between fluid forces and cardiac morphogenesis. Importantly, common strategies for interfering with cardiac function often alter several biomechanical variables simultaneously. Inhibition of cardiac contractility, for example, changes both the stretch of cardiac tissues and the various forces associated with blood flow. In addition, manipulations that alter circulation while still maintaining contractility can perturb both the velocity and the direction of flow. Hence,

most conclusions reached thus far are based on correlating particular functional scenarios with interesting phenotypes, rather than demonstrating which specific types of fluid forces cause which cellular outcomes. To evaluate the effects of distinct biomechanical cues, it will be instrumental for future studies to employ techniques that administer specific forces in a targeted fashion. Applications of single molecule spectroscopy could be adapted for this purpose: optical tweezing, for instance, could be used to manipulate erythrocyte velocity or direction in a confined region (Anton et al., 2013). Similarly, magnetic tweezers could be employed to stretch cells coated with ligand-conjugated magnetic beads, where the specificity of the ligand determines spatial control (Marjoram et al., 2016). These types of directed manipulations will help to delineate causative relationships between distinct fluid forces and specific cellular responses.

Even with experiments that uncouple the effects of specific flow parameters, limitations remain in our ability to interpret how particular forces exert their impact on both the endocardium and the myocardium. These two layers of the heart appear to respond to fluid forces in a harmonious fashion, yet it is unknown how they coordinate their morphogenesis. Does the pressure created by blood flow induce stretch of both the endocardium and the myocardium simultaneously? Or do fluid forces act primarily on the endocardium, with signals relayed to the myocardium only secondarily? Does the ECM that resides between the endocardium and myocardium transmit biomechanical cues between the layers, in addition to regulating biochemical cross-talk between them? To address these questions, it will be exciting for future studies to employ tools like tissue-specific, FRET-based tension sensors (Lagendijk

et al., 2017) or tissue-embedded, force-sensitive oil microdroplets (Campas et al., 2014) to elucidate the precise spatiotemporal dynamics of cardiac mechanosensation.

Finally, we cannot resolve the mechanical interactions between the endocardium and the myocardium without knowing the full roster of molecular pathways responding to forces in each of the two layers. Interesting candidates for future exploration include Piezo1, a mechanosensitive calcium channel (Ranade et al., 2014), Yap1, a nuclear target of Hippo signaling (Nakajima et al., 2017), TGF-β receptors like Endoglin (Sugden et al., 2017), and junctional components like VE-cadherin (Baratchi et al., 2017), all of which have been shown to have mechanoresponsive roles in the endothelium. It will also be important to consider possible functional overlap between paralogues of genes that have already been implicated in cardiac mechanobiology, especially since discrepancies between mutant and morphant phenotypes suggest compensatory interactions between related factors (Novodvorsky et al., 2015).

Altogether, the body of work examining the influence of fluid forces during zebrafish heart development has opened up a number of exciting avenues for further investigation into the mechanosensitive pathways that control essential morphogenetic mechanisms. Going forward, we foresee that future studies in this area will actively bridge the gap between biomechanical inputs and cellular outcomes. By measuring and manipulating specific flow parameters and monitoring their impacts, it will be feasible to connect the fluid mechanics, signal transduction, downstream effector genes, and cellular dynamics that are responsible for shaping

essential features of the developing heart. Ultimately, a mechanistic understanding of the roles of fluid forces during cardiac morphogenesis is likely to provide a valuable foundation for new insights regarding how hemodynamic conditions *in utero* affect the incidence of congenital heart disease.

Acknowledgements

The appendix, in full, is a reformatted reprint of the following book chapter: Sidhwani, P., Yelon, D., 2019. “Fluid forces shape the embryonic heart: insights from zebrafish”, in *Current Topics in Developmental Biology* 2019; 132: 395-416. The dissertation author was the primary investigator and author of this paper.

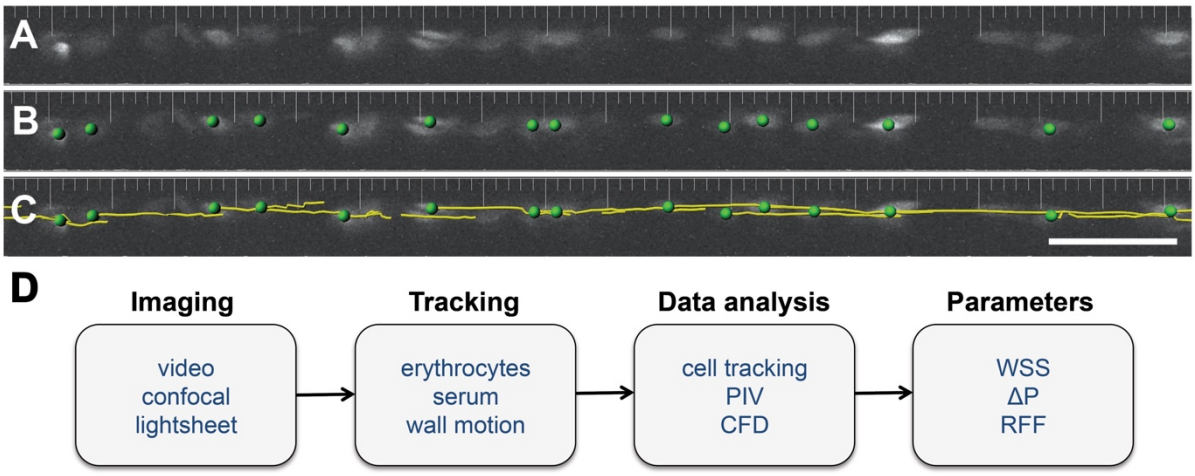

Figure A-1: Analysis of blood flow in the zebrafish. (A) Labeled erythrocytes in the dorsal aorta of an embryo carrying the transgene *Tg(gata1:dsRed)* are visualized at a single timepoint. (B) Image segmentation identifies individual erythrocytes (green dots). (C) A tracking algorithm reveals the trajectories (yellow lines) of the erythrocytes, allowing measurement of their displacement and estimation of their velocity. (D) Workflow options for analysis of blood flow in zebrafish. PIV, particle image velocimetry; CFD, computational fluid dynamics; WSS, wall shear stress; RFF, retrograde flow fraction. Panels A-C adapted from Watkins et al., 2012.

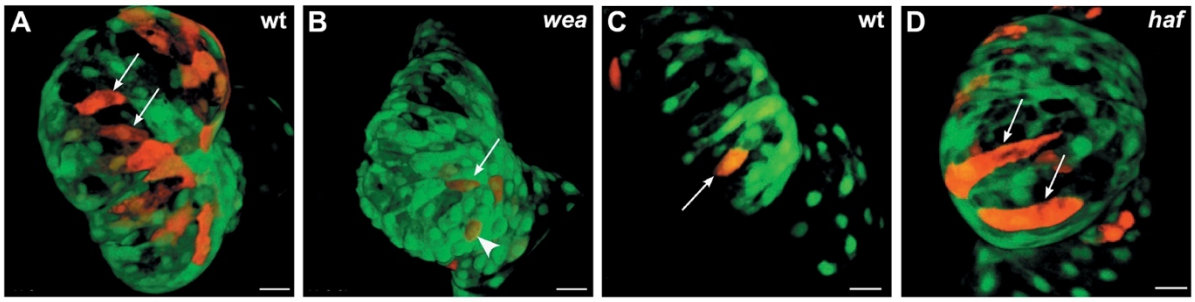

Figure A-2: Cardiac function modulates cardiomyocyte dimensions in the ventricle. Confocal projections show the ventricle in embryos carrying the transgene *Tg*(*myl7:egfp*), with mosaic expression of *Tg*(*myl7*:*dsRedt4*). (A,C) At 52 hours post-fertilization (hpf), cardiomyocytes in the outer curvature of the ventricle (arrows) have acquired a characteristic size and an elongated morphology. (B) In *weak atrium* (*wea*) mutants, blood flow into the ventricle is reduced, and the cardiomyocytes in the outer curvature are abnormally small (arrow) and circular (arrowhead). (D) In *half-hearted* (*haf*) mutants, the ventricle is non-contractile, and the outer curvature cardiomyocytes are abnormally large and distended (arrows). Images adapted from Auman et al., 2007.

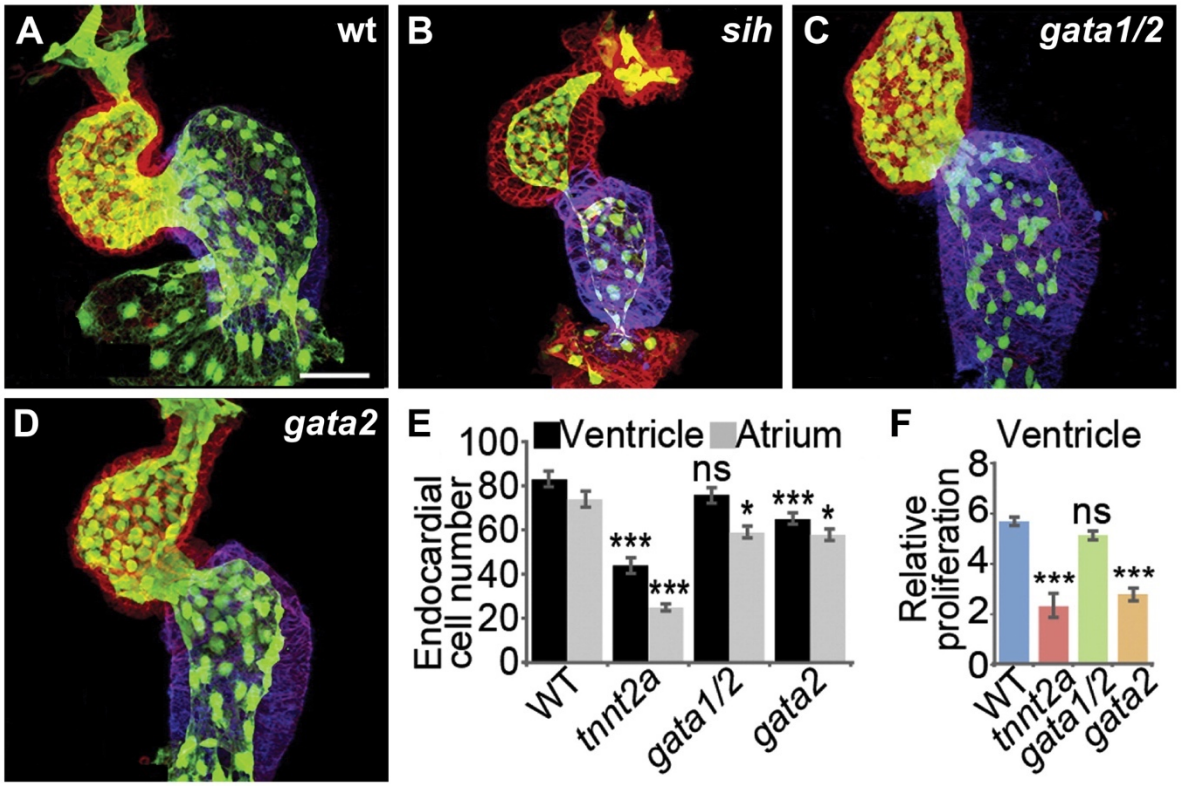

Figure A-3: Fluid forces influence endocardial cell number during chamber emergence. (A-D) Endocardial cells (green) are indicated by expression of the transgene *Tg*(*kdrl:GFP*); localization of Amhc (blue) and actin (red) are also shown. Whereas wild-type embryos have ~80 and ~70 endocardial cells in the ventricle and the atrium, respectively (A,E), the number of endocardial cells in both chambers is significantly reduced in *silent heart* (*sih; tnnt2a*) mutants (B,E), in which the heart is noncontractile. *gata1/2* morphants, which have diminished shear forces due to their reduced hematocrit, display fewer endocardial cells in the atrium (C,E). In contrast, *gata2* morphants, which have been shown to have reduced retrograde flow in addition to diminished shear forces, display fewer endocardial cells in both chambers (D,E), similar to *sih* mutants. (F) Consistent with this, endocardial proliferation in the ventricle is significantly reduced in *sih* mutants and *gata2* morphants, but not in *gata1*/*2* morphants. Images adapted from Dietrich et al., 2014.

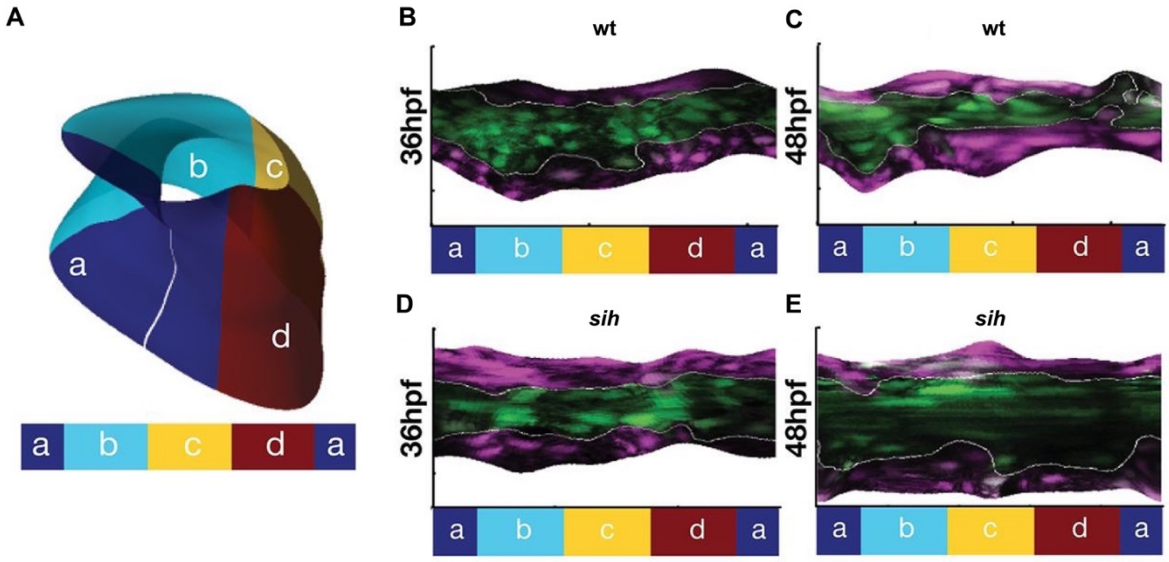

Figure A-4: Cardiac function regulates endocardial convergence at the AVC. (A) The AVC endocardium can be subdivided into four regions: superior (a), exterior (b), inferior (c) and interior (d). (B-E) Representations of the unfolded endocardium in *Tg(fli:kaede)* embryos in which the AVC endocardium has been labeled via photoconversion. In wild-type embryos, the AVC endocardial cells converge between 36 hpf (B) and 48 hpf (C). In contrast, in *sih* mutants, the AVC endocardium widens between 36 hpf (D) and 48 hpf (E). Images adapted from Boselli et al., 2017.

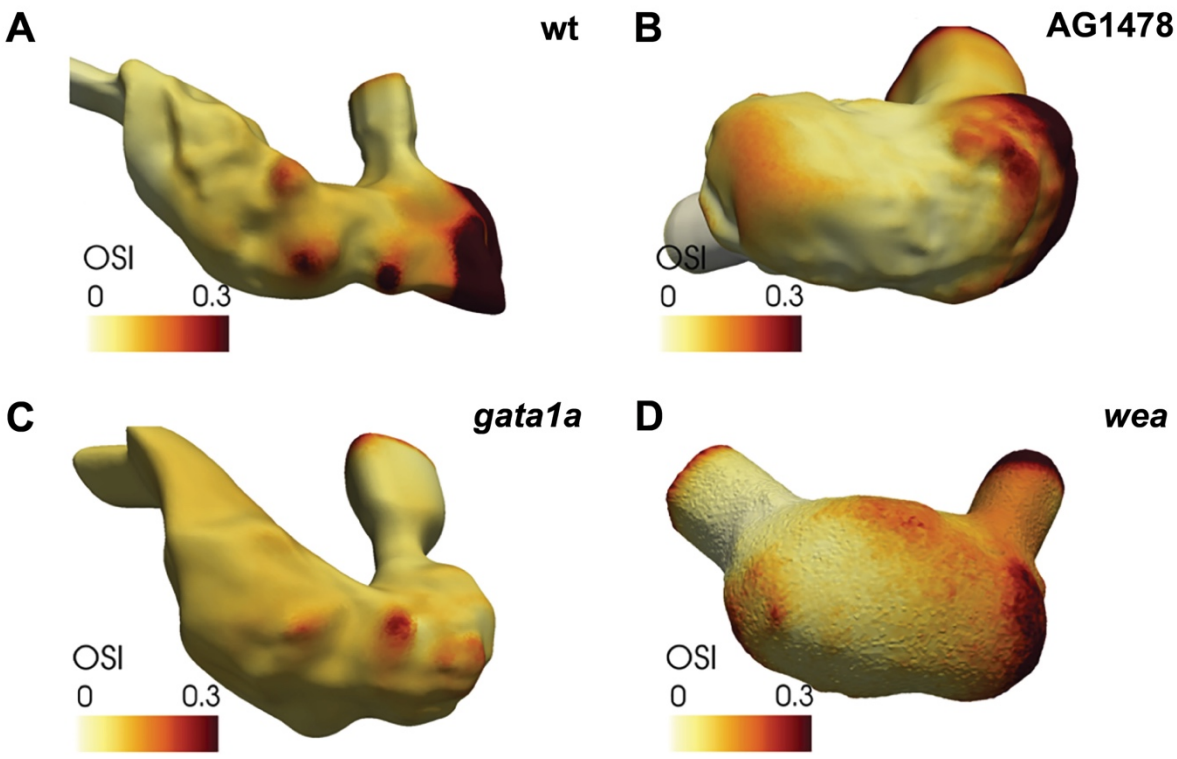

Figure A-5: Interplay between fluid forces and ventricular trabeculation. Representations of the inner surface of the ventricle, overlaid with a depiction of the oscillatory shear index (OSI) at 4 dpf. (A) In wild-type, the OSI is relatively high in trabecular grooves and relatively low in trabecular ridges. (B) In AG1478-treated embryos, the Neuregulin signaling pathway is inhibited, resulting in reduced trabeculation and a smoother inner surface of the ventricle. A similar reduction of trabeculation is observed in *gata1a* morphants (C) and *wea* mutants (D). Images adapted from Vedula et al., 2017.

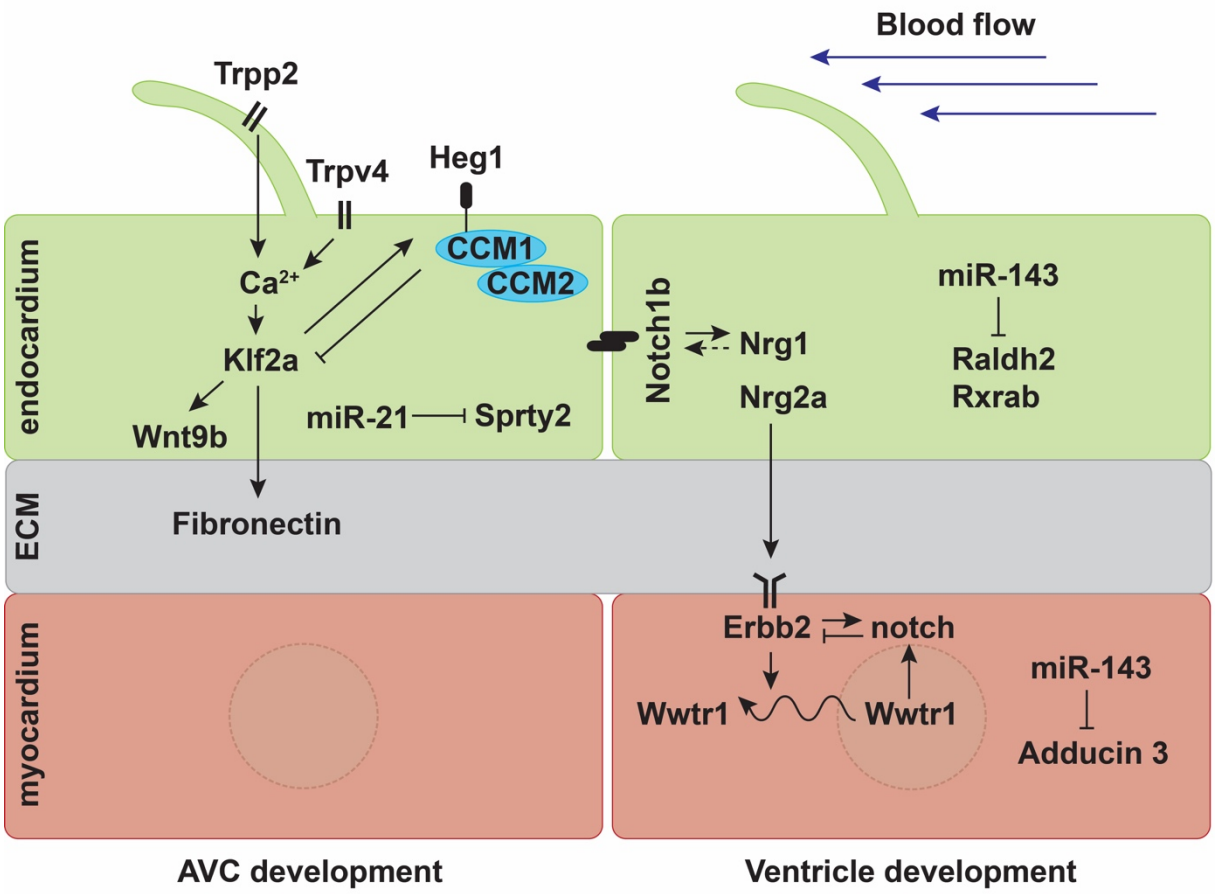

Figure A-6: Mechanoresponsive pathways regulating cardiac development in zebrafish. During AVC development, oscillatory flow activates mechanosensitive calcium channels Trpp2 and Trpv4 in the endocardium, which then promote *klf2a* expression (Heckel et al., 2015). In addition, flow-induced Heg1 represses *klf2a* expression in conjunction with the CCM complex, establishing a feedback loop for *klf2a* (Donat et al., 2018; Renz et al., 2015). Klf2a, in turn, regulates *wnt9b* expression in the endocardium (Goddard et al., 2017) and Fibronectin deposition in the extracellular matrix (ECM) (Steed et al., 2016). At the same time, flow-induced *miR-21* represses receptor tyrosine kinase signaling by targeting *sprty2* (Banjo et al., 2013). Meanwhile, during ventricle emergence, function-dependent *miR-143* inhibits retinoic acid signaling in the endocardium (Miyasaka et al., 2011) and targets Adducin3 in the myocardium (Deacon *et al*., 2010). Mechanical forces also activate Notch signaling in the endocardium, which further induces expression of the Erbb2 ligand *nrg1* (Samsa et al., 2015). During trabeculation, cardiac function regulates *nrg2a* (Rasouli and Stainier, 2017) and *erbb2* expression (Lee et al., 2016), as well as Wwtr1 localization (Lai et al., 2018). The Nrg/Erbb2 pathway can further affect Notch signaling in cardiomyocytes (Jiménez-Amilburu et al., 2016) and regulate Wwtr1 localization, which can also activate Notch signaling (Lai et al., 2018).

References

Anton, H., Harlepp, S., Ramspacher, C., Wu, D., Monduc, F., Bhat, S., Liebling, M., Paoletti, C., Charvin, G., Freund, J.B., Vermot, J. (2013). Pulse Propagation by a Capacitive Mechanism Drives Embryonic Blood Flow. *Development*, *140*, 4426-4434.

Auman, H.J., Coleman, H., Riley, H.E., Olale, F., Tsai, H.J., Yelon, D. (2007). Functional Modulation of Cardiac Form through Regionally Confined Cell Shape Changes. *PLoS Biol*, *5*, e53.

Bagatto, B., Burggren, W. (2006). A Three-Dimensional Functional Assessment of Heart and Vessel Development in the Larva of the Zebrafish (Danio Rerio). *Physiol Biochem Zool*, *79*, 194-201.

Banjo, T., Grajcarek, J., Yoshino, D., Osada, H., Miyasaka, K.Y., Kida, Y.S., Ueki, Y., Nagayama, K., Kawakami, K., Matsumoto, T., Sato, M., Ogura, T. (2013). Haemodynamically Dependent Valvulogenesis of Zebrafish Heart Is Mediated by Flow-Dependent Expression of Mir-21. *Nat Commun*, *4*, 1978.

Baratchi, S., Khoshmanesh, K., Woodman, O.L., Potocnik, S., Peter, K., McIntyre, P. (2017). Molecular Sensors of Blood Flow in Endothelial Cells. *Trends Mol Med*, *23*, 850-868.

Bartman, T., Walsh, E.C., Wen, K.K., McKane, M., Ren, J., Alexander, J., Rubenstein, P.A., Stainier, D.Y. (2004). Early Myocardial Function Affects Endocardial Cushion Development in Zebrafish. *PLoS Biol*, *2*, E129.

Behrndt, M., Salbreux, G., Campinho, P., Hauschild, R., Oswald, F., Roensch, J., Grill, S.W., Heisenberg, C.P. (2012). Forces Driving Epithelial Spreading in Zebrafish Gastrulation. *Science*, *338*, 257-260.

Beis, D., Bartman, T., Jin, S.W., Scott, I.C., D'Amico, L.A., Ober, E.A., Verkade, H., Frantsve, J., Field, H.A., Wehman, A., Baier, H., Tallafuss, A., Bally-Cuif, L., Chen, J.N., Stainier, D.Y., Jungblut, B. (2005). Genetic and Cellular Analyses of Zebrafish Atrioventricular Cushion and Valve Development. *Development*, *132*, 4193-4204.

Boselli, F., Freund, J.B., Vermot, J. (2015). Blood Flow Mechanics in Cardiovascular Development. *Cell Mol Life Sci*, *72*, 2545-2559.

Boselli, F., Steed, E., Freund, J.B., Vermot, J. (2017). Anisotropic Shear Stress Patterns Predict the Orientation of Convergent Tissue Movements in the Embryonic Heart. *Development*, *144*, 4322-4327.

Broekhuizen, M.L., Hogers, B., DeRuiter, M.C., Poelmann, R.E., Gittenberger-de Groot, A.C., Wladimiroff, J.W. (1999). Altered Hemodynamics in Chick Embryos after Extraembryonic Venous Obstruction. *Ultrasound Obstet Gynecol*, *13*, 437-445.

Campas, O., Mammoto, T., Hasso, S., Sperling, R.A., O'Connell, D., Bischof, A.G., Maas, R., Weitz, D.A., Mahadevan, L., Ingber, D.E. (2014). Quantifying Cell-Generated Mechanical Forces within Living Embryonic Tissues. *Nat Methods*, *11*, 183-189.

Chen, C.Y., Patrick, M.J., Corti, P., Kowalski, W., Roman, B.L., Pekkan, K. (2011). Analysis of Early Embryonic Great-Vessel Microcirculation in Zebrafish Using High-Speed Confocal Mupiv. *Biorheology*, *48*, 305-321.

Chen, Q., Jiang, L., Li, C., Hu, D., Bu, J.W., Cai, D., Du, J.L. (2012). Haemodynamics-Driven Developmental Pruning of Brain Vasculature in Zebrafish. *PLoS Biol*, *10*, e1001374.

Cherian, A.V., Fukuda, R., Augustine, S.M., Maischein, H.M., Stainier, D.Y. (2016). N-Cadherin Relocalization During Cardiac Trabeculation. *Proc Natl Acad Sci U S A*, *113*, 7569-7574.

Collins, M.M., Stainier, D.Y. (2016). Organ Function as a Modulator of Organ Formation: Lessons from Zebrafish. *Curr Top Dev Biol*, *117*, 417-433.

Corti, P., Young, S., Chen, C.Y., Patrick, M.J., Rochon, E.R., Pekkan, K., Roman, B.L. (2011). Interaction between Alk1 and Blood Flow in the Development of Arteriovenous Malformations. *Development*, *138*, 1573-1582.

Deacon, D.C., Nevis, K.R., Cashman, T.J., Zhou, Y., Zhao, L., Washko, D., Guner-Ataman, B., Burns, C.G., Burns, C.E. (2010). The Mir-143-Adducin3 Pathway Is Essential for Cardiac Chamber Morphogenesis. *Development*, *137*, 1887-1896.

Dekker, R.J., van Soest, S., Fontijn, R.D., Salamanca, S., de Groot, P.G., VanBavel, E., Pannekoek, H., Horrevoets, A.J. (2002). Prolonged Fluid Shear Stress Induces a Distinct Set of Endothelial Cell Genes, Most Specifically Lung Kruppel-Like Factor (Klf2). *Blood*, *100*, 1689-1698.

Diaz de la Loza, M.C., Thompson, B.J. (2017). Forces Shaping the Drosophila Wing. *Mech Dev*, *144*, 23-32.

Dietrich, A.C., Lombardo, V.A., Veerkamp, J., Priller, F., Abdelilah-Seyfried, S. (2014). Blood Flow and Bmp Signaling Control Endocardial Chamber Morphogenesis. *Dev Cell*, *30*, 367-377.

Donat, S., Lourenco, M., Paolini, A., Otten, C., Renz, M., Abdelilah-Seyfried, S. (2018). Heg1 and Ccm1/2 Proteins Control Endocardial Mechanosensitivity During Zebrafish Valvulogenesis. *Elife*, *7*.

Franco, C.A., Jones, M.L., Bernabeu, M.O., Geudens, I., Mathivet, T., Rosa, A., Lopes, F.M., Lima, A.P., Ragab, A., Collins, R.T., Phng, L.K., Coveney, P.V., Gerhardt, H. (2015). Dynamic Endothelial Cell Rearrangements Drive Developmental Vessel Regression. *PLoS Biol*, *13*, e1002125.

Freund, J.B., Goetz, J.G., Hill, K.L., Vermot, J. (2012). Fluid Flows and Forces in Development: Functions, Features and Biophysical Principles. *Development*, *139*, 1229-1245.

Goddard, L.M., Duchemin, A.L., Ramalingan, H., Wu, B., Chen, M., Bamezai, S., Yang, J., Li, L., Morley, M.P., Wang, T., Scherrer-Crosbie, M., Frank, D.B., Engleka, K.A., Jameson, S.C., Morrisey, E.E., Carroll, T.J., Zhou, B., Vermot, J., Kahn, M.L. (2017).

Hemodynamic Forces Sculpt Developing Heart Valves through a Klf2-Wnt9b Paracrine Signaling Axis. *Dev Cell*, *43*, 274-289 e275.

Goetz, J.G., Steed, E., Ferreira, R.R., Roth, S., Ramspacher, C., Boselli, F., Charvin, G., Liebling, M., Wyart, C., Schwab, Y., Vermot, J. (2014). Endothelial Cilia Mediate Low Flow Sensing During Zebrafish Vascular Development. *Cell Rep*, *6*, 799-808.

Grego-Bessa, J., Luna-Zurita, L., del Monte, G., Bolos, V., Melgar, P., Arandilla, A., Garratt, A.N., Zang, H., Mukouyama, Y.S., Chen, H., Shou, W., Ballestar, E., Esteller, M., Rojas, A., Perez-Pomares, J.M., de la Pompa, J.L. (2007). Notch Signaling Is Essential for Ventricular Chamber Development. *Dev Cell*, *12*, 415-429.

Haack, T., Abdelilah-Seyfried, S. (2016). The Force Within: Endocardial Development, Mechanotransduction and Signalling During Cardiac Morphogenesis. *Development*, *143*, 373-386.

Han, P., Bloomekatz, J., Ren, J., Zhang, R., Grinstein, J.D., Zhao, L., Burns, C.G., Burns, C.E., Anderson, R.M., Chi, N.C. (2016). Coordinating Cardiomyocyte Interactions to Direct Ventricular Chamber Morphogenesis. *Nature*, *534*, 700-704.

Heckel, E., Boselli, F., Roth, S., Krudewig, A., Belting, H.G., Charvin, G., Vermot, J. (2015). Oscillatory Flow Modulates Mechanosensitive Klf2a Expression through Trpv4 and Trpp2 During Heart Valve Development. *Curr Biol*, *25*, 1354-1361.

Herwig, L., Blum, Y., Krudewig, A., Ellertsdottir, E., Lenard, A., Belting, H.G., Affolter, M. (2011). Distinct Cellular Mechanisms of Blood Vessel Fusion in the Zebrafish Embryo. *Curr Biol*, *21*, 1942-1948.

Hove, J.R., Koster, R.W., Forouhar, A.S., Acevedo-Bolton, G., Fraser, S.E., Gharib, M. (2003). Intracardiac Fluid Forces Are an Essential Epigenetic Factor for Embryonic Cardiogenesis. *Nature*, *421*, 172-177.

Huang, C., Sheikh, F., Hollander, M., Cai, C., Becker, D., Chu, P.H., Evans, S., Chen, J. (2003). Embryonic Atrial Function Is Essential for Mouse Embryogenesis, Cardiac Morphogenesis and Angiogenesis. *Development*, *130*, 6111-6119.

Iftimia, N.V., Hammer, D.X., Ferguson, R.D., Mujat, M., Vu, D., Ferrante, A.A. (2008). Dual-Beam Fourier Domain Optical Doppler Tomography of Zebrafish. *Opt Express*, *16*, 13624-13636.

Jamison, R.A., Samarage, C.R., Bryson-Richardson, R.J., Fouras, A. (2013). In Vivo Wall Shear Measurements within the Developing Zebrafish Heart. *PLoS One*, *8*, e75722.

Jimenez-Amilburu, V., Rasouli, S.J., Staudt, D.W., Nakajima, H., Chiba, A., Mochizuki, N., Stainier, D.Y.R. (2016). In Vivo Visualization of Cardiomyocyte Apicobasal Polarity Reveals Epithelial to Mesenchymal-Like Transition During Cardiac Trabeculation. *Cell Rep*, *17*, 2687-2699.

Kalogirou, S., Malissovas, N., Moro, E., Argenton, F., Stainier, D.Y., Beis, D. (2014). Intracardiac Flow Dynamics Regulate Atrioventricular Valve Morphogenesis. *Cardiovasc Res*, *104*, 49-60.

Kochhan, E., Lenard, A., Ellertsdottir, E., Herwig, L., Affolter, M., Belting, H.G., Siekmann, A.F. (2013). Blood Flow Changes Coincide with Cellular Rearrangements During Blood Vessel Pruning in Zebrafish Embryos. *PLoS One*, *8*, e75060.

Kwon, H.B., Wang, S., Helker, C.S., Rasouli, S.J., Maischein, H.M., Offermanns, S., Herzog, W., Stainier, D.Y. (2016). In Vivo Modulation of Endothelial Polarization by Apelin Receptor Signalling. *Nat Commun*, *7*, 11805.

Lagendijk, A.K., Gomez, G.A., Baek, S., Hesselson, D., Hughes, W.E., Paterson, S., Conway, D.E., Belting, H.G., Affolter, M., Smith, K.A., Schwartz, M.A., Yap, A.S., Hogan, B.M. (2017). Live Imaging Molecular Changes in Junctional Tension Upon Ve-Cadherin in Zebrafish. *Nat Commun*, *8*, 1402.

Lai, J.K.H., Collins, M.M., Uribe, V., Jimenez-Amilburu, V., Gunther, S., Maischein, H.M., Stainier, D.Y.R. (2018). The Hippo Pathway Effector Wwtr1 Regulates Cardiac Wall Maturation in Zebrafish. *Development*, *145*.

Lee, J., Fei, P., Sevag Packard, R.R., Kang, H., Xu, H., Baek, K.I., Jen, N., Chen, J., Yen, H., Kuo, C.C., Chi, N.C., Ho, C.M., Li, R., Hsiai, T.K. (2016). 4-Dimensional Light-Sheet Microscopy to Elucidate Shear Stress Modulation of Cardiac Trabeculation. *J Clin Invest*, *126*, 3158.

Lee, J., Moghadam, M.E., Kung, E., Cao, H., Beebe, T., Miller, Y., Roman, B.L., Lien, C.L., Chi, N.C., Marsden, A.L., Hsiai, T.K. (2013). Moving Domain Computational Fluid Dynamics to Interface with an Embryonic Model of Cardiac Morphogenesis. *PLoS One*, *8*, e72924.

Li, M., Zhao, L., Page-McCaw, P.S., Chen, W. (2016). Zebrafish Genome Engineering Using the Crispr-Cas9 System. *Trends Genet*, *32*, 815-827.

Liebling, M., Forouhar, A.S., Wolleschensky, R., Zimmermann, B., Ankerhold, R., Fraser, S.E., Gharib, M., Dickinson, M.E. (2006). Rapid Three-Dimensional Imaging and Analysis of the Beating Embryonic Heart Reveals Functional Changes During Development. *Dev Dyn*, *235*, 2940-2948.

Lin, Y.F., Swinburne, I., Yelon, D. (2012). Multiple Influences of Blood Flow on Cardiomyocyte Hypertrophy in the Embryonic Zebrafish Heart. *Dev Biol*, *362*, 242-253.

Liu, J., Bressan, M., Hassel, D., Huisken, J., Staudt, D., Kikuchi, K., Poss, K.D., Mikawa, T., Stainier, D.Y. (2010). A Dual Role for Erbb2 Signaling in Cardiac Trabeculation. *Development*, *137*, 3867-3875.

Lu, J., Pereira, F., Fraser, S.E., Gharib, M. (2008). Three-Dimensional Real-Time Imaging of Cardiac Cell Motions in Living Embryos. *J Biomed Opt*, *13*, 014006.

Marjoram, R.J., Guilluy, C., Burridge, K. (2016). Using Magnets and Magnetic Beads to Dissect Signaling Pathways Activated by Mechanical Tension Applied to Cells. *Methods*, *94*, 19-26.

Miyasaka, K.Y., Kida, Y.S., Banjo, T., Ueki, Y., Nagayama, K., Matsumoto, T., Sato, M., Ogura, T. (2011). Heartbeat Regulates Cardiogenesis by Suppressing Retinoic Acid Signaling Via Expression of Mir-143. *Mech Dev*, *128*, 18-28.

Nakajima, H., Yamamoto, K., Agarwala, S., Terai, K., Fukui, H., Fukuhara, S., Ando, K., Miyazaki, T., Yokota, Y., Schmelzer, E., Belting, H.G., Affolter, M., Lecaudey, V., Mochizuki, N. (2017). Flow-Dependent Endothelial Yap Regulation Contributes to Vessel Maintenance. *Dev Cell*, *40*, 523-536 e526.

Novodvorsky, P., Watson, O., Gray, C., Wilkinson, R.N., Reeve, S., Smythe, C., Beniston, R., Plant, K., Maguire, R., A, M.K.R., Elworthy, S., van Eeden, F.J., Chico, T.J. (2015). Klf2ash317 Mutant Zebrafish Do Not Recapitulate Morpholino-Induced Vascular and Haematopoietic Phenotypes. *PLoS One*, *10*, e0141611.

Pan, X., Yu, H., Shi, X., Korzh, V., Wohland, T. (2007). Characterization of Flow Direction in Microchannels and Zebrafish Blood Vessels by Scanning Fluorescence Correlation Spectroscopy. *J Biomed Opt*, *12*, 014034.

Peshkovsky, C., Totong, R., Yelon, D. (2011). Dependence of Cardiac Trabeculation on Neuregulin Signaling and Blood Flow in Zebrafish. *Dev Dyn*, *240*, 446-456.

Pestel, J., Ramadass, R., Gauvrit, S., Helker, C., Herzog, W., Stainier, D.Y. (2016). Real-Time 3d Visualization of Cellular Rearrangements During Cardiac Valve Formation. *Development*, *143*, 2217-2227.

Ranade, S.S., Qiu, Z., Woo, S.H., Hur, S.S., Murthy, S.E., Cahalan, S.M., Xu, J., Mathur, J., Bandell, M., Coste, B., Li, Y.S., Chien, S., Patapoutian, A. (2014). Piezo1, a Mechanically Activated Ion Channel, Is Required for Vascular Development in Mice. *Proc Natl Acad Sci U S A*, *111*, 10347-10352.

Rasouli, S.J., Stainier, D.Y.R. (2017). Regulation of Cardiomyocyte Behavior in Zebrafish Trabeculation by Neuregulin 2a Signaling. *Nat Commun*, *8*, 15281.

Renz, M., Otten, C., Faurobert, E., Rudolph, F., Zhu, Y., Boulday, G., Duchene, J., Mickoleit, M., Dietrich, A.C., Ramspacher, C., Steed, E., Manet-Dupe, S., Benz, A., Hassel, D., Vermot, J., Huisken, J., Tournier-Lasserve, E., Felbor, U., Sure, U., Albiges-Rizo, C., Abdelilah-Seyfried, S. (2015). Regulation of Beta1 Integrin-Klf2-Mediated Angiogenesis by Ccm Proteins. *Dev Cell*, *32*, 181-190.

Rochon, E.R., Menon, P.G., Roman, B.L. (2016). Alk1 Controls Arterial Endothelial Cell Migration in Lumenized Vessels. *Development*, *143*, 2593-2602.

Samsa, L.A., Givens, C., Tzima, E., Stainier, D.Y., Qian, L., Liu, J. (2015). Cardiac Contraction Activates Endocardial Notch Signaling to Modulate Chamber Maturation in Zebrafish. *Development*, *142*, 4080-4091.

Schwerte, T., Pelster, B. (2000). Digital Motion Analysis as a Tool for Analysing the Shape and Performance of the Circulatory System in Transparent Animals. *J Exp Biol*, *203*, 1659-1669.

Schwerte, T., Uberbacher, D., Pelster, B. (2003). Non-Invasive Imaging of Blood Cell Concentration and Blood Distribution in Zebrafish Danio Rerio Incubated in Hypoxic Conditions in Vivo. *J Exp Biol*, *206*, 1299-1307.

Sedmera, D., Pexieder, T., Rychterova, V., Hu, N., Clark, E.B. (1999). Remodeling of Chick Embryonic Ventricular Myoarchitecture under Experimentally Changed Loading Conditions. *Anat Rec*, *254*, 238-252.

Shyer, A.E., Rodrigues, A.R., Schroeder, G.G., Kassianidou, E., Kumar, S., Harland, R.M. (2017). Emergent Cellular Self-Organization and Mechanosensation Initiate Follicle Pattern in the Avian Skin. *Science*, *357*, 811-815.

Staudt, D.W., Liu, J., Thorn, K.S., Stuurman, N., Liebling, M., Stainier, D.Y. (2014). High-Resolution Imaging of Cardiomyocyte Behavior Reveals Two Distinct Steps in Ventricular Trabeculation. *Development*, *141*, 585-593.

Steed, E., Faggianelli, N., Roth, S., Ramspacher, C., Concordet, J.P., Vermot, J. (2016). Klf2a Couples Mechanotransduction and Zebrafish Valve Morphogenesis through Fibronectin Synthesis. *Nat Commun*, *7*, 11646.

Sugden, W.W., Meissner, R., Aegerter-Wilmsen, T., Tsaryk, R., Leonard, E.V., Bussmann, J., Hamm, M.J., Herzog, W., Jin, Y., Jakobsson, L., Denz, C., Siekmann, A.F. (2017). Endoglin Controls Blood Vessel Diameter through Endothelial Cell Shape Changes in Response to Haemodynamic Cues. *Nat Cell Biol*, *19*, 653-665.

Vedula, V., Lee, J., Xu, H., Kuo, C.J., Hsiai, T.K., Marsden, A.L. (2017). A Method to Quantify Mechanobiologic Forces During Zebrafish Cardiac Development Using 4-D Light Sheet Imaging and Computational Modeling. *PLoS Comput Biol*, *13*, e1005828.

Vermot, J., Forouhar, A.S., Liebling, M., Wu, D., Plummer, D., Gharib, M., Fraser, S.E. (2009). Reversing Blood Flows Act through Klf2a to Ensure Normal Valvulogenesis in the Developing Heart. *PLoS Biol*, *7*, e1000246.

Watkins, S.C., Maniar, S., Mosher, M., Roman, B.L., Tsang, M., St Croix, C.M. (2012). High Resolution Imaging of Vascular Function in Zebrafish. *PLoS One*, *7*, e44018.

Yalcin, H.C., Amindari, A., Butcher, J.T., Althani, A., Yacoub, M. (2017). Heart Function and Hemodynamic Analysis for Zebrafish Embryos. *Dev Dyn*, *246*, 868-880.

Zickus, V., Taylor, J.M. (2018). 3d + Time Blood Flow Mapping Using Spim-Micropiv in the Developing Zebrafish Heart. *Biomed Opt Express*, *9*, 2418-2435.